APPLICATION OF AN LC-MS/MS METHOD FOR THE ANALYSIS OF POLY (LACTIC-CO-GLYCOLIC ACID) NANOPARTICLES FOR TAXANE CHEMOTHERAPY

A Thesis Submitted to the
College of Graduate and Postdoctoral Studies
In Partial Fulfillment of the Requirements
For the Degree of Master of Science
In the College of Pharmacy and Nutrition
University of Saskatchewan
Saskatoon

By

AMIR KHAJAVINIA

PERMISSION TO USE AND DISCLAIMER

In presenting this thesis in partial fulfillment of the requirements for a Postgraduate degree from the University of Saskatchewan, I agree that the Libraries of this University may make it freely available for inspection. I further agree that permission for copying of this thesis in any manner, in whole or in part, for scholarly purposes may be granted by the professor who supervised my thesis work or, in their absence, by the Head of the Department or the Dean of the College in which my thesis work was done. It is understood that any copying or publication or use of this thesis or parts thereof for financial gain shall not be allowed without my written permission. It is also understood that due recognition shall be given to me and to the University of Saskatchewan in any scholarly use which may be made of any material in my thesis.

Requests for permission to copy or to make other uses of materials in this thesis/dissertation in whole or part should be addressed to:

Dean
College of Pharmacy and Nutrition
University of Saskatchewan
Health Sciences Building, 107 Wiggins Road
Saskatoon, Saskatchewan S7N 5E5
Canada

OR

Dean
College of Graduate and Postdoctoral Studies
University of Saskatchewan
116 Thorvaldson Building, 110 Science Place
Saskatoon, Saskatchewan S7N 5C9
Canada

ABSTRACT

Docetaxel and other compounds in the taxane drug family are among the most effective chemotherapeutic agents used for the treatment of solid tumors, such as breast cancer. Specific targeting of docetaxel to the tumor site would increase the safety and efficacy of the treatment. The focus of the project was to prepare optimized Poly lactic-co-glycolic acid (PLGA) nanoparticles loaded with docetaxel, establish tandem mass spectrometric (MS/MS) fingerprints for taxane drugs, and develop a liquid chromatography (LC)-MS/MS method to quantify the encapsulated drug.

Several nanoparticle formulations were prepared to optimize the nanoparticles based on their size and yield percentage using a modified solvent evaporation technique. The MS/MS fragmentation behavior of taxane compounds, namely paclitaxel, docetaxel, cabazitaxel, cephalomannine, and Baccatin III were studied in detail and a generalized MS/MS fingerprint was established for the first time. A hybrid quadrupole orthogonal time-of-flight (Q-TOF) mass spectrometer was used to obtain accurate mass measurements while MS/MS and second-generation MS/MS (MS^3) analyses were performed using a triple quadrupole-linear ion trap (QqQ-LIT) device. The established MS/MS fingerprints were used to develop a multiple reaction

monitoring (MRM) LC-MS/MS method to quantify docetaxel in PLGA nanoparticles.

The optimized nanoparticles had a zeta potential of -23.2 ± 1.4 mV and mean particle sizes of 202.2±4.7 nm and 251.7±8.2 nm before and after freeze-drying (FD), respectively. Polydispersity index values of the nanoparticles confirmed their uniform size distribution. The taxane compounds showed common MS/MS fragmentation behavior, which allowed for the production of a universal fragmentation pattern. In addition, diagnostic product ions originated from a cleavage in the ester bond between the core diterpene ring-structure and the sidechain. The developed LC-MS/MS method could quantify docetaxel in the PLGA matrix with accuracy and precision at a quantification limit of 15.6 ng/ml. Method validation was conducted using the regulatory guidelines of the Food and Drug Administration (FDA) and the European Medicines Agency (EMA) and showed acceptable values for all the tested criteria. The established general fragmentation pattern of taxanes can be used to predict the dissociation behavior of new compounds with similar structural characteristics. The developed LC-MS/MS method will be beneficial for the future analysis of docetaxel loaded polymeric nano-delivery systems.

Keywords: Taxane; Nanoparticle; liquid chromatography; tandem mass spectrometry

ACKNOWLEDGEMENTS

I would like to express my sincere gratitude to my supervisor, Dr. Azita Haddadi, for her guidance and help. I would like to thank my committee members, Dr. Jane Alcorn and Dr. Anas El-Aneed for their constructive criticism and insight which helped improve my research. The invaluable support and motivation from Dr. El-Aneed were instrumental in the development of the final outcome. I also acknowledge the time and consideration of Dr. Ekaterina Dadachova for chairing my committee meetings.

I would like to express my deep gratitude to Ms. Deborah Michel for the training she provided on the use of mass spectrometer. I am grateful to Dr. Mehran Yarahmadi who offered valuable assistance with the formulation of nanoparticles. I also acknowledge Mr. Ken Thoms for his technical assistance on using the QSTAR system as well as Dr. Randy Purves for his valuable discussions.

I acknowledge the financial support from the College of Pharmacy and Nutrition through the Apotex Graduate Award for years 2019 and 2020.

Finally, I would also like to thank my siblings, Reza, Mona, Amin, and Omid for their care, love, and support during my MSc program.

DEDICATION

To my lovely parents, Ali Khajavinia and Hajar Sina who are my source of inspiration.

Thank you for your limitless and unconditional support in every step of my life.

TABLE OF CONTENTS

LIST OF TABLES

LIST OF FIGURES

LIST OF ABBREVIATIONS

Å	Angstrom
AF2	Excitation energy
AJCC	American Joint Committee on Cancer
ANOVA	Analysis of variance
APCI	Atmospheric pressure chemical ionization
API	Atmospheric pressure ionization
ATP	Adenosine triphosphate
AUC	Area under the curve
℃	Degrees Celsius
CD	Cluster of differentiation glycoprotein
CE	Collision energy
CID	Collision-induced dissociation
CUR	Curtain gas
CV	Coefficient of variation
CXP	Collision cell exit potential
DP	Declustering potential
EGFR	Epidermal growth factor receptor
EMA	European medicines agency
ESI	Electrospray ionization
FD	Freeze-drying
FDA	Food and Drug Administration
FTIR	Fourier-transform infrared spectroscopy
g	Gram
×g	Times gravitational force
GS1	Nebulizer gas

GS2	Heater gas pressure
HER2	Human epidermal growth factor 2
HR	Hormone receptor
HPLC	High performance liquid chromatography
HQC	High quality control
IS	Internal standard
ISV	Ion spray voltage
kDa	Kilo Dalton
kg	kilogram
LC	Liquid chromatography
LC-QqQ	Liquid chromatography triple quadrupole mass spectrometry
LIT	Linear ion trap
LLE	Liquid-liquid extraction
LLOQ	Lower limit of quantification
LOD	Limit of detection
LOQ	Limit of quantification
LQC	Low quality control
MDR	Multi-drug resistance
MF	Matrix factor
mg	milligram
µg/ml	micrograms per milliliter
µl	microliter
ml	milliliter
min	Minute
mm	millimeter
M_{mi}	Mono isotopic mass
MQC	Middle quality control

MRM	Multiple reaction monitoring
MS	Mass spectrometry
MS/MS (MS^2)	Tandem mass spectrometry
MS^n	Multiple stage tandem mass spectrometry
mV	Millivolts
m/z	Mass to charge ratio
n	Number
ng	nanogram
nm	nanometer
o/w	Oil-in-water emulsion
PdI	Polydispersity index
PEG	Polyethylene glycol
P-glycoprotein	Permeability glycoprotein
pH	Power of hydrogen
PLA	Poly (lactic acid)
PLGA	Poly (lactic-co-glycolic acid)
PK	Pharmacokinetic
PVA	Polyvinyl alcohol
QC	Quality control
Q-Trap	Quadrupole ion trap
SD	Standard deviation
SPE	Solid phase extraction
R^2	Regression coefficient
rcf	Relative centrifugal force
u	Atomic mass unit
ULOQ	Upper limit of quantification
UHPLC	Ultrahigh-performance liquid chromatography

UV	Ultraviolet
V	Volts
v/v %	Volume per volume percentage
w/o/w	Water-in-oil-in-water emulsion
w/v %	Weight per volume percentage
w/w	Weight by weight concentration

1. INTRODUCTION

Breast cancer is one of the most prevalent types of cancer and remains an unmet clinical need. Nearly 1 in 8 women will be diagnosed with invasive breast cancer over the course of their lifetime and 1 in 39 women will die from breast cancer (1,2). A review of 29 studies showed that, in patients with early breast cancer, chemotherapy regimens that contained a taxane, such as paclitaxel or docetaxel had higher disease-free survival rates compared to regimens without a taxane (3,4). Despite the advantages of these drugs, patients who receive these chemotherapeutic agents experience severe side effects. Anemia, thrombocytopenia, sensory neurotoxicity, and skin toxicity are among the main side effects of taxanes (5). The lack of selectivity causes the healthy cells to be affected by these drugs and indicates the need for improved therapeutic strategies (6).

Nano-carriers have been the focus of many studies trying to overcome the limitations of chemotherapy (7). After formulating the nanoparticles, it is essential to determine the loading parameters prior to *in vivo* testing and assessing the properties of the particles in an animal model. The goal of my M.Sc. study is to formulate PLGA nanoparticles encapsulating docetaxel. To measure loading level, tandem mass spectrometric (MS/MS) analysis is conducted, and a subsequent liquid chromatography (LC)-MS/MS method is developed. The rationale behind this

research was to have a robust analytical method with accurate, precise, and reproducible results. In the future, these nanoparticles will be conjugated with trastuzumab, a monoclonal antibody approved by the FDA for treating breast cancers that overexpress HER2 receptors. Our final goal in in the future is that the actively targeted drug delivery system would lower the side effects and enhance the therapeutic effects of docetaxel.

2. LITERATURE REVIEW

2.1. Breast cancer overview

Breast cancer is the most commonly diagnosed type of cancer in the world (11.7% of the total cases) and the first cause of cancer death among women (8). In 2020 alone, there were more than 2 million newly diagnosed cases of breast cancer, worldwide (8). This indicates the need for finding more efficient diagnostic techniques and treatment methods for the disease.

Surgery, radiotherapy, endocrine-based treatment, and chemotherapy are the main treatment options of breast cancer therapy that are generally chosen based on the type of cancer, severity of the disease, patient condition, and patient compliance (9). Neoadjuvant therapy, i.e. chemotherapy as the first treatment, has long been used either to downstage the advanced and inflammatory cancers, or to reduce the size of the large operable tumors. Chemotherapy can also be applied after the surgery or endocrine treatment to decrease the chance of recurrence, in which case it is called adjuvant therapy (10). Several standard chemotherapy regimens typically contain an anthracycline, such as doxorubicin or daunorubicin, and a taxane (e.g., paclitaxel or docetaxel). Trastuzumab plus paclitaxel or docetaxel has been, for many years, the standard first-line treatment for HER2-positive metastatic breast cancer (11).

Based on different criteria, breast cancer can be categorized into different subgroups. The American Joint Committee on Cancer (AJCC) uses an anatomical staging system which mainly considers the extent of the cancer spread that is in the breast tissue, lymph nodes in the area, and/or spread to distant tissues (12). However, they recently added the prognostic stage groups to include the molecular markers associated with each type of cancer (13). This new staging approach helps with the decision-making process to choose the best treatment (12). In addition, prognosis of the disease and patient's response to the chosen treatment regimen are easier to predict using AJCC's new staging system (12).

2.2. Breast cancer molecular subtypes

Breast cancer molecular subtypes either can be determined through the analysis of gene expression or approximated with the help of routine processes of clinical biological marker evaluation. These markers include hormone receptor (HR) of estrogen or progesterone, human epidermal growth factor receptor 2 (HER2), and/or extra copies of the HER2 gene (2,14). Based on the presence or absence of HR and HER2, breast cancer can be categorized into four different molecular subtypes:

A) Luminal A (HR+/HER2-):

The cancer growth in this subtype is slower and less aggressive than other groups (12). Luminal A tumors are the most common type and are associated with the most favorable prognosis among other breast cancers partly due to the fact that, in most cases, these tumors respond well to hormonal therapy (15).

B) Luminal B (HR+/HER2+):

The luminal B tumor cells are positive for both hormone receptors and protein Ki67 (a cellular marker for active proliferation) and/or HER2. This type of breast cancers tends to cause higher grade tumors than luminal A, and poorer outcomes are expected with them (15).

C) Basal-like (HR-/HER2-):

Since basal-like cancer cells lack the receptors of estrogen, progesterone, and also HER2, they are also called triple negative cells (16). Finding effective treatments for this type of cancer has not been as successful as for other types, and hence, it has poorer prognosis than other groups (17).

D) HER2-enriched (HR-/HER2+):

This subgroup had the worst prognosis, in the past; However, the introduction of the treatments that target HER2 has tremendously improved the outcomes for the patients with HER2-enriched cancer (18). Several anti-HER2 agents, including

trastuzumab, are available that can target the HER2 family intracellularly as well as extracellularly in HER2-positive breast cancer (19).

2.3. Taxane drug family

In 1971, Wani et al. (20) reported the extraction of a novel anti-tumor agent, taxol, from the bark of western yew, *Taxus brevifolia*. Since then, the taxane drug family has evolved dramatically, and the drugs in this family have become one of the most successful chemotherapeutic agents against a range of solid tumors (21) (Table 2.1). The success of taxanes stems from the ability to inhibit a fundamental process involved in cell proliferation. These drugs bind to the β-tubulin subunit in the structure of the microtubule, causing mitotic arrest and subsequent cell death by inhibiting the microtubule depolymerization (22).

The taxane family represents a diverse range of natural and semi-synthetic compounds. Paclitaxel, cephalomannine, and baccatin III are naturally found in *Taxus* plants while docetaxel and cabazitaxel are semi-synthetic derivatives. Table 2.1 shows the structures of the drugs in this family- paclitaxel, docetaxel, and cabazitaxel- as well as the two related compounds- cephalomannine and Baccatin III. The structures of these compounds generally consist of a tricyclic diterpene backbone (taxadiene) and an ester side chain (5).

Although the drugs in the taxane family share many structural similarities, small differences in their chemical structures have led to dissimilarities in their clinical use, pharmacokinetic (PK) behavior, and frequency of their side effects (23). For instance, the chemical formula of cabazitaxel is different from that of docetaxel in two functional groups on the diterpene ring: cabazitaxel has two methyl-ester groups instead of two hydroxyl groups in the docetaxel structure (Table 2.1). This change makes cabazitaxel molecule more lipophilic and gives it the ability to cross the blood-brain barrier, a property that docetaxel lacks (24). On the other hand, having very similar structures makes it harder to separate or quantify these compounds in the plant extracts (25), unless we have a highly selective method for the analysis; paclitaxel and cephalomannine, for instance, differ only in that paclitaxel has a benzoyl group but cephalomannine has a tigloyl group in their side chains.

Table 2.1. Taxane drug family and related compounds; (*) indicates a synthetic compound.

No.	Compound	Structure	M_{mi} (u)	Use
1	Paclitaxel	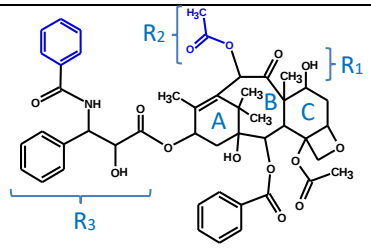	853. 33	- Breast cancer (26) - Ovarian cancer (21) - Non-small cell lung cancer (27) - Kaposi's sarcoma (28)
2	Docetaxel*	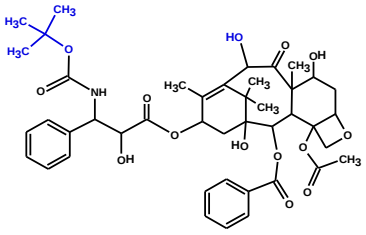	807.35	- Breast cancer (29) - Non-small cell lung cancer (30) - Prostate cancer (31) - Gastric cancer (32) - Head and neck cancer (33)
3	Cabazitaxel*	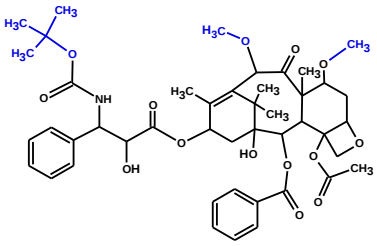	835.38	- Prostate cancer (34)
4	Cephalomannine	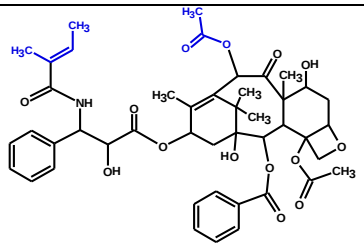	831.35	Laboratory use: - Identification of fungal taxol (35) - Paclitaxel synthesis (25)
5	Baccatin III	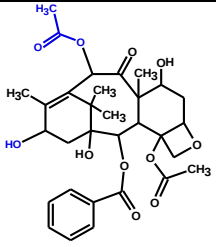	586.24	Laboratory use: - Paclitaxel synthesis (36)

M_{mi}: Monoisotopic mass

2.4. Docetaxel characteristics and pharmacokinetics

Docetaxel is the semi-synthetic derivative of paclitaxel and is one of the most successful agents used for the treatment of breast cancer. Docetaxel enhances the stabilization of microtubules resulting in anti-mitotic effects, similar to other taxanes (21). It has recently been widely used to treat breast cancer in neoadjuvant, adjuvant and metastatic cases (37). In addition, docetaxel is an important component in the chemotherapeutic regimens of prostate, ovarian, and non-small cell lung cancer (38).

Despite its meritorious effects, the clinical use of docetaxel is limited due to its poor aqueous solubility, rapid elimination, low selective distribution, and severe adverse effects (38). Severe and febrile neutropenia and severe peripheral neurotoxicity are among its main adverse reactions (39). As is the case with many other cancer medications, rapidly proliferating cells, such as hematological and gastrointestinal cells are affected to a larger extent by docetaxel (40). Thrombocytopenia, hypersensitivity, fluid retention, anemia, nausea, diarrhea, vomiting, alopecia, myalgia, and skin reactions are some of the other side effects that have been reported with docetaxel (23). The emergence of these toxicities frequently requires reduction of the dose or therapy cessation, despite desirable clinical outcome. Improving the specificity of the treatment and reducing the adverse reactions, especially those which limit the dose, are among the main goals of successful cancer therapy (23).

Resistance of the cancerous cells to the drug is another major problem that causes limitations with a treatment regimen that includes microtubule targeting agents (41). P-glycoprotein efflux has known to be one of the main mechanisms of docetaxel resistance (42). P-glycoprotein is an ATP-dependent drug efflux pump which can transport docetaxel from inside the cells, where it can exert its effect, to outside of the cell (38). The emergence of resistance can increase the risk of cancer relapse (43). Moreover, a higher dose of the drug would be needed to reach the same intercellular concentration of the docetaxel. An increase in dose can result in increased side effects of the medication and decreased patient compliance (38,44). Therefore, combating or avoiding resistance is another important consideration needed to achieve a successful treatment.

Due to its low solubility in water, a combination of ethanol and tween 80 (polysorbate 80) has been used in the formulation of the commercially available product of docetaxel, Taxotere®, to increase the solubility of the drug (45). Some problems observed with Taxotere® such as hypersensitivity reactions and increased exposure of body compartments to the drug are believed to be related to the excipients (i.e., ethanol/tween 80) (46,47).

Docetaxel concentration profile in plasma is characterized by triphasic elimination kinetics after intravenous administration (48). Its elimination half-life ranges between 11 to 19 h (48). Docetaxel partitions into many tissues and as a result has a

relatively high volume of distribution. However, it has poor oral bioavailability due to significant first-pass effect, and low penetration into the central nervous system due to its efflux by the P-glycoprotein drug efflux pump (49). Plasma α-1- acid glycoprotein concentrations and the liver enzyme activity are the main determinants of drug clearance (48). Approximately 70–80% of the administered drug is eliminated in the form of metabolites in the feces through bile and about 10% is excreted in the urine (42).

2.5. PLGA nanoparticles

Poly (lactic-co-glycolic acid) (PLGA) is a polymer synthesized by the copolymerization of glycolic acid and lactic acid monomers (50). The monomeric units are consecutively linked together by ester linkages to produce a linear polyester macromolecule (51). The commercially available forms of PLGA are labeled to identify the ratio of the monomers in the compound, for example PLGA 50:50 indicates that the copolymer is composed of 50% lactic acid and 50% glycolic acid (52).

PLGA has a number of desirable properties to be used vastly in the biomedical fields. It is completely biocompatible and biodegradable, has controllable properties, and also is approved by the FDA for human therapy (51,53). Due to these characteristics,

PLGA has been used extensively to prepare novel drug delivery systems and *in-vivo* imaging systems such as nanoparticles (54).

By changing the parameters of the synthesis method, the characteristics of the nanoparticles produced can be modified. Several different methods of preparation have been investigated in different studies (51). Solvent evaporation is the most common method used to prepare PLGA nanoparticles. Both oil-in-water (o/w) and water-in-oil-in-water (w/o/w) emulsions can be prepared using the solvent evaporation technique. A w/o/w emulsion consists of oil phase droplets which are dispersed in an outer bulk aqueous phase while each oil droplet has an internal aqueous phase. While w/o/w techniques are mainly suitable to encapsulate water soluble drugs, o/w emulsions are better carriers for lipophilic drugs (55). In order to prepare an o/w emulsion, PLGA is dissolved in an organic water-immiscible solvent such as ethyl acetate or chloroform (56). This solution is then dispersed in the aqueous phase containing an emulsifier such as poly vinyl alcohol (PVA). The organic solvent is evaporated to yield the nanoparticle suspension (57).

In addition to the aforementioned advantages of PLGA, another beneficial feature of the polymer is having several functional groups (e.g., OH and COOH) which make it easier to attach targeting ligands to the polymer (Figure 2.1). A number of peptides and proteins have been used in different studies to serve as the targeting agent for PLGA nanocarriers (7,58,59). For example, fab fragments of a humanized

anti-HER2 monoclonal antibody have been covalently bound on the surface of PLGA nanoparticles carrying *Pseudomonas* exotoxin (PE38KDEL) (60). The targeted nanoparticles were internalized into HER2-overexpressing breast cancer cells, which resulted in significantly higher cytotoxicity compared to non-targeted nanoparticles (60). In another study, trastuzumab was physically conjugated to the surface of PLGA/montmorillonite nanoparticles using the electrostatic attraction forces between the OH groups of polymer and the functional groups of trastuzumab (OH and NH_2) (61). The results of *in vitro* cytotoxicity experiment on SK-BR-3 cells showed that the IC_{50} of paclitaxel-loaded plain nanoparticles was 12.74 times higher than paclitaxel-loaded nanoparticles surface modified with trastuzumab (61).

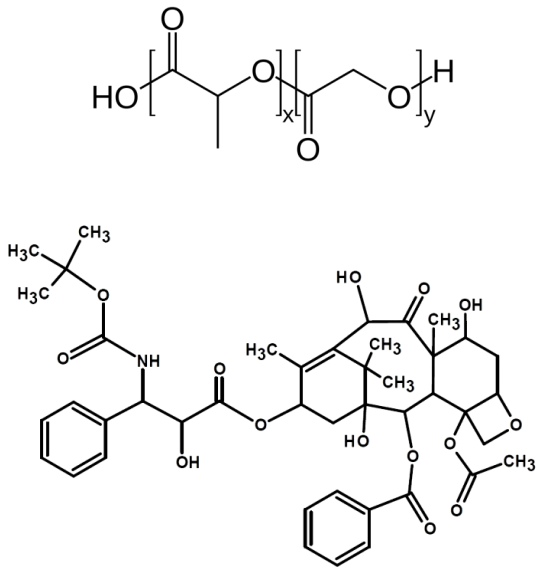

Figure 2. 1. Chemical structures of PLGA (up) and docetaxel (down).

2.6. Docetaxel nanoparticles

Nanoparticles are being extensively used as drug delivery systems. Nanoparticles can enhance the dissolution rate of the encapsulated drug which, in turn, enhances its bioavailability and absorption (62–64). Nanoparticles can also be employed to prolong the effect of a drug by providing more protection against metabolism and renal clearance (65–69). Moreover, nanoparticles can improve the tissue distribution of a drug by enhancing its delivery to certain tissues (targeted drug delivery); this can lower the side effects of the drug (70–72). Nanoparticles can provide prolonged circulation of the drug which can lead to a decrease in clearance and an increase in the half-life, mean residence time, and area under the curve (AUC) of the drug. Although the efficacy and toxicity of a drug is largely correlated with the blood concentration of the drug, tissue distribution data provides valuable understanding of the relationship between drug distribution and observed side effects (73). By comparing the PK and biodistribution of a drug with the encapsulated form, efficacy and side effects of the drug could be monitored and predicted.

Nanoparticle-encapsulated docetaxel has been evaluated in several studies. PLA-PLGA nanoparticles have been compared to free drug solution showing enhanced PK parameters and biodistribution in mice with adenocarcinoma (74). In another study conducted in our group, PLGA and PLGA-PEG nanoparticles were used to

study the PK and biodistribution of docetaxel in BALB/c mice (75). Both types of nanoparticles showed long circulating sustained release profiles when administered intravenously. Surface modification of nanoparticles with PEG increased the residence time of docetaxel in blood compared to non-modified PLGA nanoparticles (75).

2.7. Mass spectrometry uses in drug development and analysis

The use of mass spectrometry (MS) for drug analysis have been expanding over the past 20 years. MS is used in different steps of the drug discovery and development process, including high-throughput screening, metabolite studies, quantification of active ingredients and pharmacokinetic studies (76–82).

Due to the high speed and sensitivity of liquid chromatography-MS (LC-MS) (83,84), many researchers have chosen this technique for quantitative analyses in the drug development processes (85–88). The combination of the separation ability of LC with the selectivity of MS allows for the determination of a group of analytes in a complex mixture. To ensure the validity of the quantitative analysis, isotopically labelled internal standards should be used, which can correct variability in an assay, such as the extraction procedure and the ionization with the MS instrument (89).

Electrospray ionization (ESI) and atmospheric pressure chemical ionization (APCI) are the two most commonly used ionization techniques in LC-MS analysis of pharmaceuticals. Both ESI and APCI fall under the umbrella of atmospheric pressure ionization (API) interfaces. Before the development of API, the introduction of the mobile phase from the LC system into the vacuum of the mass spectrometer was a major challenge. API sources do not interrupt the high vacuum in the MS analyzer since the analyte ionizes at atmospheric pressure. Moreover, ESI technique is considered to be a "soft" ionization technique meaning that the protonated or deprotonated ions or adduct ions are generated without much fragmentation. This feature is ideal for the selection of precursor ion.

The rapid improvement of MS instrumentations as well as hyphenated MS technologies, such as LC-MS, have made MS a powerful technique for quantitative purposes (90). A wide range of pharmaceuticals have been investigated using LC-MS. For example, collision-induced dissociation tandem mass spectrometry (CID-MS/MS) analysis of a series of diquaternary ammonium gemini surfactants, used as gene-delivery systems, was first established (91–93). The fragmentation patterns were then used to develop a universal MS/MS fingerprint for the studied gemini surfactants (94) and subsequently, multiple reaction monitoring (MRM) MS-based methods were successfully developed to determine gemini surfactants in biological

samples (95–98). In addition, the established MS/MS fingerprints were essential to establish the metabolic pathways of the studied compounds (99).

Elucidation of chemical structures of the newly discovered or synthesized compounds can be achieved by exact-mass measurement and CID-MS/MS. For example, Cui and coworkers used ESI-multiple stage tandem mass spectrometry (MS^n) to analyze saponins in a plant extract from *Panax ginseng* (100). Saponins are natural glycosides with a wide range of biological activity. ESI-MS^n allowed for the differentiation of structures of several types of ginsenosides and led to the establishment of a general fragmentation pathway for these compounds (100). Finally, an HPLC-MS/MS method was developed that was capable of rapid screening of different saponins in plant extract (100). The work of Cui et al. shows how establishing fragmentation pathways for pharmaceutical agents helps to identify diagnostic product ions and neutral losses allowing for the development of identification and quantification methods. In a similar example, the MS/MS dissociation behavior of plant phytosterols and tocopherols were studied (101). The results paved the way for the establishment of an APCI-LC-MS/MS method for simultaneous quantification of four phytosterols and four tocopherols entrapped in a liposomal formulation (102).

Metabolite identification and quantification is an integral stage in the drug discovery process (103–106). Establishing the elimination rate of a drug, identification of its clearance route, drug lead optimization, and detection of potentially toxic metabolites are some of the main applications of drug metabolism studies (107,108). In addition to the aforementioned applications, LC-MS is also a relatively easy-to-use strategy, capable of rapid and sensitive analysis of metabolites (109,110). Different LC-MS methods have been used to identify and quantify drug metabolites in a number of human tissues and bodily fluids (111–114). For instance, targeted metabolomic profiling has been used in a study to identify novel diagnostic biomarkers for early breast cancer detection (115). Plasma samples from 39 women with breast cancer were compared to 21 samples from a control group to examine 232 endogenous metabolites using LC-MS. The results suggested acylcarnitines and 9,12-linoleic acid as potential diagnostic biomarkers for breast cancer (115). In another example, an LC-ESI-MS/MS method was developed for the quantification of 27 free and conjugated estrogen-related metabolites in urine (116). Studies have shown that an imbalance in the estrogen metabolism can be associated with a higher risk of developing breast cancer (117,118). The developed LC-ESI-MS/MS method was able to quantify the metabolites in the low nanograms per milliliter range. The results of the study can be used to help diagnose breast cancer in its early stages in the future.

HPLC-MS/MS systems have also been extensively used for *in vitro* metabolic stability assays, aiming at providing a prediction of the *in vivo* intrinsic clearance of the drugs (119,120). For example, stable and reactive metabolites of tetrahydropiperine, a natural arylpentamide compound isolated from *Piper nigrum* L., were investigated (121). The metabolic profiles of tetrahydropiperine were elucidated via incubation with hepatocytes of mouse, rat, dog, monkey and human. The samples were analyzed using ultrahigh-performance liquid chromatography (UHPLC)-MS/MS to characterize the structures of the metabolites and establish the metabolic pathway of the compound (121).

Employing MS in drug development and pharmaceutical studies mentioned above are only a few examples among its various applications. New MS instrumentations and techniques continue to pave the way for easier, faster, and more sensitive analytical methods.

2.8. Mass spectrometric techniques for the quantification of docetaxel

Mass spectrometry (MS) has widely been used in bio-medical assays mainly due to its high sensitivity, selectivity, and high throughput capacity (122). Liquid chromatography triple quadrupole mass spectrometry (LC-QqQ) is the major type of MS used for quantification purposes (123). MS/MS allows for high selectivity over other analytical methods, such as UV-spectroscopy. In MS/MS analysis, the first MS analyzer separates a single ion from a mixture of ions in the sample to be dissociated in the collision cell while the second MS analyzer separates the produced product ions (124).

Many different analytical methods have already been applied to quantify docetaxel in polymeric or biologic samples. High performance liquid chromatography coupled with ultraviolet detector (HPLC-UV) and mass spectrometry (HPLC-MS/MS) are the most widely used methods for the analysis of docetaxel (Table 2.1). While UV-based analysis is simpler, MS-based methods provide higher selectivity and lower quantification limits. In a recently published study, the limit of quantification for docetaxel was found to be 700 ng/ml in a PLGA nanoparticle matrix using an HPLC-UV technique (125), while MS-based methods can have a quantification limit as low as a few nanograms per milliliter (126).

There are two main methods of sample introduction to the MS: flow injection analysis (FIA), and LC. Although direct injection of the sample to the mass spectrometer is a rapid method of sample introduction, it has several disadvantages when more complex matrices such as plasma or urine are analyzed. For example, with flow injection analysis of a complex matrix, higher limits of detection and quantification could be achieved compared to LC analysis (127). Incorporation of chromatographic separation eliminates such problems (123). Despite the disadvantage of being more time-consuming than FIA, LC provides better signal to noise ratios by effectively separating the analytes within the matrix; the result is having a lower detection limit. In a study conducted previously in our group, FIA-MS/MS analysis of docetaxel in PLGA nanoparticle matrix resulted in a detection limit of 62.5 ng/ml (128).

HPLC-MS/MS has been adapted by many researchers to quantify docetaxel in different matrices (129–131) (Table 2.2). For example Gao et al. developed an HPLC-ESI-MS/MS method for the determination of docetaxel in human plasma (131). A liquid-liquid extraction procedure was employed using a mixture of ether-dichloromethane and acetonitrile-ammonium acetate buffer followed by chromatographic separation with a C18 column. The developed HPLC-MS/MS method was able to quantify docetaxel in plasma with 10 ng/ml lower limit of quantification (LLOQ) and had a detection limit (LOD) of 2 ng/ml (131).

Table 2.2. Different analytical techniques used to quantify docetaxel. (LLE: liquid-liquid extraction, SPE: solid-phase extraction, MS: mass spectrometry, UV: ultra-violet)

No	Extraction	Medium	Column	detection	Retention time	Reference
1	LLE	plasma	C18	MS	$\approx 4min$	(132)
2	SPE	Plasma	C18	MS	$\approx 1.8min$	(133)
3	LLE	Plasma	C18	MS	$\approx 1.32\ min$	(134)
4	SPE	Plasma	C8	UV	$\approx 11\ min$	(135)
5	LLE	Plasma	C18	UV	$\approx 7.6\ min$	(136)
6	SPE	Plasma	C8	MS	$\approx 4.7\ min$	(137)
7	SPE	Plasma	C18	MS	$\approx 3.7\ min$	(138)
8	LLE	Plasma	C18	MS	$\approx 4.4\ min$	(139)

3. PURPOSE OF THE PROJECT

3.1. Rationale for research

Docetaxel is among the medications used as the first-line treatment in HER2-receptor-positive breast cancer. Despite the meritorious effects of docetaxel, in some cases, its use is being limited due to the drug's adverse effects. In addition, there are formulation issues associated with Taxotere® such as the incorporation of ethanol and tween 80 in the formulation of the product. Therefore, we aimed at developing a novel formulation to overcome the observed side effects and make use of the benefits of the nano-delivery systems. Measuring the loading parameters of the newly developed formulation is a crucial step in the characterization of the formulation. Knowing the total amount of drug encapsulated in the nanoparticle formulation is needed for the calculation of the dose and for the conduct of *in vitro* and *in vivo* tests, in the future. Hence, we attempted to develop a new LC-MS/MS method to quantify docetaxel in the PLGA polymer matrix using a phenyl column. A phenyl column has not been used before for this purpose despite its potential benefits.

First, we decided to establish the MS/MS fragmentation fingerprints of the drugs in the taxane family and identify common dissociation patterns of these drugs for the first time. Establishing MS/MS fingerprints has also the benefit of identifying

product ions that are both diagnostic and abundant allowing for the development of qualitative and quantitative methods. To ensure the validity of the analytical method, the FDA and EMA method validation guidelines were applied.

3.2. Hypotheses

In this study we hypothesize that:

- Optimization of the formulation conditions of PLGA nanoparticles will lead to the production of particles no larger than 250 nm and a yield of more than 50%.
- The structural similarities between the drugs in the taxane family result in similar dissociation pathways among various structures, allowing for the establishment of a general fragmentation pattern for the five studied taxane compounds.
- LC-MS/MS method employing a combination of phenyl column stationary phase and methanol-based analyte recovery will enhance analytical sensitivity of the method in comparison to methods using flow injection-MS/MS.

3.3. Objectives

PLGA nanoparticles can be utilized to deliver docetaxel. This will possibly lead to the optimization of the drug's biodistribution and will minimize the adverse effects. Therefore, the following objectives are considered in this study:

1. To prepare PLGA nanoparticle formulations loaded with docetaxel, and to characterize the nanoparticles in terms of their particle size, polydispersity index (PdI), zeta potential, yield percentage, and loading parameters.
2. To establish the MS/MS fragmentation fingerprints of the taxane-based structures.
3. To develop an HPLC-MS/MS method for the quantification of docetaxel in nanoparticle formulations.

4. MATERIALS AND METHODS

4.1. Materials

Ester-terminated PLGA (50:50) with an inherent viscosity of 0.15-0.25 dL/g was purchased from Birmingham Polymers (LA, USA). Paclitaxel (>99.5% purity) and docetaxel (>99%) were from LC laboratories (Woburn, MA, USA). Cabazitaxel (98%), cephalomannine (96%), and Baccatin III (95%) were purchased from Toronto Research Chemicals (Toronto, ON, Canada). Polyvinyl alcohol (PVA) was from Sigma-Aldrich Co. (St Louis, USA). Methanol and acetone were LC-MS grade, purchased from Fisher Scientific (Fairlawn, NJ, USA), and formic acid was from BDH Chemicals (Toronto, ON, Canada).

4.2. Preparation of the nanoparticles

PLGA nanoparticles were prepared based on a method established previously in our laboratory using the solvent evaporation technique (128). Briefly, 10% w/v ester-ended PLGA and 3% w/v docetaxel were dissolved in ethyl acetate to serve as the organic phase. 2.2% w/v polyvinyl alcohol (PVA) was added as the aqueous phase and vigorously mixed followed by high energy sonication for two minutes using a digital tip-sonifier (Branson digital sonifier 250, Danbury, USA). The resulting suspension was stirred at room temperature to allow for the evaporation of the organic solvent, and the prepared nanoparticles were washed to remove the extra

PVA and free drug residues. Finally, nanoparticles were freeze dried for 48 hours (Labconco Co., Kansas City, USA) and stored at -20°C.

4.3. Characterization of the nanoparticles

Particle size, zeta potential and polydispersity index (PdI) were measured using Malvern Zetasizer (Nano series, Montreal, Canada).

The yield percentage of the process was calculated using the following equation:

$$\text{Yield (\%)} = \frac{\text{weight of the obtained particles}}{\text{the initial weight of polymer,drug and other ingredients}} \times 100 \quad \text{(Equation 1)}$$

After the determination of the amount of drug encapsulated in the nanoparticles (section 4.5), drug loading and encapsulation efficiency of nanoparticles were calculated as follows:

$$\text{Drug loading (\%)} = \frac{\text{weight of the drug in the particles}}{\text{weight of the particles}} \times 100 \quad \text{(Equation 2)}$$

$$\text{Encapsulation efficiency (\%)} = \frac{\text{weight of drug in particles}}{\text{initial weight of drug added}} \times 100 \quad \text{(Equation 3)}$$

4.4. MS/MS fragmentation analysis

4.4.1. Sample preparation

Stock solutions of all the compounds were prepared at 5 µg/ml with methanol containing 0.1% (v/v) formic acid. Using the formic acid solution in methanol, each sample was further diluted by 5× before full scan MS and MS/MS analysis.

4.4.2. Mass spectrometric analysis

4.4.2.1. Single stage MS analysis

The single stage MS analysis of the taxane-related compounds was performed using a QSTAR XL quadrupole orthogonal time-of-flight hybrid (QqTOF) mass spectrometer equipped with an electrospray ionization (ESI) source (AB SCIEX, Redwood City, CA, USA). The instrument parameters were optimized as follows: declustering potential 60V and focusing potential of 180 V. Samples were directly infused into the source chamber at a flow rate of 15 µl/min using an integrated Harvard syringe pump. The voltage of the Turbo ion spray was set at 5500 V and the mass spectrometer was operated in a positive ion mode while nitrogen was used as the ESI nebulizing gas. Prior to the analysis of the compounds, the external calibration of the instrument was performed using cesium iodide (CsI, *m/z* 132.9055, Sigma-Aldrich, Oakville, ON, Canada) and sex pheromone inhibitor iPD1 (*m/z* 829.5320, Bachem Bioscience Inc., PA, USA).

4.4.2.2. MS/MS analysis

Taxane-related compounds were analyzed using an AB SCIEX 6500 QTRAP® triple quadrupole-linear ion trap mass spectrometer (QqQ-LIT-MS) equipped with a Turbo V Ion Spray electro-spray ionization (ESI) source.

Samples were directly infused into the mass spectrometer using an integrated syringe pump that delivered constant supply of the sample at a flow rate of 7 µl/min. Nitrogen gas was used as the ESI nebulizing gas. The temperature of the ion source was set at default value of 150 ºC, and no drying gas was used. The instrument was operated in the positive ion mode with an ion spray voltage of 5500 V and a declustering potential (DP) of 40 V.

To perform MS/MS, and second-generation MS/MS (MS^2) the collision energy (CE) was optimized separately for each compound and determined to be 23 eV for docetaxel, 18 eV for cephalomannine, 10 eV for cabazitaxel, and 20 eV for both paclitaxel and Baccatin III. The optimized CEs induce fragmentation while the precursor ion remained abundant. MS^3 analysis of the compounds was performed under the same optimized conditions described above. The excitation energy (AF2) was optimized to have the highest possible abundance of the second-generation product ions while maintaining the presence of the precursor ion peak. The excitation energy ranged from 50 V to 110 V for docetaxel, 80 V to 200 V for

cephalomannine, 50 V to 110 V for cabazitaxel, 80 V to 150 V for paclitaxel, and 90 V to 200 V for baccatin III.

4.4.3. Data analysis

Structures of all the taxanes and their respective product ions generated during MS/MS analysis were drawn using the open source ACD/ChemSketch software, version 2018.1.1 (Advanced chemistry Development Inc.). The software was also used to calculate the theoretical monoisotopic masses of the ions.

4.5. LC-MS quantification of encapsulated docetaxel

4.5.1. Sample preparation

4.5.1.1. Standard sample preparation

Stock solutions of docetaxel (4 µg/ml) and paclitaxel (2 µg/ml) were prepared in methanol. Paclitaxel was used as the internal standard (IS) in the analysis. All stock solutions were prepared freshly before each experiment. Working solutions of the standards were made by serial dilution of the stock solution in methanol to prepare eight concentrations: 15.6, 31.2, 62.5, 250, 1000, 2000, 3500, 4000 ng/ml.

To prepare standards, 0.5 ml of each standard working solution and 100 µl of the IS stock solution (to obtain a final concentration of 400 ng/ml) were transferred to 2ml tubes and vortexed for 60s. The solvent was evaporated using a centrifugal vacuum concentrator (Labconco, USA) and 0.5 mg plain (drug-free) nanoparticles were added to the tube. Each prepared standard was extracted using the method described in section 4.5.1.4.

4.5.1.2. Quality control (QC) preparation

Quality control (QC) samples were prepared at four concentration levels to be used in validation experiments. A stock solution of 3000 ng/ml was used to prepare a concentration set of 15.625, 40, 1500, and 3000 ng/ml. According to the FDA

guidelines, the high-quality control (HQC) sample should be at least 75% of the upper limit of quantification (ULOQ); the middle quality control (MQC) sample should be in the mid-range, and the low-quality control (LQC) sample should be within 3 times the concentration of LLOQ (140). Based on this, the HQC had a concentration of 3000 ng/ml, equal to 75% of the ULOQ (4000 ng/ml), the MQC had a concentration of 1500 ng/ml (37.6% of the calibration range), and LQC had a concentration of 40 ng/ml (2.6 ×LLOQ).

To prepare QC samples, 0.5 ml of each QC working solution and 100 µl of the internal standard stock solution were transferred to 2ml tubes and vortexed for 60s. The solvent was evaporated using a centrifugal vacuum concentrator (Labconco, USA) and 0.5 mg plain (drug-free) nanoparticles were added to the tube. Each prepared QC sample was extracted using the method described in section 4.5.1.4.

4.5.1.3. Preparation of samples with unknown drug content

100 µl IS stock solution was placed in 2 ml tubes. The solvent was evaporated, and 0.5 mg drug-loaded nanoparticle formulation was placed in the tube. Each sample was extracted using the method described in section 4.5.1.4. Samples were diluted 20 times with blank (an extracted matrix sample to which the internal standard had been added i.e., zero calibrator) before analysis. An analytical run included the

following samples: double blank (an extracted matrix sample without the analyte i.e., matrix blank), blank, eight calibration standards, four levels of QC, and unknown samples.

4.5.1.4. Docetaxel extraction from nanoparticles

To quantify the docetaxel content, the samples were extracted prior to injection in the mass spectrometer. An extraction method established previously in our laboratory (128) was used with some modifications. Paclitaxel was added at the beginning of the extraction process as the internal standard at a concentration of 400 ng/ml.

0.5 ml acetone was added to 0.5 mg drug-loaded or drug-spiked nanoparticles to dissolve both the polymer and the drug. The obtained mixture was vigorously shaken (VWR Mini Vortexer, USA) for one minute and was subjected to bath sonication (Branson 5510 bath sonicator, USA) for 30 minutes. Then it was centrifuged for 30 minutes at 20,000 g (Beckman J2-21 Ultracentrifuge, USA). The supernatant was separated and transferred to new Eppendorf tubes. The same procedure was repeated by dissolving the precipitate in acetone. The collected supernatants from the first and second centrifugation steps were mixed and evaporated. 0.5 ml methanol was added to the residue, vortexed for one minute and centrifuged for 30 minutes at 20,000 g. The supernatant was transferred to HPLC vials (Figure 4.1).

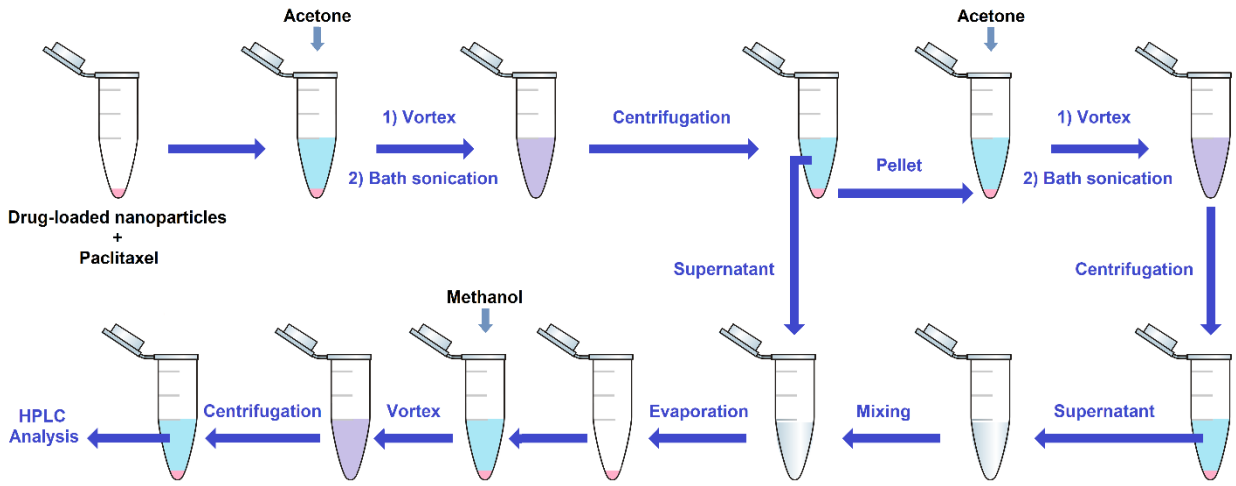

Figure 4.1. Illustration of the steps of docetaxel extraction from nanoparticles.

4.5.2. LC-MS/MS method development

A new LC-MS/MS method was developed for the quantification of docetaxel in the nanoparticle matrix.

Chromatographic separation was achieved on a 1260 Agilent Infinity II (Waldbronn, Germany) High Performance Liquid Chromatography (HPLC) system. A sample volume of 5 µl was injected using the 1200 Agilent autoinjector set to 4°C for the separation on a Nova-Pak® Phenyl column (60 Å, 4 µm, 3.9 mm × 75 mm) maintained at 40°C. A gradient binary mobile phase composed of (A) 0.1% (v/v) formic acid in water and (B) 0.1% (v/v) formic acid in methanol was set to a flow rate of 0.3 ml/min for a run time of 10 min. The gradient program started with 70% B for the first 0.5 min and changed to 90% B over 6.5 min. The initial composition

was restored within the next 0.5 min and was held constant for an additional 2.5 min for equilibration. Figure 4.2 shows the changes in the percentage of the organic phase vs. time during one chromatographic run.

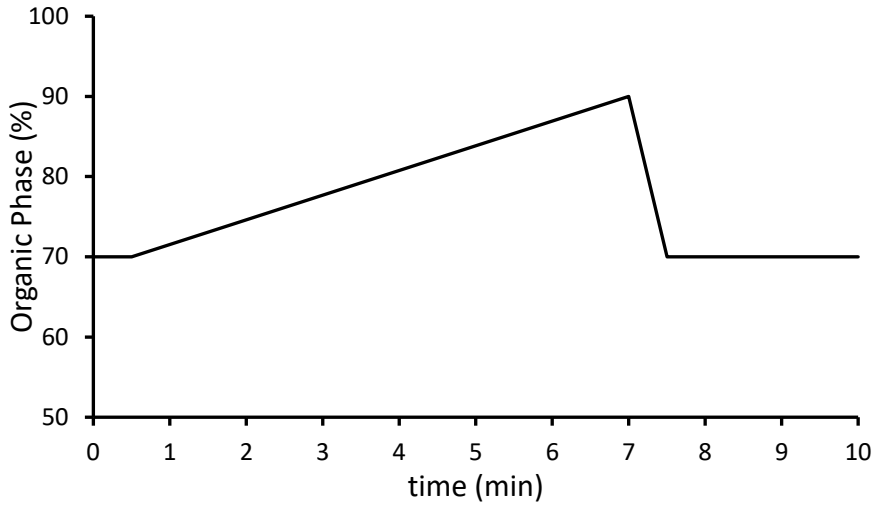

Figure 4.2. Changes in the organic phase (0.1% formic acid in methanol) vs time during one chromatographic run.

A Valco® switching valve was used to deliver the flow to the column between time-points of 4 min and 7 min. At time periods of 0 to 4 min and 7 to 10 min, the flow was diverted into waste to decrease the contamination of the ion source and increase the sensitivity. System control and data processing were achieved on Analyst® software, version 1.7.0 (AB Sciex, ON, Canada).

After HPLC separation, column effluent was directed to a Hybrid Triple Quadrupole-linear Ion trap mass spectrometer (AB Sciex 4000 QTRAP MS/MS system, Framingham, MA, US) equipped with a Turboionspray® interface. Quantitation was achieved in the multiple reaction monitoring (MRM) mode in positive ionization using electrospray ionization (ESI) source. The monitored precursor ion → product ion for docetaxel to serve as quantifier and qualifier transitions were *m/z* 808.4 → *m/z* 527.3 and *m/z* 808.4 → *m/z* 226.1, respectively. The monitored transitions for paclitaxel were *m/z* 854.4 → *m/z* 569.3 and *m/z* 854.4 → *m/z* 286.2. Table 4.1 summarizes these data.

The source temperature was set to 400°C, ion spray voltage (ISV) 5500V, curtain gas (CUR) 40, nebulizer gas (GS1) 40, heater gas pressure (GS2) 40 and using an entrance potential of 10 for all transitions. The declustering potentials (DP), collision energy (CE), and collision cell exit potential (CXP) were optimized for each MRM transition to ensure ion abundance and stability (Table 4.1). Dwell time for all transitions was 50ms at unit resolution. The interface heater was on and nitrogen was used as the gas for all cases.

Table 4. 1. MRM transitions for docetaxel and paclitaxel (IS) and optimized MS conditions.

	Docetaxel		Paclitaxel	
	808.4 → 527.3 (Quantifier)	808.4 → 226.1 (Qualifier)	854.4 → 569.3	854.4 → 286.2
De-clustering potential (DP)	76	76	101	101
Collision energy (CE)	15	21	15	27
Cell exit potential (CXP)	14	14	16	18

Validation of the developed LC-MS/MS method was conducted according to the Guidance for Bioanalytical Method Validation issued by the FDA (140) and the EMA Guidelines on Bioanalytical Method Validation (141).

4.5.2.1. Accuracy and precision

The four levels of QCs were used in sextuplicates during the same day (intra-day) and on three consecutive days (inter-day).

For each sample, the accuracy was calculated as the difference in percentage between its measured and nominal concentrations. Precision was determined by calculating the coefficient of variation (CV).

To accept the accuracy from a single run, the mean calculated value should be within ±15% of the nominal value of each QC level, except the LLOQ for which it should be within ±20%. The acceptance criteria for precision is a CV% of less than 15% for

each QC level, except for the LLOQ where it should not be more than 20% (140,141).

4.5.2.2. Linearity

An 8-point standard curve was constructed by plotting known concentrations of docetaxel in the range of 15.625 ng/ml to 4000 ng/ml against the peak area ratio of docetaxel to paclitaxel. A linear regression analysis weighting the standard curve with $1/x$ was implemented. A double blank sample and a blank sample were also analyzed with each set of calibration standards. The regression coefficient (R^2), slope, intercept, and equation of the resulting standard curves were determined.

4.5.2.3. Limit of detection and limit of quantification

The standard that has a signal to noise ratio of 3:1 was considered as the limit of detection (LOD). The limit of quantitation (LOQ) of the method was measured based on a signal-to-noise ratio of 10:1 with the acceptable precision and accuracy (within ±20% of the nominal value).

4.5.2.4. Selectivity

To assess the method selectivity, double blank solution (n=6) was injected, and the peak area observed at channels of the analyte and the internal standard at their expected retention times were compared to the mean peak area of the LLOQ. The method was considered selective if the observed interference is less than 20% of the LLOQ for the analyte and less than 5% for the IS (141).

To make sure that there is no interference between the analyte and the internal standard, six blank solutions (an extracted solution containing only IS) were injected. The observed interference at the analyte channel was measured and compared to the mean peak area of the LLOQ. An interference of less than 20% of the LLOQ was considered acceptable (141–143).

4.5.2.5. Matrix effects

EMA guidelines were used to evaluate the matrix effects (141). To perform this, the peak areas were compared between post-spiked samples at two concentration levels (LQC and HQC) and samples prepared in neat solvent. The same procedure was performed for the internal standard (IS) at the concentration of 400 ng/ml.

Six samples of drug-free nanoparticles were extracted as described in section 4.5.1.4. After extraction, the samples were spiked with the analyte or the IS. An equivalent

set of samples were also prepared in methanol (n=6 at each level of concentration). The matrix factor (MF) and the IS-normalized MF were calculated according to equations (4) and (5), respectively. The CV% was determined for each factor. Based on the EMA guidelines, the CV% of the IS-normalized MF should not be greater than 15% (141).

$$\text{Matrix Factor (MF)} = \frac{\text{Peak area}_{(\text{post-extraction spiked sample})}}{\text{Peak area}_{(\text{non-extracted neat solvent sample})}} \quad \text{(Equation 4)}$$

$$\text{IS-normalized MF} = \frac{\text{MF}_{\text{analyte}}}{\text{MF}_{\text{IS}}} \quad \text{(Equation 5)}$$

4.5.2.6. Extraction procedure efficiency

To determine the efficiency of the extraction method, the peak areas were compared between pre-spiked samples and samples prepared in neat solvent, at three concentration levels (LQC, MQC, and HQC). The same procedure was performed for the internal standard (IS) at a concentration of 400 ng/ml.

Six samples of drug-free nanoparticles were spiked with the analyte or the IS and extracted as described in section 4.5.1.4. An equivalent set of samples were also prepared in methanol (n=6 at each level of concentration). The extraction efficiency percentage was calculated using equation (6).

$$\text{Extraction Efficiency \%} = \frac{\text{Peak area}_{(\text{pre-extraction spiked sample})}}{\text{Peak area}_{(\text{non-extracted neat solvent sample})}} \times 100 \quad \text{(Equation 6)}$$

4.5.2.7. Extraction Recovery

To determine the extraction recovery percentage, the peak areas were compared between pre-spiked samples and post-spiked samples, at three concentration levels (LQC, MQC, and HQC). The same procedure was performed for the internal standard (IS) at a concentration of 400 ng/ml.

Six samples of plain (drug-free) nanoparticles were extracted as described in section 4.5.1.4. After extraction, the samples were spiked with the analyte or the IS. An equivalent set of samples were also prepared by spiking the plain nanoparticles with the analyte or the IS (n=6 at each level of concentration). The second set was also extracted and then analyzed with LC-MS. The extraction recovery percentage was calculated according to equation (7).

$$\text{Extraction Recovery } \% = \frac{\text{Peak area}_{(\text{pre-extraction spiked sample})}}{\text{Peak area}_{(\text{post-extraction spiked sample})}} \times 100 \quad \text{(Equation 7)}$$

4.5.2.8. Carry-over effects

The FDA and EMA guidelines were used to calculate the carry-over effects for the analyte (140,141) and EMA guidelines were used to calculate this parameter for the IS (141). To minimize the carry-over effects, a double blank sample was injected after each highly concentrated sample (ULOQ, HQC, or unknown samples with an expected high concentration) (141). Equations 8 was used to assess the carry-over

effect of the analyte and the internal standard. A double blank sample was injected after the ULOQ to determine the peak areas of the analyte and the IS in the double blank sample.

$$\text{Carry-over Effect \%} = \frac{\text{Peak area of the double blank after ULOQ}}{\text{Peak area of the LLOQ}} \times 100 \qquad \text{(Equation 8)}$$

Carry over was deemed insignificant if it was less than or equal to 20% of the LLOQ for the analyte (140,141), and less than or equal to 5% in for the internal standard (141).

4.5.2.9. Dilution integrity

Dilution integrity test was carried out to make sure that the diluted samples have the same precision and accuracy as the undiluted samples. Nanoparticles were spiked with the internal standard (400 ng/ml) and docetaxel to yield a final concentration of 20,000 ng/ml. The sample was extracted (section 4.5.1.4) and 10, 20, and 40-fold diluted with the blank solution. (n=6 at each dilution level)

The test was accepted if the accuracy and precision were between 85% and 115% (141).

4.5.2.10. Stability tests

Stability tests were conducted at conditions encountered during analysis using QC samples to ensure that the steps taken during sample preparation and sample analysis have no effect on the concentration of the analyte. The samples were measured by a standard curve developed from freshly prepared calibration standards.

4.5.2.10.1. Stock solution stability

Although the analyte and the IS stock solutions were prepared freshly for each experiment, we assessed the stock solution stability for our future studies.

A stock solution of the analyte was stored at $-20\,℃$ for one month, and used to prepare two calibration standards (n=6 at each level); 4×LLOQ (62.5 ng/ml) and 50% of ULOQ (2000 ng/ml) which were then analyzed against a freshly prepared standard curve. Plain nanoparticles were not spiked in these samples because the main purpose of this experiment was to determine the stability of the stock solutions. A sample was considered stable if its actual concentration was within $\pm 15\%$ of its nominal concentration (140).

To assess the stability of the internal standard stock solution, six samples were prepared at a concentration of 400 ng/ml form a one-month-old stock solution stored

at −20 ℃. The peak areas of these samples were compared to the peak areas of the samples prepared from a fresh IS stock solution.

4.5.2.10.2. Auto-sampler stability

The auto-sampler stability test was performed to assess the stability of the analyte in the processed sample under the conditions in the auto-sampler. LQC and HQC samples (n=6 at each level) were extracted (section 4.5.1.4) and analyzed then reinjected after being placed for 24 h in the auto-sampler at 4 ℃, and analyzed against a freshly prepared standard curve.

Samples were considered stable if their actual concentrations were within ±15% of their nominal concentration (140).

4.5.2.10.3. Storage stability

A set of six replicates of LQC and HQC samples were prepared and stored at −20 ℃ for one month. Fresh IS solution was added, then samples were extracted (section 4.5.1.4) and analyzed against a freshly prepared standard curve. Samples were considered stable if accuracy was within ±15% of the nominal value (140).

4.6. Statistical analysis

Data were analyzed by descriptive statistics calculating the mean and standard deviation (mean±SD) for continuous variables. Analysis of variance (ANOVA) with multiple comparison (Tukey's and Pairwise Comparison) tests were performed to demonstrate statistical difference at an α-level of 0.05 using SPSS software. The paired student's t-test were used to evaluate the differences when we had two groups with a level of significance set at $P<0.05$.

5. RESULTS

5.1. Preparation and characterization of the nanoparticles

Although the method of nanoparticle preparation was developed in our lab previously (128), we needed to optimize the preparation conditions due to the changes in the equipment such as the ultra-centrifuge and the ultra-sonicator probe. Changes in the production procedure can change the characteristics of the resulting nanoparticles. In addition, nanoparticle formulations show inherent variabilities in their properties which necessitates the repetition of the processes to ensure the regular production of formulations with consistent properties (144).

In order to optimize the preparation process of the PLGA nanoparticles with the new equipment, different technical parameters were investigated to reach an optimum formulation with the lowest particle size and highest yield percentage. Various formulations were developed, and the results were summarized in Table 5.1. The evaluated parameters included centrifugation time, centrifugation force, sonication amplitude, PVA solution volume, and PLGA weight. It should be noted that some of the results in Table 5.1 are lacking as either the production conditions did not lead to a nanoparticle formulation or produced highly aggregated particles.

Table 5. 1. Various tested formulation conditions and their respective results. The cells with no information are representation of the production conditions which did not lead to a nanoparticle formulation or produced highly aggregated particles. Not all the tested parameters have been presented due to intellectual property limitations.

Code	PLGA (%w/v)	Sonication Amplitude (%)	Centrifugation		Size (nm)				Yield (%)
			Time (min)	rcf	Before FD	PdI	After FD	PdI	
F1	10.8	40	30	57840	271.6±6.4	0.238± 0.10	248.5±5.8	0.351±0.047	-
F2	10.8	40	30	57840	167.8±5.5	0.336±0.02	-	-	-
F3	10.8	40	17	34860	126.4±2.2	0.180±0.012	-	-	38
F4	16.7	30	40	34860	184.9±0.1	0.180±0.012	241.5±7.3	0.281± 0.054	38.9
F5	16.7	40	50	48250	-	-	-	-	-
F6	10.8	40	60	48250	-	-	-	-	-
F7	16.7	40	60	48250	-	-	-	-	-
F8	10.8	40	50	48250	187.5±5.5	0.322±0.039	204.7±3.5	0.328±0.091	88.5
F9	10.8	40	50	48250	159.9±1.7	0.351±0.028	254.56±5.9	0.281±0.090	78.7
F10	16.7	40	50	48250	140.5±3.1	0.381±0.023	186.9±3.8	0.351±0.398	62.6
F11	16.7	40	50	48250	180.9±7.3	0.303±0.14	235±4.2	0.303±0.077	70.3
F12	16.7	40	45	48250	171.4±7.3	0.342±0.002	4374±1935	1.000	76.6
F13	16.7	40	40	48250	133.5±1.2	0.241±0.004	-	-	44.1
F14	16.7	35	40	48250	245.0±4.1	0.249±0.02	270.0±6.3	0.306±0.081	59.9
F15	16.7	35	50	48250	156.1±1.9	0.232±0.012	195.3±4.7	0.304±0.047	58.5
F16	16.7	35	40	48250	165.8±6.1	0.321±0.019	250.1±12.3	0.294±0.048	49.8
F17	16.7	30	40	48250	161.8±2.6	0.303±0.01	278.0±6.8	0.321±0.105	71.6
F18	16.7	30	45	48250	157.4±8.6	0.308±0.01	-	-	47.7
F19	16.7	30	45	48250	198.6±1.1	0.245±0.028	234.1±4.5	0.271±0.035	59.9
F20	14.5	30	50	48250	-	-	-	-	-
F21	16.7	30	30	48250	208.6±6.1	0.346±0.04	278.3±12.5	0.245±0.028	41.4
F22	16.7	30	40	39080	236.7±11.5	0.361±0.059	298.6±0.126	0.370±0.971	46.5
F23	16.7	30	40	48250	202.2±4.7	0.237±0.005	251.7±8.2	0.320±0.038	64.5
F24	16.7	30	40	39080	176.3±5.5	0.288±0.044	250.8±7.4	0.314±0.04	46.8
F25	16.7	30	40	39080	159.3±3.7	0.201±0.007	234.1±4.5	0.271±0.035	41.8
F26	16.7	30	40	48250	209.3±5.8	0.361±0.025	287.1±8.2	0.364±0.109	63.7
F27	16.7	30	40	48250	170.2±4.2	0.274±0.032	232.0±5.1	0.289±0.025	63.8

rcf: Relative centrifugal force; FD: Freeze-drying; PdI: Poly-dispersity Index

Z-average is the mean hydrodynamic size of the collection of particles in a suspension measured by dynamic light scattering (145). Poly-dispersity Index (PdI) is a measure of heterogeneity of size and shows the size distribution of the particles in a sample (146). A suspension with a PdI of more than 0.7 is commonly considered to have a broad size distribution of particles (146). The optimum plain formulation in our study had a z-average of 170.2 ± 4.2 nm and a poly-dispersity Index of 0.274 ± 0.032. Table 5.2 summarizes the conditions leading to the production of the optimum formulation.

Table 5. 2. The optimized conditions yielding the final nanoparticle formulation.

PLGA (% w/v in oil phase)		16.7
PVA (% w/v in aqueous phase)		2.2
Oil Phase: Aqueous Phase		1 : 7.6
Ultra-sonication time (min)		2
Centrifugation	time	40 min
	rcf	48250
Freeze-drying		Sucrose 1.7 %w/v

After freeze-drying (FD), the particle size and PdI values changed to 232.0 ± 5.1 nm and 0.289 ± 0.025, respectively. The formulation yield percentage was measured to be 63.8%. Drug-loaded nanoparticles showed a larger mean particle size of

202.2±4.7 nm and a PdI of 0.237±0.005 before FD. The freeze-dried nanoparticles had also a larger particle size (251.7±8.2 nm) and PdI (0.320±0.038) than plain nanoparticles. Therefore, PdI value of the nanoparticle formulations remained around 0.3 and did not change meaningfully after FD, confirming the uniform size distribution of the particles. Figure 5.1 illustrates a representative particle size report for the prepared nanoparticles.

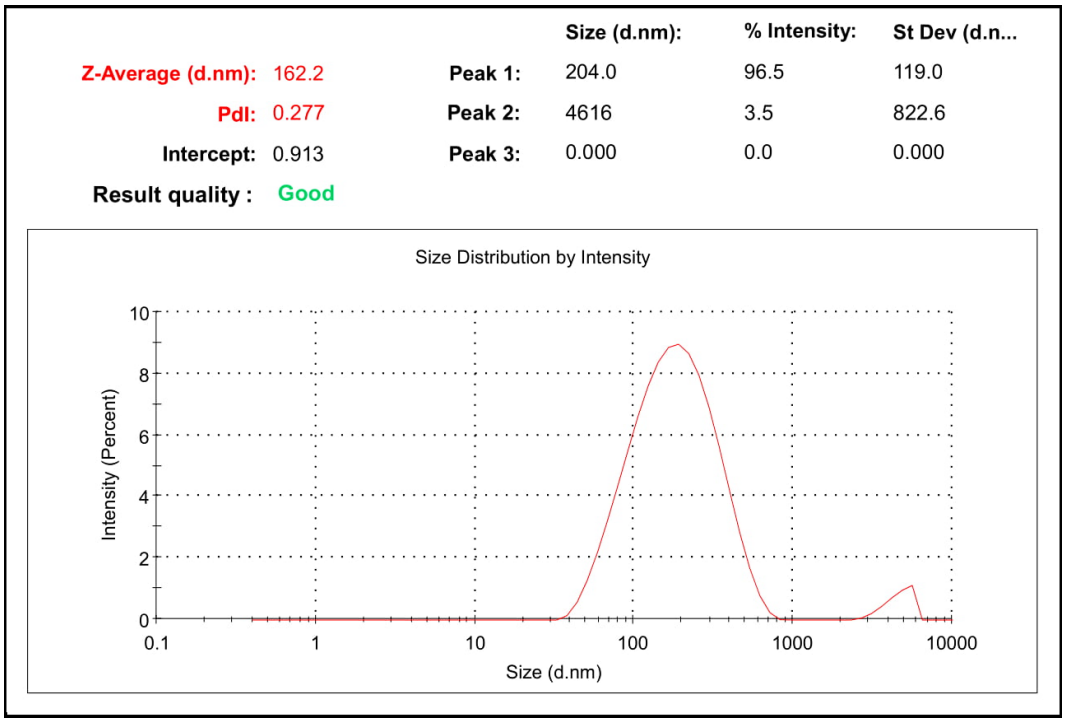

Figure 5. 1. A representative particle size report of a plain nanoparticle formulation.

The plain nanoparticles showed a zeta potential of -23.2 ± 1.4 mV, and the drug loaded nanoparticles had a zeta potential of -22.5 ± 0.8 mV. This surface charge will

allow for long circulation times in the blood (147). Statistical analysis of the zeta potential measurements showed no significant difference between plain and docetaxel-loaded nanoparticles or before and after FD. Figure 5.2 illustrates a representative zeta potential report for the prepared nanoparticles.

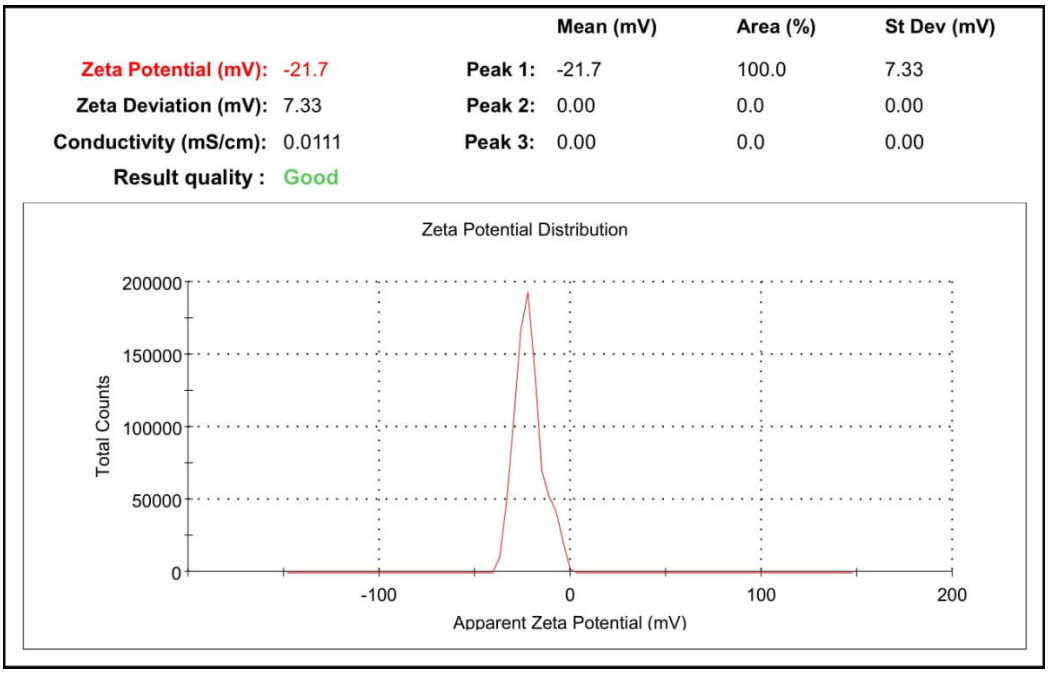

Figure 5. 2. A representative zeta potential report of a drug-loaded nanoparticle formulation.

5.1.1. The effect of sonication amplitude on particle size

Figure 5.3 shows the effect of three ultra-sonication amplitudes on the size for the nanoparticles, before and after FD. Increasing the amplitude from 30% to 40% decreased the size of the particles in both groups. Before FD, particles that were prepared with ultra-sonication amplitude of 30% had a size of 198.6 ± 1.1 nm, while

particles that were prepared with 40% amplitude had a size of 140.5 ± 3.1 nm. A similar trend was observed after FD as particles prepared with ultra-sonication amplitude of 30% showed a size of 234.1 ± 4.5 nm, while a size of 186.9 ± 3.8 nm was observed for those that were prepared with 40% amplitude.

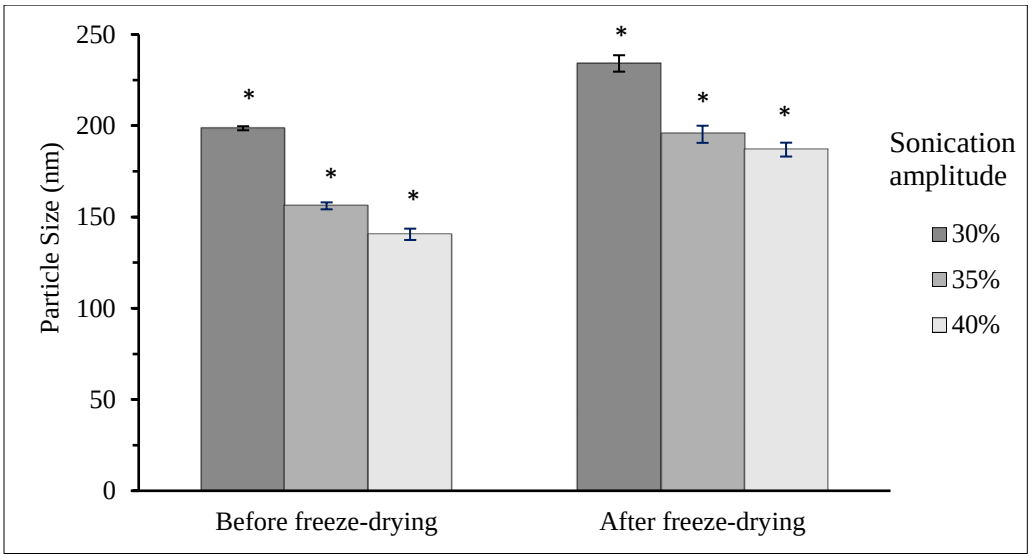

Figure 5. 3. The effect of sonication amplitude on the particle size of the nanoparticles, before and after freeze-drying. Each bar represents the size of the particles ±SD (n=3). The size differences between before and after freeze-drying are statistically significant (ANOVA test) between all groups, indicated by the (*) sign.

The increase in the mean particle sizes after FD was significantly different for all the formulations, regardless of the sonication amplitude. However, the size difference between the 35% and 40% groups was not statistically significant after FD. The formulation that was prepared at an ultra-sonication amplitude of 35% had an average particle size of 195.3 ± 4.7 nm after FD, and the formulation with the ultra-sonication amplitude of 40% had a z-average of 186.9 ± 3.8 nm. On the contrary,

the sonication amplitude of 30% produced particles with a size (234.1 ± 4.5 nm) that was significantly larger than the particle size of both 35% or 40%.

5.1.2. The effect of ultra-sonication amplitude on nanoparticle yield percentage

Yield of a process is a measure of the quantity of the product formed in relation to the quantity of the materials with which the process was initiated (148). A higher yield percentage is an indication of a more efficient process with minimal waste and lower cost. Moreover, yield percentage is needed to calculate the loading efficiency of a nanoparticle formulation.

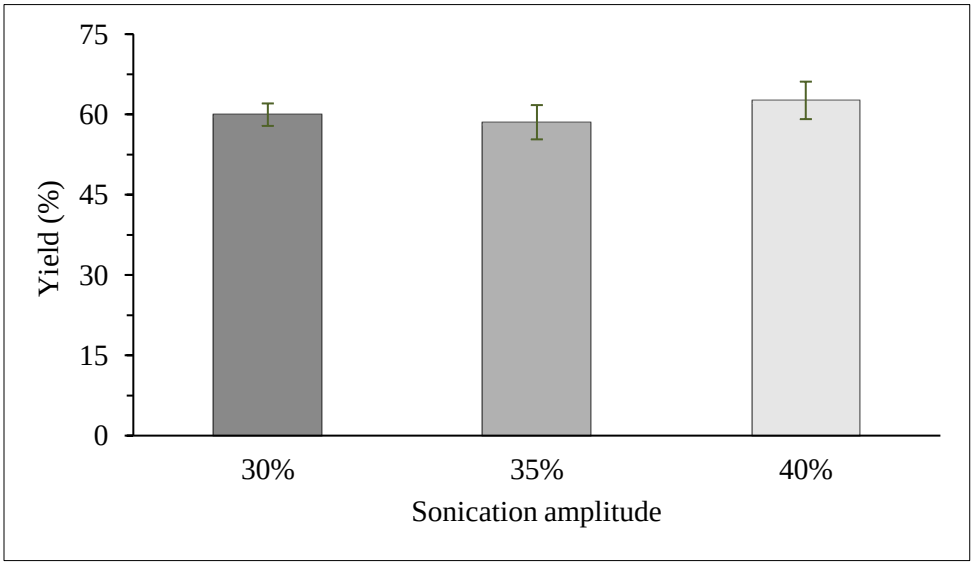

Figure 5. 4. The effect of sonication amplitude on the yield percentage of the nanoparticle formulations. Each bar represents the size of the particles ±SD (n=3). The differences between the three amplitudes are not significant (ANOVA test).

Plotting the yield percentage of the nanoparticle formulations against the ultra-sonication condition used during their preparation showed that the yield percentage hovered around 60% for all the sonication amplitudes (Figure 5.4). Statistical analysis of the data indicated that the differences between the yield percentages are not significant between different preparation conditions. An average yield percentage of 59.96% ± 2.1 was observed when the sonication amplitude of 30% was used in the preparation process, while the yield% was 58.55 % ± 3.2 and 62.63 % ± 3.5 when the ultra-sonication was performed at the amplitudes of 35% and 40%, respectively (Figure 5.4).

5.1.3. The effect of centrifugation speed on nanoparticle particle size

During preparation of the formulations, the nanoparticles were washed with distilled water to dissolve and eliminate any extra PVA or unencapsulated drug from the produced nanoparticles. Subsequently, ultra-centrifugation was used to separate the nanoparticles from water containing PVA and free drug. Figure 5.5 shows how increasing the centrifugal force affects the average sizes of the nanoparticles. An increase in the relative centrifugal force (rcf) from 34860×g to 48250×g resulted in a statistically significant decrease in the size of the particles from 184.9 ± 0.1 nm to

161.8 ± 2.6 nm. However, the difference between the sizes of the two formulations with a rcf of 34860×g and 39080×g was not statistically significant.

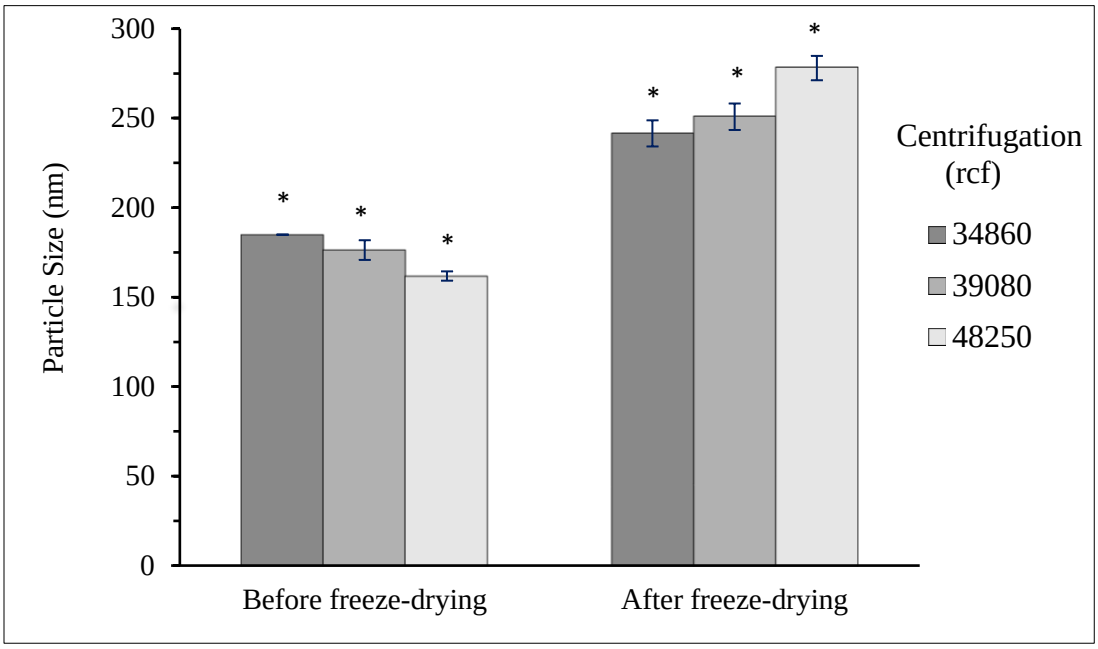

Figure 5. 5. The effect of centrifugation rcf (×g) on the particle size of the nanoparticles, before and after freeze-drying. Each bar represents the size of the particles ±SD (n=3). The size differences between before and after freeze-drying are statistically significant (ANOVA test) between all groups, indicated by the (*) sign.

After FD, the average size of the particles increased for all the formulations compared to their size before FD (Figure 5.5), while the difference between the size of the formulations with a rcf of 34860×g and 39080×g remained statistically insignificant after FD. The formulation which had the highest z-average before FD (rcf of 34860×g and size of 184.9 ± 0.1 nm) became the smallest sized nanoparticle formulation after FD with a mean particle size of 241.5 ± 7.3 nm. Similarly, the

formulation with a rcf of 48250×g which had the smallest size between the three groups before FD (Figure 5.5) showed the largest size after being freeze-dried (278.0 ± 6.8 nm).

5.1.4. The effect of centrifugation speed on nanoparticle yield

Figure 5.6 shows the effect of centrifugation force on the yield percentage of the prepared formulations. The yield increased with the increase of the centrifugation speed. The highest yield (71.6% ± 5.5) was obtained with a rcf of 48250×g and the lowest yield was observed when a rcf of 34860×g was used in the preparation procedure (38.9% ± 1.1).

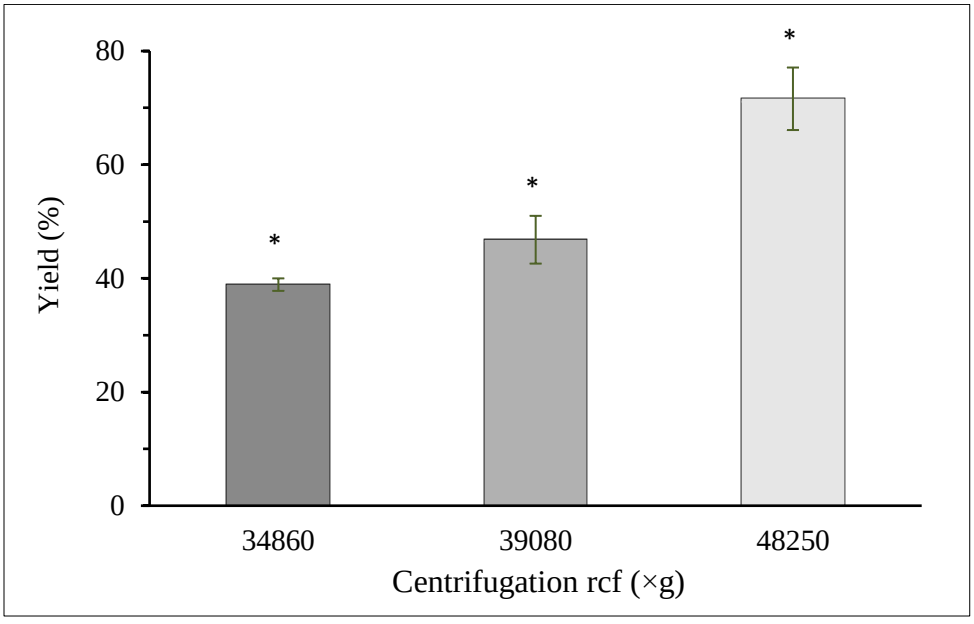

Figure 5. 6. The effect of centrifugation rcf (×g) on the yield percentage of the nanoparticle formulations. Each bar represents the size of the particles ±SD (n=3). The differences between all groups are statistically significant (ANOVA test) indicated by the (*) sign.

5.2. MS/MS fragmentation analysis

5.2.1. Full scan analysis

Full scan ESI-MS in the positive ion mode of the tested taxanes showed an abundant singly charged ion $[M+H]^+$ and low abundant sodium $[M+Na]^+$ and potassium $[M+K]^+$ adducts for all compounds. Exact mass measurements of the taxanes showed mass accuracies of less than 3 ppm mass errors (Table 5.3). The ESI-Q-ToF analysis confirmed the molecular structures of the compounds.

Table 5. 3. Full scan MS analysis of the studied taxanes using QqTOF instrument.

Compound	Monoisotopic mass	*m/z* (theoretical) $[M+H]^+$	*m/z* measured	ppm
Paclitaxel	853.3309	854.3382	854.3377	0.62
Docetaxel	807.3466	808.3539	808.3538	0.10
Cabazitaxel	835.3779	836.3852	836.3861	1.10
Cephalomannine	831.3466	832.3539	832.3529	1.18
Baccatin III	586.2414	587.2487	587.2472	2.53

5.2.2. Tandem mass spectrometric analysis

The $[M+H]^+$ species were selected as the precursor ion for MS/MS (Figure 5.7, Appendix Figures S2-S5) and MS^3 analysis (Table 5.4, Appendix Tables S1-S4). It should be noted that MS/MS analysis using the QqQ-LIT and the QqTOF produced the same product ions. All tested taxanes have the same backbone structure of a

diterpene ring (Table 2.1) that showed similar fragmentation behavior with bond cleavage occurring at the substituent groups during MS/MS analysis. The variation within the side chain (R_3) of the structures resulted in the production of compound-specific product ions upon CID-MS/MS analysis in positive ionization. Formation of these unique product ions happens with a similar fragmentation pattern for all the taxanes with side chains (i.e., paclitaxel, docetaxel, cabazitaxel, and cephalomannine) and involves the eventual loss of the diterpene ring core structure as illustrated by the loss designated as B5 → S5 in Figure 5.8.

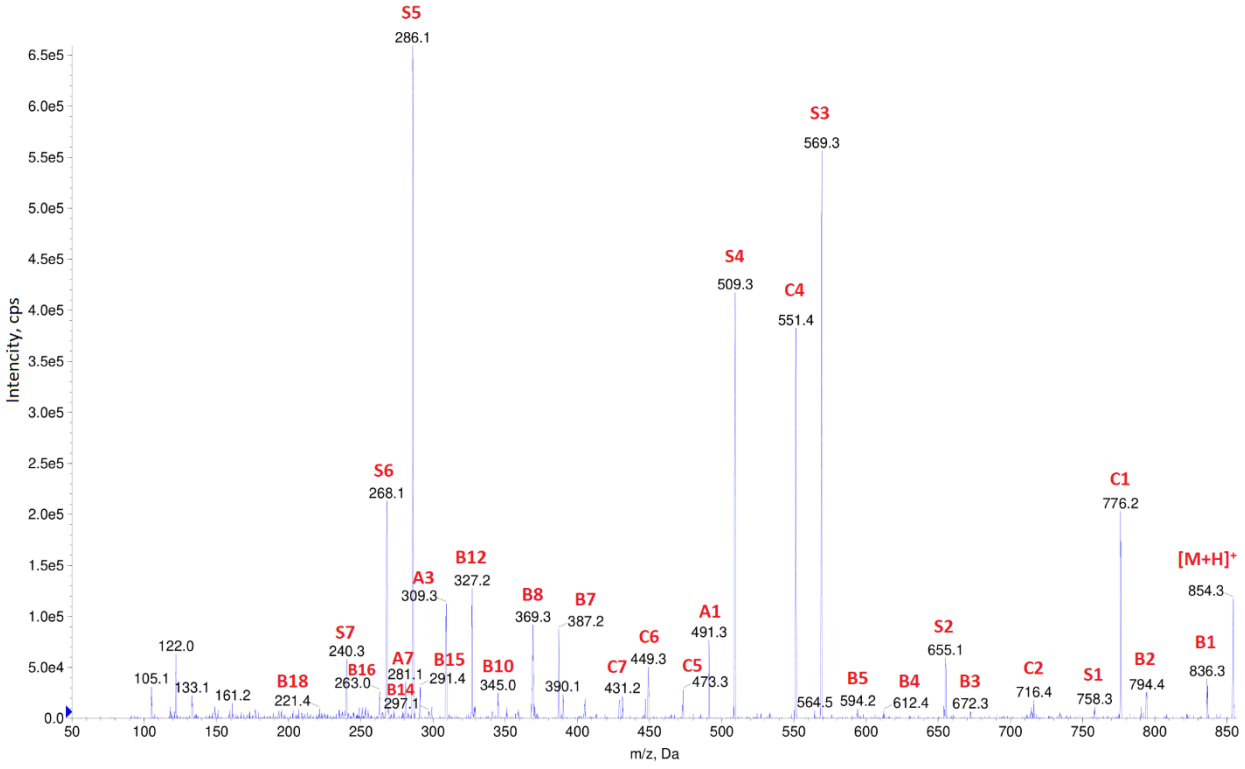

Figure 5. 7. The ESI-QqLIT-MS/MS spectrum of paclitaxel as a representative example of taxane-related compounds.

As mentioned above, differences in the fragmentation patterns occurred due to the presence of different side chains in the tested compounds. Such differences could be used as diagnostic product ions for the qualitative and quantitative analysis of taxanes. However, most of the product ions were formed by neutral losses of the substituents on the B-ring. The detailed general fragmentation behavior of taxanes is discussed in the following section using paclitaxel as a representative structure to highlight the common MS/MS pathways among various taxane-related analogues. To aid in the illustration of the fragmentation routes, the location of the cleavage dictates the letter designation for the observed product ions while the number indicates the sequence in which the ions are formed. The letters A, B, C and S were used in naming the product ions, where A refers to a cleavage on ring A, B refers to dissociation in the B-ring, C indicates a loss from ring C, and S shows a cleavage on the sidechain (Table 2.1 and Figure 5.8).

Table 5. 4. MS3 analysis for paclitaxel.

Precursor ion	First generation product ions (MS/MS)	Second generation product ions (MS^3)
854.3 $[M+H]^+$	836.3 [B1]	794.4 [B2], 776.2 [C1], 594.2 [B5],569.3 [S3], 551.4 [C4], 509.3 [S4], 491.3 [A1], 369.3 [B8], 309.3 [A3], 286.1 [S5]
	794.4 [B2]	776.2 [C1], 734.3 [C3], 716.4 [C2], 672.3 [B3], 612.4 [B4], 509.3 [S4], 491.3 [A1], 449.3 [C6], 327.2 [B12], 286.1 [S5]
	776.2 [C1]	758.3 [S1], 716.4 [C2], 655.1 [S2], 309.3 [A3], 286.1 [S5]
	716.4 [C2]	594.2 [B5], 309.3 [A3], 286.1 [S5], 268.1 [S6], 239.9 [S7]
	655.1 [S2]	509.3 [S4], 449.3 [C6], 327.2 [B12], 309.3 [A3]
	612.4 [B4]	594.2 [B5], 309.3 [A3], 286.1 [S5], 268.1 [S6], 239.9 [S7]
	594.2 [B5]	309.3 [A3], 286.1 [S5]
	569.3 [S3]	551.4 [C4], 509.3 [S4], 387.2 [B7], 327.2 [B12], 309.3 [A3]
	551.4 [C4]	509.3 [S4], 491.3 [A1], 473.3 [C5], 369.3 [B8], 309.3 [A3]
	509.3 [S4]	491.3 [A1], 449.3 [C6], 431.2 [C7], 387.2 [B7], 327.2 [B12], 309.3 [A3]
	491.3 [A1]	473.3 [C5],449.3 [C6], 431.2 [C7], 369.3 [B8], 327.2 [B12], 309.3 [A3]
	473.3 [C5]	431.2 [C7], 309.3 [A3]
	449.3 [C6]	431.2 [C7], 387.2 [B7], 327.2 [B12], 309.3 [A3]
	431.2 [C7]	429.1 [C8], 369.3 [B8], 309.3 [A3]
	429.1 [C8]	401.1 [B6], 387.2 [B7]
	387.2 [B7]	369.3 [B8], 359.0 [B9], 345.0 [B10], 327.2 [B12]
	369.3 [B8]	341.0 [B11], 327.2 [B12], 297.1 [B14]
	345.0 [B10]	327.2 [B12], 299.0 [A4]
	327.2 [B12]	313.0 [A2], 311.0 [B13], 297.1 [B14]
	313.0 [A2]	311.0 [B13], 299.0 [A4], 297.1 [B14]
	309.3 [A3]	295.3 [A5], 291.4 [B15], 281.1 [A6], 263.0 [B16], 235.0 [B17], 221.4 [B18]
	295.3 [A5]	281.1 [A6], 263.0 [B16], 221.4 [B18]
	286.1 [S5]	268.1 [S6], 239.9 [S7]
	281.1 [A6]	263.0 [B16], 235.0 [B17], 221.4 [B18]
	268.1 [S6]	239.9 [S7]
	263.0 [B16]	235.0 [B17], 221.4 [B18]

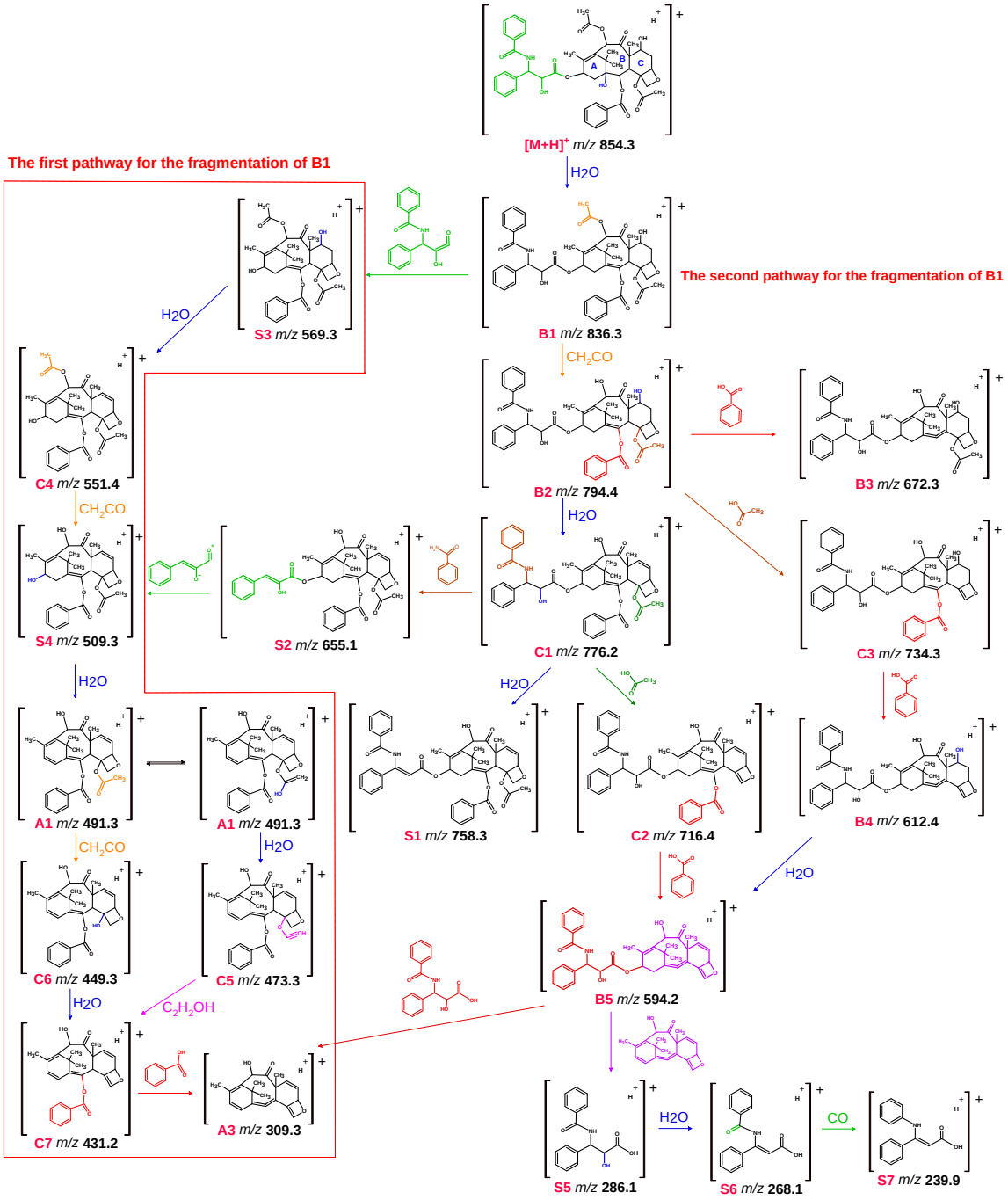

Figure 5. 8. The proposed MS/MS fragmentation of paclitaxel. After the generation of ion B1 at m/z 836.3, the first pathway for the fragmentation of ion B1 begins with the loss of the sidechain (B1→S3). The dotted red line includes the first pathway for the fragmentation of ion B1 begins with the loss of the sidechain (B1→S3). The dotted red line includes the first pathway for the fragmentation of ion B1. Letter A refer to a cleavage on ring A, B refers to dissociation in the B-ring, C indicates a loss from ring C, and S shows a cleavage on the sidechain.

5.2.2.1. Fragmentation of paclitaxel

The MS/MS analysis of paclitaxel resulted in the formation of numerous product ions (Figure 5.7) and it was the most complex spectra among all tested compounds. The observed product ions were mainly generated via the fragmentation of the substituent groups on the diterpene ring (Figure 5.8). MS^3 analysis was used to confirm the genesis of the observed product ions (Table 5.4).

The MS/MS dissociation is initiated by a loss of H_2O molecule to produce the ion designated as B1 (B indicates a cleavage from the B-ring) observed at *m/z* 836.3. This loss of water molecule is possible in two locations and will not affect the overall fragmentation behavior. It is shown on ring B in Figure 5.8 for illustrative purposes. B1 then dissociates in two unique pathways to produce the highly abundant S3 (S indicates a cleavage from the sidechain) at *m/z* 569.3 (B1 → S3, i.e., first pathway) or the minor product ion observed at *m/z* 794.4 (B1 → B2, i.e., second pathway). In fact, the second dissociation pathway is initiated with the loss of one of the CH_2CO groups yielding the formation of the B2 ion. It should be noted that the loss of CH_2CO can also occur at the C ring. For simplicity, it was illustrated as a loss on the B ring. In any case, a second similar elimination occurs resulting in the eventual removal of the two CH_3COO groups, as seen in ions C2 and C3.

The first dissociation pathway involves the cleavage of the ester bond on the sidechain for B1 ion that results in the loss of the side chain and the production of the ion designated as S3. Both B2 and S3 ions undergo further fragmentation as explained below. The fragmentation pattern of the diterpene ring is different when the side chain is not eliminated (i.e., the second pathway) compared to the first pathway, where the side chain has been lost. However, the subsequent fragmentation of B2 and S3 results in the formation of some shared product ions between the two pathways.

In the first pathway, product ion S3 dissociates via the loss of H_2O molecule followed by a loss of CH_2CO to form the highly abundant ions C4 observed at *m/z* 551.4 (C indicates a cleavage from the C-ring) and S4 at *m/z* 509.3, respectively. The MS/MS spectrum shows two minor peaks at *m/z* 491.3 and *m/z* 473.3, near the ion observed at *m/z* 509.3. Each of these ions have a difference in *m/z* value of 18, indicating sequential losses of H_2O molecules. The first neutral loss of water yields A1 at *m/z* 491.3 (A indicates a cleavage from the A-ring) but the loss of the second H_2O, can only be related to the keto–enol tautomerism on the carbonyl group of the C-ring to generate the ion observed at *m/z* 473.3, C5. The subsequent loss of hydroxyacetylene (C_2H_2O) from C5 results in the formation of C7 at *m/z* 431.2. The keto form of A1 can also dissociate via loss of CH_2CO from the C-ring yielding ion C6 at *m/z* 449.3, followed by a loss of water to form C7. MS^3 data (Table 5.4)

confirms the proposed fragmentation behavior as the MS^3 spectrum of C5 does not show, despite possible theoretical formation, a second-generation product ion at *m/z* 449.3 (C6). However, both C5 and C6 ions at *m/z* 473.3 and *m/z* 449.3 are present in the MS^3 spectrum of A1 (*m/z* 491.3). In addition, the ion C7 at *m/z* 431.2 is present in the MS^3 spectra of both C5 and C6 (Table 5.4), confirming the genesis of the observed product ions.

The ion C7 then undergoes two main fragmentation processes (Appendix, Figure S1). The first one involves the elimination of the benzoic acid moiety from the B-ring forming ion A3 (*m/z* 309.3). Ion A3 is further dissociated by the neutral losses of CH_2, H_2O, and CO species to form ions A5, A6, and B15-B18 (Appendix, Figure S1). The second fragmentation process involves formation of ions C8, A2, A4, and B6-B14 by sequential dissociation of substituents CO, CH_2, H_2O, and H_2, mainly from the B-ring. In order to rationalize the loss of water from ion B7 at *m/z* 387.2, a resonance form of the structure of ion B7 allows for the elimination of the water molecule as shown in Appendix, Figure 5.3.

The second major pathway during CID-MS/MS fragmentation of paclitaxel involves dissociation of the substitute groups without the initial elimination of the sidechain. Ion B2 at *m/z* 794.4 can undergo three different elimination mechanisms, yielding product ions observed at *m/z* 672.3, *m/z* 734.4, and *m/z* 776.2, designated as ions B3, C3, and C1. Ion B3 results from the elimination of benzoic acid and do not produce

any additional product ions. On the other hand, both ions C1 and C3 resulting from the elimination of water molecule and acetyl acid, respectively, are further dissociated producing additional product ions. Ion C3 loses benzoic acid moiety to form the ion B4 observed at *m/z* 612.4, while ion C1 can go through three different fragmentation pathways by either neutral loss of acetic acid forming ion C2 at *m/z* 716.4, loss of water molecule yielding the ion designated S1 at *m/z* 758.3, or the elimination of benzamide producing the ion S2 at *m/z* 655.1. MS^3 data show that many of the product ions in the first major pathway of paclitaxel fragmentation are also present in the MS^3 spectra of some of the product ions in the second pathway (ions B2, C1, and S2, Table 5.4). This phenomenon is justifiable by the fact that the ion S4 (*m/z* 509.3) already formed after the elimination of the side chain can also be formed from ion S2 via the loss of the side chain.

A major final ion that will result in the formation of the remaining product ions in the proposed fragmentation pathway is the ion designated as B5 observed at *m/z* 594.2. It is generated by either a loss of water or benzoic acid from B4 and C2, respectively. Subsequent elimination of the R_3 sidechain from B5 yields ion A3 (*m/z* 309.3) that was described already in the first fragmentation pathway. A unique elimination for B5 involves the loss of the diterpene ring, which is the core of the structure. Such elimination forms the base peak, the highly abundant ion S5, observed at *m/z* 286.1. In fact, the loss of the core structure is unique in the proposed

fragmentation pathway, which leaves the highly conjugated ion of the side chain. It can be speculated that the high level of conjugation and stability of this ion makes it the base peak in the observed spectra (Figure 5.7). Further dissociation of S5 is self-explanatory with the loss of water and carbonyl substituents to form S6 (*m/z* 268.1) and S7 (*m/z* 240.3), respectively.

5.2.2.2. Comparison of the MS/MS fragmentation pattern of the tested taxanes

One prominent feature in the CID-MS/MS dissociation of the studied taxanes is the similar fragmentation of their core structure which mainly includes losing the substituent groups on the diterpene ring (Table 5.5). However, the presence of varying functional groups in these compounds results in the formation of unique product ions that are specific to each structure (Appendix Tables S1-S4).

A notable ion is the ion designated as S4 observed in the fragmentation of paclitaxel (*m/z* 509.3), cephalomannine (*m/z* 509.2), and baccatin III (*m/z* 527.0). S4, however, was not present in the case of docetaxel or cabazitaxel (Table 5.5). Examining the structures of docetaxel and cabazitaxel shows that both compounds lack a CH_3CO substitute on their B-ring, unlike the remaining compounds (Table 2.1). It can be proposed that the loss of a CH_3CO group from the C-ring is less favorable in all these compounds due to possible steric hindrance from the benzoic acid substitute on the

B-ring. Therefore, it is logical to assume that the loss of CH_3CO occurs predominantly on the B-ring where this functional group is more exposed. As such, ion S4 was not observed in the compounds that lack CH_3CO on the B ring, namely docetaxel and cabazitaxel (Table 2.1).

Another key elimination that dictates the overall dissociation behavior is the loss of water as shown in the case of paclitaxel, such as B7→B8 and B10→B12 (Appendix Figure S1). Ions B8 and B12 are also present in the MS/MS dissociation of cabazitaxel (Appendix, Table S1). These two product ions are formed by a neutral loss of H_2O from the B-ring in paclitaxel (Appendix, Figure S1). However, in the case of cabazitaxel, the loss of water cannot occur because both R_1 and R_2 substituents are methoxy groups (Table 2.1) and instead, we observe a loss of 32, indicating a loss of methanol. In addition, dissociation of the sidechain resulting in the formation of S5 product ion is seen with paclitaxel (*m/z* 286.1), docetaxel (*m/z* 282.2), cabazitaxel (*m/z* 281.9), and cephalomannine (*m/z* 264.1). The S5 species is observed at unique *m/z* values for each compound since the structure of R_3 is different except in the cases of docetaxel and cabazitaxel (Table 2.1). Therefore, as expected, S5 product ion was observed at the same *m/z* values in the spectrum of docetaxel and cabazitaxel.

A unique structural feature for baccatin III among all structures is the lack of a sidechain, meaning that some ions that are the result of dissociations in the core

structure before the loss of the side chain (e.g., B1, B2, and B3) are not present in the MS/MS analysis of baccatin III (Table 5.5). Likewise, product ions that are the direct result of the sidechain dissociation (e.g., S6 and S7) cannot exist in the MS/MS profile of baccatin III (Table 5.5 and Appendix Table S4).

During the analysis, the ion at *m/z* 309.3 could theoretically be attributed to two different structures: $C_{20}H_{21}O_3$ and $C_{22}H_{13}O_2$ (Appendix Figure S7). MS^3 of the ion observed at *m/z* 309.3 produces six ions of B15, A5, A6, B16, B17, and B18 (Table 5.4) and their proposed structures are shown in Appendix Figure S1. The ion with the molecular formula of $C_{22}H_{13}O_2$ cannot produce these six ions; therefore, the ($C_{20}H_{21}O_3$) ion is the only logical structure for 309.3 as it can further fragment into the six other ions (Appendix Figure S7).

Table 5. 5. Product ions observed during MS/MS analysis of tested taxanes. Checkmark √ indicates the observation of the ion during MS/MS analysis while x indicates that the ion was not observed.

	Paclitaxel	Baccatin III	Docetaxel	Cephalomannine	Cabazitaxel
S3	√	x	√	√	√
C4	√	√	√	√	√
S4	√	√	x	√	X
A1	√	√	√	√	√
C5	√	√	x	√	x
C6	√	√	√	√	√
C7	√	√	√	√	√
A3	√	√	√	√	x
B15	√	√	x	√	x
A5	√	√	√	√	x
A6	√	√	√	√	x
B16	√	x	√	x	x
B17	√	√	√	x	√
B18	√	√	x	√	x
C8	√	√	√	√	√
B6	√	√	√	√	√
B7	√	√	√	√	x
B8	√	√	√	√	√
B9	√	√	√	x	x
B11	√	√	√	√	√
B10	√	√	√	x	x
B12	√	√	√	√	√
B13	√	√	√	√	x
A2	√	√	√	√	√
A4	√	x	√	x	x
B14	√	x	x	x	x
B1	√	x	√	√	√
B2	√	x	x	√	x
B3	√	x	√	x	x
C3	√	√	√	x	x
B4	√	x	x	x	x
C1	√	x	√	√	√
S2	√	x	x	√	x
C2	√	x	x	√	x
S1	√	x	√	√	√
B5	√	x	√	x	x
S5	√	x	√	√	√
S6	√	x	x	√	x
S7	√	x	√	√	x

5.3. LC-MS/MS method development

A LC-MS/MS method was developed for the quantification of docetaxel in the nanoparticle matrix using the MRM mode to attain the needed specificity and selectivity. Paclitaxel, a structural analogue of docetaxel, was used as the internal standard (IS) at a final concentration of 400 ng/ml. IS was added to all standard curve, quality control (QC), and experimental samples prior to sample analysis.

Based on the MS/MS spectra (Figure 5.7 and Appendix Figure S2) and the fragmentation patterns of docetaxel and paclitaxel, two diagnostic and relatively abundant product ions were selected and monitored to ensure the identity of the target compounds. Figure 5.9 shows the structures of the selected product ions and the monitored MRMs.

Different ratios of methanol and water were evaluated to examine the possibility of having an isocratic mobile phase during method development. The efforts were not successful because the analyte eluted from the column very early (< 1 min) when using an isocratic solvent system. Due to the fact that a reverse-phase stationary phase was used, water-soluble impurities eluted from the column at the beginning of the chromatographic run, which resulted in a significant baseline noise that interferes with the analysis. Therefore, a gradient solvent system was adopted to ensure adequate separation from interferences (Figure 4.2). As seen in Figure 5.9, the IS

eluted from the phenyl column shortly after the analyte meaning that the two compounds were subjected to very similar chromatographic conditions. In addition, the peaks of the analyte and IS were observed at the mid-range of the run, which enabled to direct the chromatographic flow to waste from time 0 to 4 min protecting the MS instrument from unwanted analytes, yielding a low LOD.

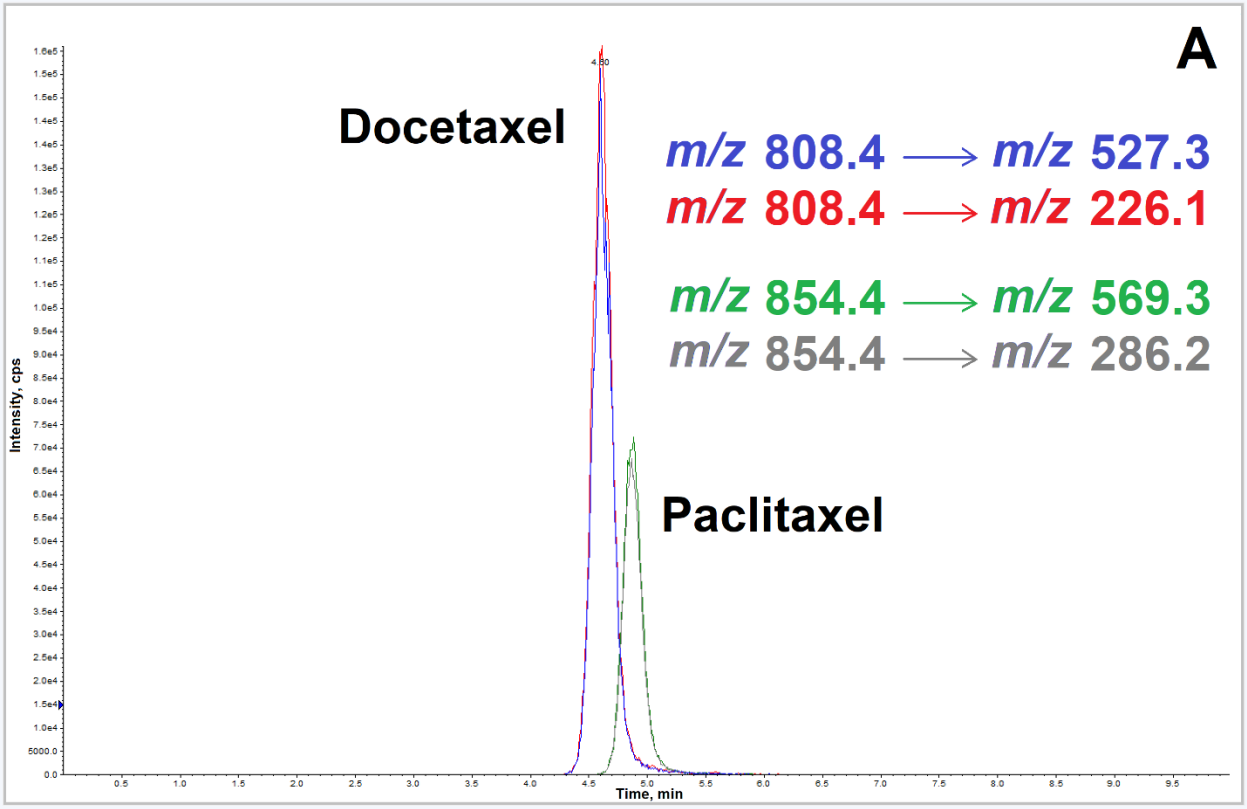

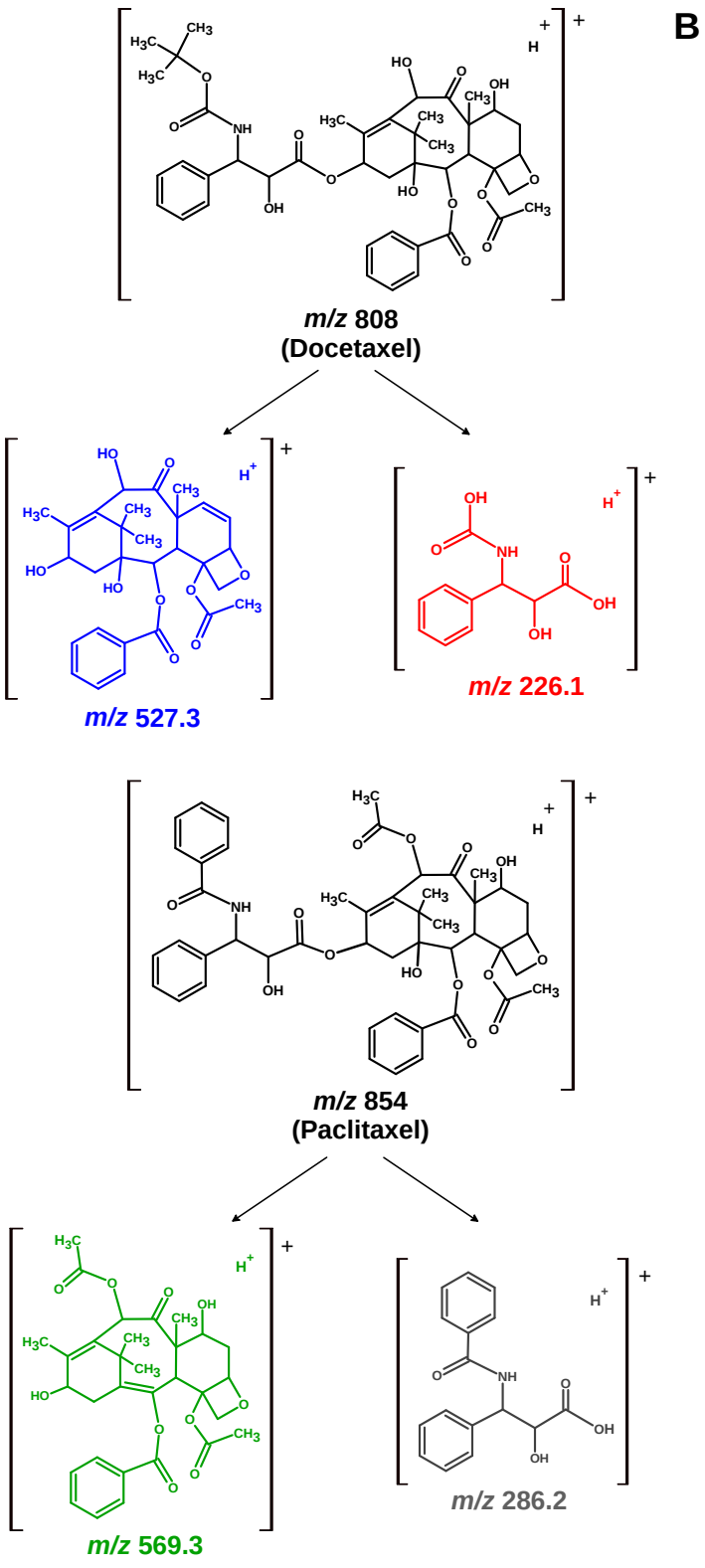

Figure 5. 9. (A) Representative LC-MS/MS chromatogram of a calibration standard sample (1000 ng/ml). Monitored transitions are shown in the figure. (B) The structures of the monitored ions.

5.4. Method validation

5.4.1. Accuracy and precision

Intraday precision and accuracy were determined by analyzing four sets of QCs (LLOQ, LQC, MQC, and HQC) in three separate days, with six replicates at each QC level. Accuracy was calculated as the percent of the theoretical value. The calculated accuracies ranged from 101.2 to 117.1% for LLOQ and 90.4 to 112.0 for other QCs (Table 5.6). The precision, reported as CV%, did not exceed 15% for the four QCs as reported in Table 5.6.

Table 5. 6. Intra-day accuracy and precision values of docetaxel determination by HPLC-MS/MS in PLGA nanoparticles.

QC	Replicates	Analysis day (#)	Observed Concentration (mean ± SD; ng/ml)	Precision (CV%)	Accuracy (%)
LLOQ (15.625 ng/ml)	6	1	16.37 ± 2.16	13.2	104.8
	6	2	15.81 ± 1.86	11.8	101.2
	6	3	18.30 ± 178	9.7	117.1
LQC (40 ng/ml)	6	1	43.50 ± 3.54	8.1	108.8
	6	2	43.97 ± 5.42	12.3	109.9
	6	3	38.63 ± 5.52	14.3	96.5
MQC (1500 ng/ml)	6	1	1648.45 ± 87.50	5.3	109.9
	6	2	1402.99 ± 163.12	11.6	93.5
	6	3	1650.37 ± 48.06	2.9	110.0
HQC (3000 ng/ml)	6	1	3360.56 ± 268.54	8.0	112.0
	6	2	2712.13 ± 403.29	14.9	90.4
	6	3	3210.41 ± 214.91	6.7	107.1

The inter-day accuracy and precision, using 18 replicates of each QC level, yielded accuracy ranging from 103.1 to 107.7% and a precision between 7.0 and 10.9%.

Table 5. 7. Inter-day accuracy and precision values of docetaxel determination by HPLC-MS/MS in PLGA nanoparticles.

QC	Concentration (ng/ml)	Replicates	Observed Concentration (mean ± SD; ng/ml)	Precision (CV%)	Accuracy (%)
LLOQ	15.625	18	16.83 ± 1.31	7.8	107.7
LQC	40	18	42.03 ± 2.95	7.0	105.1
MQC	1500	18	1567.27 ± 142.27	9.1	104.5
HQC	3000	18	3094.37 ± 339.43	10.9	103.1

5.4.2. Linearity

A standard curve with eight calibration standards was constructed by plotting the peak area ratio of the analyte to IS versus the analyte concentration and a linear regression analysis was performed to fit a linear model to the data with a weighting factor of $1/x$. A series of concentrations from 1 to 16000 ng/ml were analyzed to identify the linear range. Linearity was attained from 15.6 ng/ml to 4000 ng/ml (quantification range) and the average correlation coefficient was found to be 0.9984 (n=3). Figure 5.10 shows a representative standard curve and its respective

regression equation. The limit of quantification (LOQ) was 15.6 ng/ml, and the limit of detection (LOD) was 4 ng/ml.

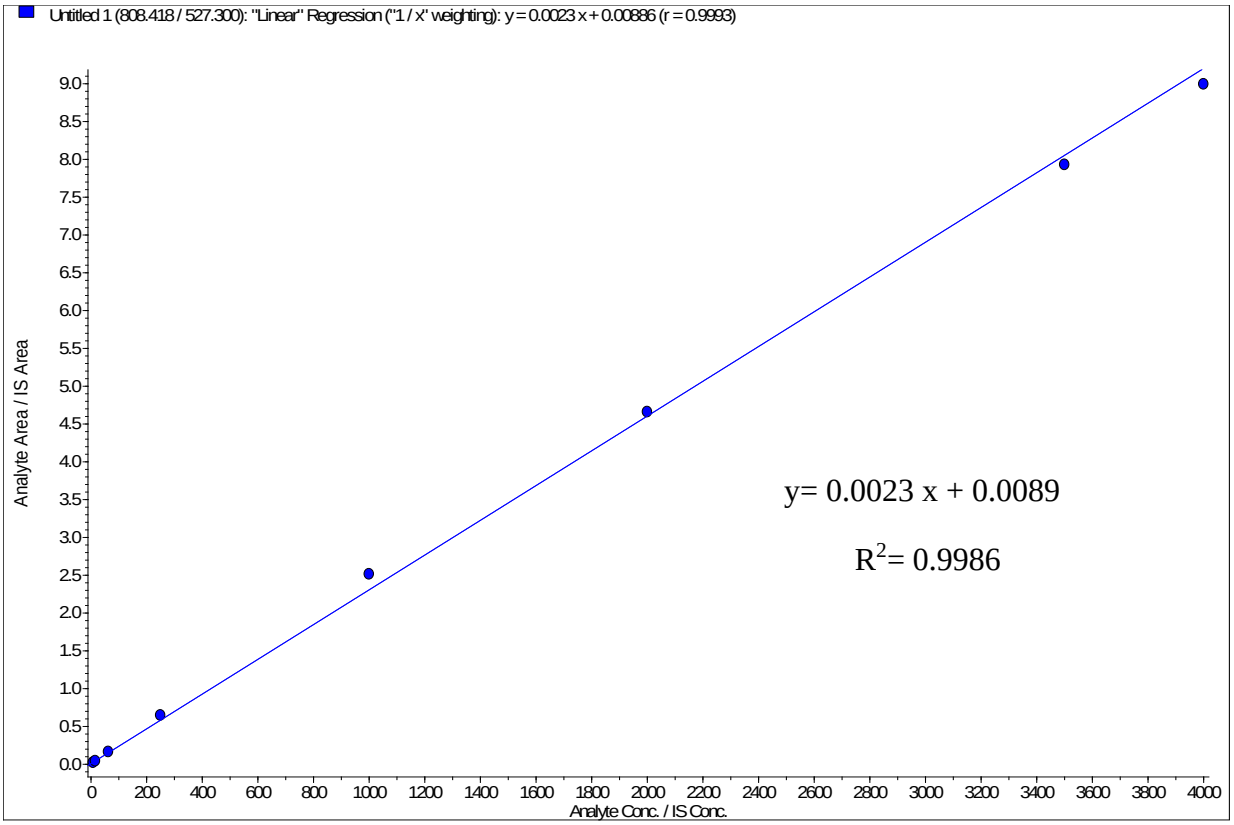

Figure 5. 10. Representative standard curve of docetaxel in the PLGA nanoparticle matrix.

5.4.3. Selectivity

The assessment of selectivity of the method for docetaxel and paclitaxel as per regulatory requirements (140) showed that the interference observed at the analyte

channel was 4.16 ± 2.33 % of the LLOQ (for the analyte) and the interference at the IS channel was 0.07 ± 0.02 %.

The analysis of double blank revealed no interferences in the analyte channel (Figure 5.11A) or the IS channel (Figure 5.11B) at the retention time of the analyte or IS. Monitoring the transitions of the analyte and the IS in a blank sample (a matrix containing IS) and an analyte solution (without the IS) showed no interference between the analyte and the IS (Figures 5.12 and 5.13).

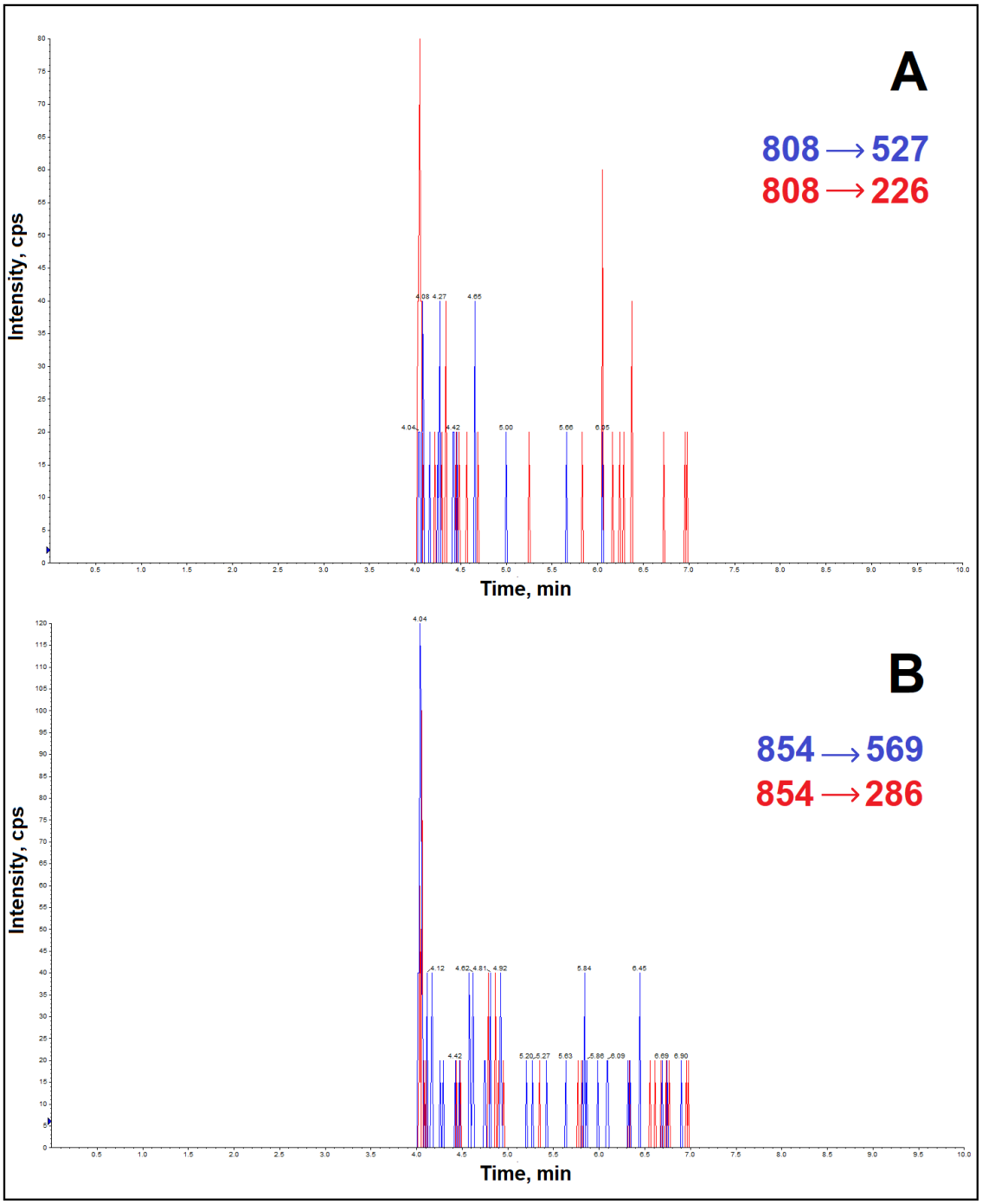

Figure 5. 11. LC-MS/MS chromatogram of a double blank sample while monitoring the transitions of analyte (A) and internal standard (B). No interference from the co-eluting compounds was observed at the channels of analyte or IS.

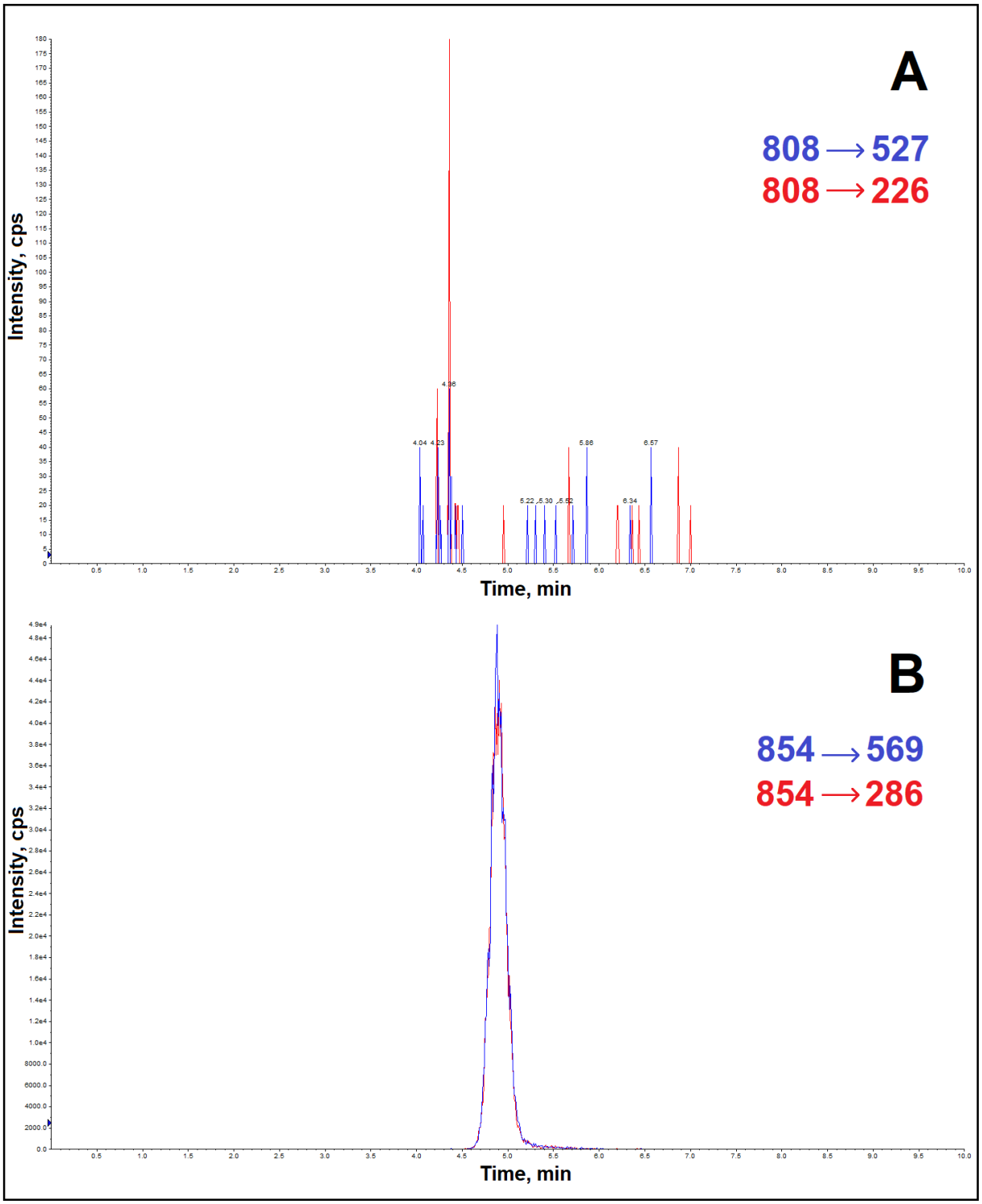

Figure 5. 12. LC-MS/MS chromatogram of a blank sample (a matrix containing IS) while monitoring the transitions of analyte (A) and internal standard (B). No interference was observed from IS at the channels of analyte.

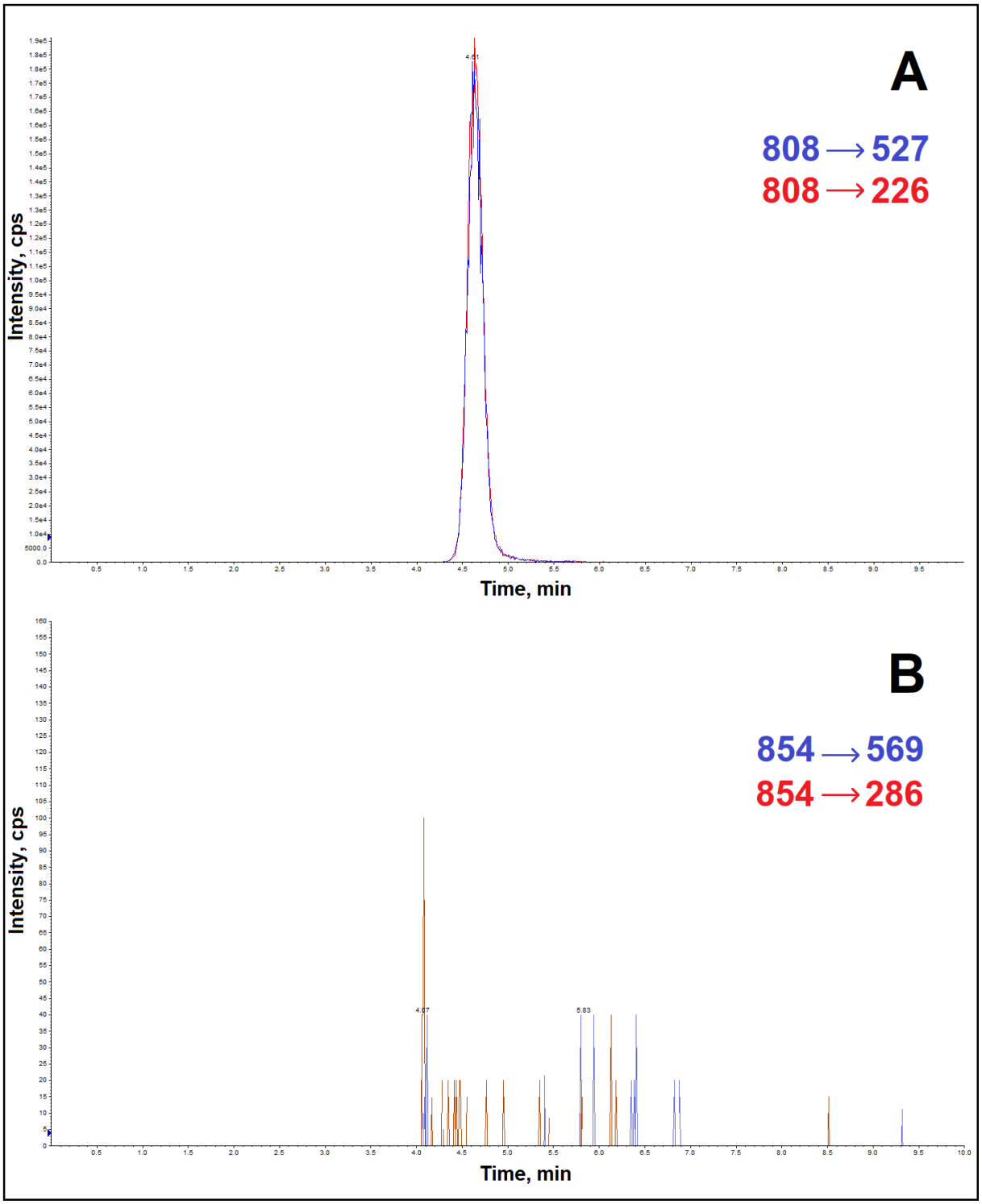

Figure 5. 13. LC-MS/MS chromatogram of a docetaxel solution (1000 ng/ml) without IS, while monitoring the transitions of the analyte (A) and internal standard (B). No interference was observed from the analyte at the channels of the IS.

5.4.4. Matrix effects

The matrix factor (MF) was evaluated by calculating the ratio of the response of a post-extracted spiked sample (analyte added to extracted matrix) and a non-extracted neat sample (analyte added to methanol) (Equation 4). The experiment was performed in replicates of 6 and the MF was found to be around 0.6 at three QC concentrations (Table 5.8). The results show that the analyte suffers from some level of ion suppression which could be attributed to the competition for charge between the analyte and the co-eluting species during ionization. However, the observed matrix effect did not undermine the quantification of the analyte for the intended application.

Table 5. 8. Evaluation of the matrix effects (MF) and IS-normalized matrix effects for the quantification of docetaxel in the nanoparticle matrix using the developed HPLC-MS/MS method at two QC levels (LQC, HQC) and IS level.

	MF	IS-normalized MF	CV%
LQC (n=6)	0.613 ± 0.036	0.919 ± 0.054	5.9
HQC (n=6)	0.672 ± 0.029	1.007 ± 0.043	4.3
IS (n=6)	0.667 ± 0.026	___	___

5.4.5. Extraction efficiency and recovery

The extraction efficiency was calculated as the ratio of the analyte peak in a pre-extraction spiked matrix sample to the peak area of the analyte in the absence of matrix (analyte solution in methanol) (Equation 6). Table 5.9 demonstrates the extraction efficiency values that range from 60.70% to 71.73% at three QC levels. Statistical analysis showed no significant differences between the three tested concentrations.

Table 5. 9. Evaluation of the extraction efficiency percentage for the quantification of docetaxel in the nanoparticle matrix using the developed HPLC-MS/MS method at three QC levels (LQC, MQC, HQC) and IS level.

	Extraction Efficiency %	CV%
LQC (n=6)	71.73 ± 8.44	11.8
MQC (n=6)	60.70 ± 7.58	12.5
HQC (n=6)	68.78 ± 4.34	6.3
IS (n=6)	89.81 ± 9.60	10.7

In addition to extraction efficiency, the evaluation of the extraction recovery (Equation 7) is important since the extraction efficiency does not take matrix effects into account. Table 5.9 shows the results of the extraction recovery determination that is calculated as the ratio of the peak area of the analyte spiked before extraction

in the matrix to the peak area of the analyte spiked after extraction of the matrix (Equation 7). As shown in Table 5.9, the extraction recovery percentage ranged from 81.67% to 100.28% across low, medium, and high QC levels. The difference between the observed extraction recoveries was not statistically significant. Such high recovery values show the high efficiency of the extraction method and ensures that the majority of the analyte is extracted from the matrix. A high recovery percentage contributes to the quantification of lower analyte concentrations.

Table 5. 10. Evaluation of the extraction recovery percentage for the quantification of docetaxel in the nanoparticle matrix using the developed HPLC-MS/MS method at three QC levels (LQC, MQC, HQC) and IS level.

	Extraction recovery %	CV%
LQC (n=6)	97.98 ± 5.27	5.4
MQC (n=6)	81.67 ± 10.50	12.8
HQC (n=6)	100.28 ± 5.40	5.4
IS (n=6)	87.32 ± 3.92	4.5

5.4.6. Carry-over effects

A needle-washing step with methanol was added between injections to avoid cross-contamination between samples. In addition, a double blank sample was injected after each sample with a high concentration (i.e., ULOQ, HQC, and experimental

samples) to minimize carry-over effects as recommended by the EMA guidelines (141).

Based on the FDA (140) and the EMA (141) guidelines, carry-over effects for the analyte should not exceed 20% of the LLOQ. While FDA does not specify any guidelines for acceptable range of carry-over effects for the IS, according to the EMA guidelines, it should not be more than 5% (141). The carry-over effect after the ULOQ was calculated to be 15.698 ± 0.653 % of the LLOQ for the analyte and 4.888×10^{-5} % ± 3.711×10^{-7} for the IS, indicating negligible carry-over effects during the analysis of a samples.

5.4.7. Dilution integrity

Table 5.11 shows the accuracy and precision of the samples which were diluted 10, 20, and 40 times. Three different dilution factors were chosen to ensure that the dilution integrity test will cover the dilution applied to the experimental samples. All the samples met the FDA guidelines for accuracy and precision (±15% for accuracy and CV%) (140) . Since the samples with an unknown concentration were 20-fold diluted with blank, the observed results indicate that diluting the samples does not affect the analytical results during the analysis of the nanoparticle formulations loaded with docetaxel.

Table 5. 11. Evaluation of the dilution integrity for the quantification of docetaxel in the nanoparticle matrix using double blank as the diluent at three levels (10-, 20-, and 40-times dilution) following analysis by HPLC-MS/MS.

	Replicates	Observed Concentration (mean±SD; ng/ml)	Precision (CV%)	Accuracy (%)
10 × Diluted (2000 ng/ml)	6	2215.17± 201.39	9.1	110.8
20 × Diluted (1000 ng/ml)	6	923.33 ± 137.6	14.9	92.3
40 × Diluted (500 ng/ml)	6	504.16 ± 70.01	13.9	102.1

5.4.8. Stability evaluation

Stability tests were designed and performed based on the conditions that were encountered during sample handling and analysis. For example, a freeze-thaw test was not necessary because the samples were stored in the freezer in a powder form. All the prepared samples for the stock solution stability test (at two concentration levels for the analyte, i.e. 4×LLOQ and 50% of ULOQ, and one concentration for the IS, i.e. 400 ng/ml) met the accuracy limits as specified in the FDA guidelines (140) (Table 5.12). This implies that the stock solutions of docetaxel and paclitaxel can be stored at -20℃ for one month and remain stable.

Auto-sampler stability for 24h at 4℃ passed the required accuracy limits (±15% of the nominal value) showing that the analyte was stable during data acquisition (Table 5.12). In addition, storing LQC and HQC samples at -20℃ for one month before

extraction showed accurate measurement of the concentration of the samples with accuracy values of 112.4% and 95.5%, respectively. This indicates that nanoparticle samples can be stored at the mentioned conditions without any concerns of analyte degradation.

Table 5. 12. Stability data of the developed method in different conditions used for the preparation and HPLC-MS/MS analysis of the docetaxel-loaded nanoparticles.

Stability test	Condition	Sample (n=6)	Concentration (ng/ml)	Observed Concentration (mean ± SD; ng/ml)	Accuracy (%)
Stock solution stability	30 days, −20 ℃	4×LLOQ	62.5	59.43 ± 6.05	95.1
		50% of ULOQ	2000	2200 ± 207.65	110
		IS	400	358.83 ± 37.55	89.7
Auto-sampler stability	24 h, 4 ℃	LQC	40	34.53 ± 3.55	86.3
		HQC	3000	2745.17 ± 168.76	91.5
Storage stability	30 days, −20 ℃	LQC	40	44.97 ± 8.47	112.4
		HQC	3000	2864.50 ± 274.21	95.5

5.4.9. Application of the method for the quantification of docetaxel-loaded nanoparticles

The developed LC-MS/MS method was applied for the quantification of docetaxel in the optimized PLGA nanoparticles. The concentration of the drug was determined

in the extracted samples of the nanoparticle formulation and the encapsulation efficiency of the formulation was calculated to be 52.28% ± 10.18 (n=4). This means that the developed method for the preparation of PLGA nanoparticles was able to encapsulate 52.28% of the docetaxel with which the preparation was started.

the drug loading (%) was determined to be 4.28% ± 0.27 indicating that the loaded docetaxel accounts for 4.28% of the weight of the final nanoparticle formulation.

6. DISCUSSION

Nano-encapsulation is one of the most studied methods to overcome the side effects of chemotherapeutic agents such as docetaxel used in the treatment of breast cancer. In order to prepare nanoparticle formulations with optimum particle size and yield percentage, it was essential to adjust different parameters such as Polyvinyl alcohol (PVA) solution volume, PLGA amount, centrifugation force and time, and ultra-sonication amplitude. To further biologically assess the produced PLGA nanoparticles, a quantification method was needed to be established to measure the entrapped drug within the nanoparticles. Determining diagnostic product ions to monitor during MRM analysis is one of the initial requirements of establishing a LC-MS/MS quantitative method. Therefore, the MS/MS fragmentation of the compounds in taxane drug family was studied and a generalized fragmentation pattern was established for the first time. In addition, the data was used to develop a liquid chromatography (LC)-MS/MS method to quantify the encapsulated drug.

6.1. Preparation and characterization of nanoparticles

As mentioned before, there are two main steps in the preparation of polymeric nanoparticles using the solvent evaporation technique. The first step is to form an o/w emulsion by dispersing an organic phase (polymer dissolved in an organic

solvent) in an aqueous phase (surfactant dissolved in water). The second step involves the subsequent evaporation of the organic solvent to form a nanoparticle suspension. A variety of organic solvents, such as ethyl acetate (149,150) and chloroform (151,152) have been used to prepare polymeric nanocarriers.

In my M.Sc. project, we evaluated the use of chloroform and ethyl acetate to choose the optimal organic solvent for the preparation of PLGA nanoparticles. Measurement of the size of the plain formulations prepared using chloroform showed larger particles (198.0 nm) than the nanoparticles that were prepared by ethyl acetate (170.2 nm). Chloroform has higher toxicity than ethyl acetate, meaning that ethyl acetate is a more favorable solvent than chloroform. In a study, toxicologic effects of administration of *Ocimum tenuiflorum* L. extracts were evaluated in streptozotocin-induced diabetic rats (153). Different oral crude leaf extracts were prepared in hexane, chloroform, ethyl acetate, methanol, and water. Biochemical tests on blood and histopathological assessment of different tissues (such as liver, kidney, and stomach) showed that all the extracts were well-tolerated by the animals with the exception of chloroform which caused side effects such as increased number of white blood cells (153). Therefore, we chose ethyl acetate as the organic solvent to prepare the nanoparticles due to its relatively high safety in comparison to chloroform, as well as its ability to produce smaller nanoparticles.

The *in vivo* fate of a nano-sized particle is highly dependent on its size (154). For example, the size of a nanoparticle has a strong correlation with its recognition by the macrophages (155) or its pharmacokinetic properties (156). It was shown that smaller methoxy-PEG nanoparticles with a size of 80 nm had double the elimination half-life in mice (11.33 ± 1.46 h) in comparison to particles with a size of 243 nm (4.67 ± 1.35 h) (157). These findings were explained by the results of macrophage phagocytosis assay, using RAW264.7 mouse macrophage cell line, showing remarkably higher uptake of lager nanoparticles compared with smaller particles (157). On the other hand, very small-sized particles (less than 20-30 nm) will undergo renal excretion and get eliminated quickly from the body (158), before exerting their therapeutic effects. Therefore, it is important to initially determine the desired size range based on the specific purpose of the nanoparticles and then optimize the parameters associated with the production method to obtain formulations with sizes within the optimal range. For the purpose of targeting dendritic cells, for example, a nanoparticle formulation should have a size of less than 500 nm (159,160). In my project, the aim was to prepare nanoparticles with a size around 250 nm to avoid high phagocytosis by the macrophages, while maintaining the ability of the nanoparticles to cross the discontinuous endothelium of the tumor vessels with fenestration sizes of 200-780 nm (161). The intracellular

uptake of the nanoparticles with a size of around 500 nm has been confirmed in many studies (162,163).

Among the methods applied to decrease the size of the particles and prepare a nano-emulsion, ultrasonication is one of the most effective techniques capable of controlling the distribution of particle size (164). The collapse of microbubbles (cavities), created by the ultrasound waves in the emulsion, generate transient localized regions with high pressure (up to 1000 bar) (165). This phenomenon, known as ultrasonic cavitation, reduces the sizes of droplets in an emulsion by putting mechanical stress on the particles (166). In addition, ultrasonic cavitation creates high speed liquid microjets which leads to the breakup and dispersion of emulsion droplets (166).

As such, the evaluation of the effect of sonication amplitude on the size of nanoparticles showed that increasing the sonication amplitude in the range of 30% - 40% decreases the average particle size of the formulation by 58.1 nm (Figure 5.3). The high energy received by the emulsion droplets during sonication might be the reason for the smaller size of the formulation prepared at 40% ultrasonication amplitude. In fact, many studies have evaluated the effects of ultrasonication on the size of nanoparticle formulations (167–169). The effect of increasing the ultrasonication amplitudes of 20, 40, 60, and 80% for 5 min was studied on the size of chitosan nanoparticles (170). The prepared nanoparticles showed decreased mean

diameters by increasing ultrasonication amplitudes. In other words, nano-suspension prepared with an amplitude of 20% had an average size of 350 ± 3 nm, while an amplitude of 80% produced formulations with a mean size of 302 ± 2 nm (170). The rate of reduction in the size of the particles slowed down beyond the amplitude of 60%, and the resulting particles maintained a size of about 300 nm. This leveling effect was attributed to the fact that a very high sonication amplitude can create more cavitation and decrease the efficacy of ultrasonication by reducing the transmission of energy (170). In addition, an overly high sonication amplitude can produce higher heat in the emulsion, affecting the structure of the polymer (171).

Changing the ultrasonication amplitude from 30% to 40% did not significantly change the yield percentage of the nanoparticle formulations ($p > 0.05$). The yield percentage is affected by any factor that changes the weight of the produced formulation. Therefore, it can be stated that the ultrasonication amplitude is not among the factors changing the weight of the produced nanoparticle formulations.

In the final stage of nanoparticle production, the produced nano-suspension was freeze-dried to increase the stability of the formulation and decrease the release of the encapsulated drug from the nanoparticles over time (172,173). Freeze-drying of the formulations increased the size of the nanoparticles (Figures 5.3 and 5.5) because the particles tend to aggregate during the removal of water (174). This effect has been observed in many studies (175–177). A common method to minimize the effect

of freeze-drying on the size and facilitate the redispersion of the particles is the use of cryoprotectant excipients such as sugars to prevent the aggregation of particles (178,179). Sucrose, trehalose, and mannitol molecules can provide steric hinderance between the nanoparticles and prevent them from sticking together (180). It has also been reported that slower freezing rates might increase the re-dispersibility of a formulation by creating a sugar-concentrated aqueous phase around the nanoparticles making the protection of the cryoprotectant more effective (181).

Ultra-centrifugation of the nanoparticle formulation is an essential step in the production of the particles and the removal of any excessive surfactant or unencapsulated drug. It is worth mentioning that the particles in a formulation do not have the same size (Figure 5.2) meaning that every nanoparticle sample is consisted of a mixture of particles from small to large. The reported value for the size of a sample is the average size of all the particles in the sample. Sedimentation of larger particles is expected to be easier than smaller particles. A higher centrifugal force collects more smaller particle and decreases the observed average size of the formulation. A sufficiently high centrifugal force is, therefore, needed to provide enough force to sediment nearly all small particles in a sample. This phenomenon can explain why an increase in centrifugal force from 34860×g to 39080×g did not significantly lower the mean size of the particles, but an increase from 34860×g to

48250×g resulted in a statistically significant decrease in the size of the particles from 184.9 ± 0.1 nm to 161.8 ± 2.6 nm (Figure 5.5).

Although increasing the rcf sediments more particles and, therefore, decreases the size and increases the resulting yield of the formulation (Figure 5.6), it also has the disadvantage of forcefully packing the particles together. These gathered clusters of nanoparticles can act as nuclei in the subsequent freeze-drying step and cause the growth of aggregations. Figure 5.5 shows that the highest applied rcf (48250×g) resulted in the production of the smallest nanoparticles before freeze-drying (size: 161.8 ± 2.6 nm) and these particles became the largest nanoparticles after freeze-drying (278.0 ± 6.8 nm). The results provide proof that different factors, namely particle size before and after freeze-drying and yield percentage, should be evaluated against each other in order to choose a properly balanced centrifugal force for the production of the optimized formulation. Table 5.2 shows the final outcome of these evaluations, which resulted in the development of the optimized formulation.

As mentioned before, the formation of an o/w emulsion is the first step towards the production of nanoparticles using the solvent evaporation technique. It means that the drug molecules would be partitioned between the organic and the aqueous phases with the latter containing a surfactant. After the evaporation of the solvent and the formation of a nano-suspension, the drug molecules that have been solubilized in the aqueous phase will be removed in the washing step (ultracentrifugation process).

Therefore, only drug molecules that enter the organic phase will have the chance to become encapsulated in the nanoparticles. As a result of losing some drug molecules, the loading efficiency of a preparation method is nearly always below 100%. In order to further biologically assess the produced PLGA nanoparticles, there is a substantial need to measure the amount of drug that has been entrapped within the nanoparticles, meaning that a quantification method needs to be established. LC-MS/MS is chosen for the analysis due to its analytical superiority as discussed in previous sections (sections 2-7 and 2-8). Studying the MS/MS fragmentation of a compound and determining diagnostic product ions to monitor during MRM analysis is of great importance, as it is one of the initial requirements of establishing LC-MS/MS qualitative or quantitative methods.

6.2. MS/MS fragmentation analysis

The establishment of MS/MS fragmentation patterns of cytotoxic medications allows for the subsequent identification of metabolic pathways of these drugs and the development of identification and quantification methods. Since pharmaceuticals are becoming one of the main classes of surface water contaminants (182), the CID-MS/MS fragmentation of methotrexate and doxorubicin, two anticancer drugs used in the treatment of osteosarcoma (183), has been established (184). Such studies are important due to the cytotoxic, mutagenic, and genotoxic nature of these drugs. The

purpose of the study was to establish a qualitative method to analyze the two compounds and assess their fate in aquatic environment. The fragmentation patterns allowed for the structure elucidation of the degradation products of methotrexate and doxorubicin produced by photocatalysis in water samples and a LC-MS/MS method was developed to identify these compounds along with their transformation products (184).

The fragmentation pattern of taxane drug family has been investigated in this study. While reviewing the literature, we encountered many LC-MS/MS quantification methods for these compounds, for which no qualifier ion was monitored during the analysis (132,134,139). This shows the importance of establishing the fragmentation patterns of these compounds to allow for the selection of diagnostic product ions. A general MS/MS fragmentation pattern was established, for the first time, for the five studied taxane-related compounds.

6.2.1. Universal MS/MS fragmentation behavior of taxanes

Similarities in the fragmentation behavior of the studied taxanes resulted in the establishment, for the first time, of a universal fragmentation pattern, regardless of the substituents (Figure 6.1) that can be applied to other related structures. The

universal MS/MS fragmentation pathway begins with a neutral loss of a water molecule from the $[M+H]^+$ ion to yield the B1 ion (Figure 6.1).

Ion B1 can go through one of the two main fragmentation pathways; it can either lose the R_3 side-chain moiety to produce ion S3 (pathway 1) or lose R2 to generate ion B2 (pathway 2). In pathway 1, product ion S3 forms the ion designated C4 via a loss of R1OH group that will then dissociate by the loss of the R2 group forming S4. S4 ion subsequently eliminates H_2O molecule to produce ion A1. The loss of CH_2CO from the C-ring (A1→C6) allows for another loss of water to yield C7 that finally loses benzoic acid to produce ion A3.

In pathway 2, B2 can either lose the acetic acid moiety from the C-ring yielding ion C3 or lose the R_1OH substituent generating ion C1. C1 undergoes three fragmentation process; it either loses a water molecule yielding ion S1 or it can eliminate R_3 forming the ion designated S4, where the two main pathways join. Finally, C1 can eliminate acetic acid from the C-ring yielding ion C2. Benzoic acid is then eliminated to form the product ion B5, which still carries the sidechain (R_3). It dissociates by either the loss of the core structure or the R_3OH substituent; the former generates ion S5 and the latter forms ion A3, the second ion that is shared between the two main pathways (Figure 6.1).

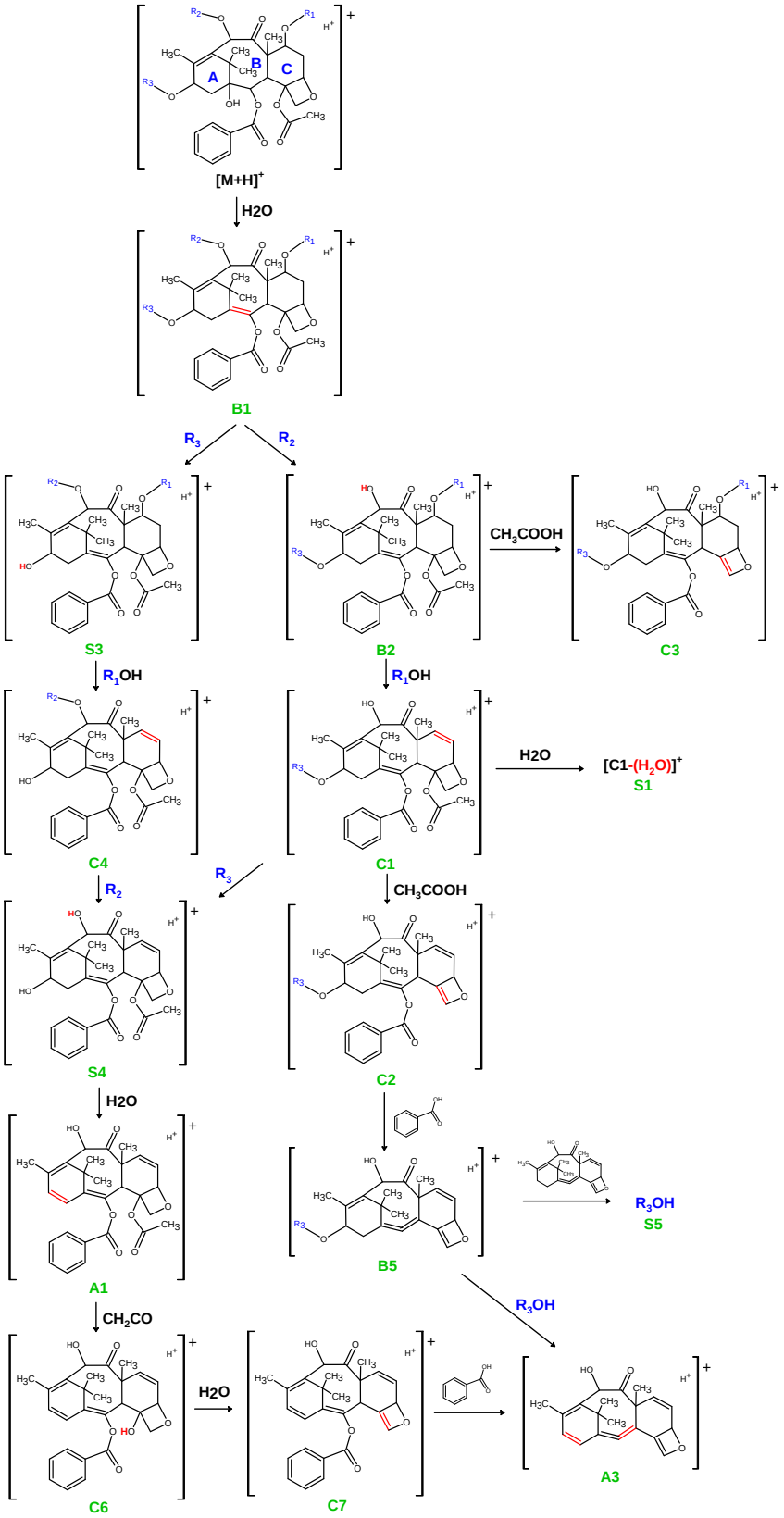

Figure 6. 1. The universal MS/MS fragmentation of taxane-related compounds.

6.3. Development and validation of the analytical method

HPLC-MS/MS has been adapted by many researchers as their quantification method to analyze docetaxel in different matrices (Table 2.2). HPLC columns used in these studies are either C8 (135,137) or C18 (132,133,136,138,139) (Table 2.2). To the best of our knowledge, a phenyl column has never been applied for the quantification of docetaxel in a polymeric formulation matrix. The stationary phase in a Nova-Pak® phenyl column is made up of silica particles with hydrophobic phenyl hexyl chains ($-(CH_2)_8-C_6H_5$) that interact with the analyte. The main impurity in the tested samples is PLGA, a linear polymer (Figure 2.1) which will have minor interactions with the stationary phase of a phenyl column. Therefore, any PLGA molecule that has not been eliminated from the sample in the extraction phase can be eliminated in the mobile phase, early in the LC-MS/MS analysis. On the other hand, docetaxel and paclitaxel have hydrophobic phenyl rings in their structures (Table 2.1) allowing for pi-pi interactions with the phenyl groups of the stationary phase, unlike PLGA molecules. Such differences in the interactions of the analyte and the polymer with the stationary phase will theoretically result in good separation of the drug molecules from PLGA impurities in the sample. PLGA elutes from the column well-before the analyte, a phenomenon which reduces the baseline noise, making the analyte peak sharper, and potentially increasing the sensitivity of the method. In a previous study in our lab (128), docetaxel was quantified in a PLGA nanoparticle matrix using a

flow-injection-MS/MS (FIA-MS/MS) method. The limit of detection (LOD) and the limit of quantification (LLOQ) were 62.5 ng/ml and 125 ng/ml, respectively. A phenyl column, on the other hand, significantly enhanced the sensitivity of the quantification and resulted in a LOD and LLOQ values of 4 ng/ml and 15.6 ng/ml, respectively. This difference between the two methods can be attributed to the effective separation capability of the phenyl column. Smaller LLOQ values will help quantify the amount of encapsulated docetaxel in formulations with low loading efficiency.

The validation of the developed method assured the repeatability and reliability of the assay results (Tables 5.6, 5.7, and 5.11) and provided proof for the high selectivity of the method (Figures 5.11, 5.12, and 5.13). Matrix factor (MF) was found to be around 0.6, meaning that the matrix suppressed the ionization of the analyte by 40%. The observed matrix effects did not hinder the quantification of docetaxel in the PLGA matrix, with the needed high sensitivity. It can be stated that matrix effects are balanced with the high extraction recovery percentage (97.98% ± 5.27 at LQC level and 100.28% ± 5.40 at HQC level, Table 5.9). Pre-MS sample treatments, such as improved extraction, will help with attaining higher MF values.

6.4. Conclusion

The focus of my MSc thesis was to prepare optimized PLGA nanoparticles encapsulated with a chemotherapeutic agent to be used in breast cancer. Several nanoparticle formulations were prepared to optimize the conditions for the fabrication of the docetaxel loaded PLGA nanoparticles. The optimized nanoparticles had a mean particle size of 251.7±8.2 nm after FD. The nanoparticles would be able to deliver their encapsulated drug to the tumor site after crossing the tumor's microvasculature pores having a size of 200-780 nm (161). Zeta potential measurements showed that the nanoparticles had a negative surface charge of -23.2 ± 1.4 mV, which did not change significantly after FD.

In order to develop an LC-MS/MS method for the determination of the loading efficiency of the drug inside the nanoparticles, it was essential to study the fragmentation fingerprint of the drug. Surprisingly, we found out that no previous study has focused on the detailed MS/MS fragmentation of the drugs in the taxane family. Therefore, the CID-MS/MS fragmentation behavior of five taxane-related compounds was evaluated. The projected molecular compositions of the studied compounds were confirmed by exact mass measurements showing mass errors of less than 3 ppm. In addition, the MS/MS analysis added another level of assurance to the chemical structures of the observed $[M+H]^+$ ions. The MS^3 data (Table 5.4

and Appendix Tables S1-S4) confirmed the genesis of the proposed product ions and allowed for the development of a generalized MS/MS fingerprint pattern that could contribute to the identification of taxane-related compounds in the future.

The MS/MS fragmentation was centered on the dissociation of the substituents from the core diterpene ring to generate diagnostic product ions. Elimination of the sidechain was observed in all the compounds except for baccatin III. Differences in the MS/MS patterns of tested compounds were attributed to the differences in the substituents. However, based on the similarities in the fragmentation behavior among all the tested compounds, a universal fragmentation pattern was developed as shown in Figure 4.2. This general fragmentation pattern can be used to predict the dissociation behavior of new compounds with similar structural characteristics. In addition, this data was used to choose diagnostic product ions to develop the LC-MS/MS quantification method.

A sensitive, specific and robust mass spectrometric method was developed and validated to quantify docetaxel in PLGA nanoparticle matrix over the range of 15.6-4000 ng/ml. The use of a phenyl column significantly increased the sensitivity of the quantification method compared to previously developed FID-MS/MS method (128). The method was successfully applied to measure the amount of docetaxel in the prepared nanoparticles. High loading efficiency of the prepared nanoparticles will allow for the injection of low amounts of the nanoparticles in an *in vivo* study.

Injecting a lower amount of nanoparticle formulation has the advantage of decreasing the injection volume, lowering the viscosity of the mixture, and reducing the adverse effects caused by possible impurity residues in the formulation (such as PVA or free drug).

6.5. Future directions

The present work was an attempt to improve the formulation of docetaxel loaded PLGA nanoparticles and develop a sensitive quantification method to measure the encapsulated drug. The following recommendations and future directions could be considered to advance the project.

A. Improving the analytical process: Using a chromatographic column was our solution to the problem of low sensitivity observed with the FIA-MS method. However, additional analytical strategies can be adopted to allow for a possibly sensitive FIA-MS method. Possible approaches can be changing the solvent system in the extraction method or the use of a solid-phase extraction. Such changes will most likely reduce impurities; and hence decrease the LLOQ without using a phenyl column. In addition, other ionization techniques such as APCI can be used to decrease the base-line noise and increase the sensitivity of the quantification method.

B. Conducting in vitro and in vivo studies: The nanoparticles can be tested in breast cancer cell lines such as MCF-7 or MDA-MB-453 to ensure the cellular uptake of the nanoparticles and compare their cytotoxic effects with free drug solution, prior to *in vivo* tests. Subsequently, a pharmacokinetic study in an animal model of the prepared nanoparticles can help evaluate the improved

biodistribution of the encapsulated drug. The fate of the nanoparticles in the tumor-bearing animal body can be studied using a fluorescent dye inside the nanoparticles (185–187).

C. Improving the formulation: PLGA nanoparticles can be surface-modified to increase their water-miscibility and decrease surface charge. A targeting agent such as trastuzumab (188–190) can fulfill this goal and increase the chance of a successful treatment by increasing the concentration of the drug at the tumor site. The antitumor effects of the modified formulations can be investigated by the injection of the nanoparticles into a xenograft animal model. Measuring the weight and volume of the tumor will provide evidence for tumor shrinkage. In addition, the data from the quantification of drug concentration in different organs of the treated animals will enable us to predict the possible side effects of the modified nanoparticle formulations. Based on these results, the modified nanoparticle formulations can be optimized to minimize potential side effects.

10. REFERENCES

1. Howlader N, Noone AM, Krapcho M, Miller D, Brest A, Yu M, Ruhl J, Tatalovich Z, Mariotto A, Lewis DR, Chen HS, Feuer EJ, Cronin KA (eds). SEER Cancer Statistics Review, 1975-2017, National Cancer Institute. Bethesda, MD, https://seer.cancer.gov/csr/1975_2.

2. American Cancer Society. Breast Cancer Facts & Figures 2019-2020. Atlanta: American Cancer Society, Inc. 2019.

3. Castiglione M P-GM. Adjuvant therapy for breast cancer. In New York: Springer; 2009. p. 126.

4. Willson ML, Burke L, Ferguson T, Ghersi D, Nowak AK, Wilcken N. Taxanes for adjuvant treatment of early breast cancer. Cochrane Database Syst Rev [Internet]. 2019;(9). Available from: https://doi.org//10.1002/14651858.CD004421.pub3

5. de Weger VA, Beijnen JH, Schellens JHM. Cellular and clinical pharmacology of the taxanes docetaxel and paclitaxel--a review. Anticancer Drugs. 2014 May;25(5):488–94.

6. Kamaly N, Xiao Z, Valencia PM, Radovic-Moreno AF, Farokhzad OC. Targeted polymeric therapeutic nanoparticles: design, development and clinical translation. Chem Soc Rev. 2012 Apr;41(7):2971–3010.

7. Dinarvand R, Sepehri nima, Manoochehri S, Rouhani H, Atyabi F. Polylactide-co-glycolide Nanoparticles for Controlled Delivery of Anticancer Agents. Int J Nanomedicine. 2011 May 27;6:877–95.

8. Sung H, Ferlay J, Siegel RL, Laversanne M, Soerjomataram I, Jemal A, et al. Global cancer statistics 2020: GLOBOCAN estimates of incidence and mortality worldwide for 36 cancers in 185 countries. CA Cancer J Clin. 2021 Feb;

9. Sibbering M, Courtney C-A. Management of breast cancer: basic principles. Surg [Internet]. 2019;37(3):157–63. Available from: https://www.sciencedirect.com/science/article/pii/S0263931919300171

10. Moo T-A, Sanford R, Dang C, Morrow M. Overview of Breast Cancer Therapy. PET Clin. 2018 Jul;13(3):339–54.

11. Loibl S, Gianni L. HER2-positive breast cancer. Lancet (London, England). 2017 Jun;389(10087):2415–29.

12. Amin MB ES, Greene FL, et al. AJCC (American Joint Committee on Cancer) Cancer Staging Manual. 8th ed. Chicago: Springer; 2018.

13. Amin MB, Greene FL, Edge SB, Compton CC, Gershenwald JE, Brookland RK, et al. The Eighth Edition AJCC Cancer Staging Manual: Continuing to build a bridge from a population-based to a more "personalized" approach to cancer staging. Vol. 67, CA: a cancer journal for clinicians. United States; 2017. p. 93–9.

14. Vuong D, Simpson PT, Green B, Cummings MC, Lakhani SR. Molecular classification of breast cancer. Virchows Arch [Internet]. 2014;465(1):1–14. Available from: https://doi.org/10.1007/s00428-014-1593-7

15. Howlader N, Cronin KA, Kurian AW, Andridge R. Differences in Breast Cancer Survival by Molecular Subtypes in the United States. Cancer Epidemiol biomarkers & Prev a Publ Am Assoc Cancer Res cosponsored by Am Soc Prev Oncol [Internet]. 2018;27(6):619–26. Available from: http://europepmc.org/abstract/MED/29593010

16. Prat A, Adamo B, Cheang MCU, Anders CK, Carey LA, Perou CM. Molecular characterization of basal-like and non-basal-like triple-negative breast cancer. Oncologist. 2013;18(2):123–33.

17. Costa RLB, Gradishar WJ. Triple-Negative Breast Cancer: Current Practice and Future Directions. J Oncol Pract [Internet]. 2017 May 1;13(5):301–3. Available from: https://doi.org/10.1200/JOP.2017.023333

18. Wolff AC, Tung NM, Carey LA. Implications of Neoadjuvant Therapy in Human Epidermal Growth Factor Receptor 2–Positive Breast Cancer. J Clin Oncol [Internet]. 2019 Jun 3;37(25):2189–92. Available from: https://doi.org/10.1200/JCO.19.01159

19. Paik S, Bryant J, Tan-Chiu E, Romond E, Hiller W, Park K, et al. Real-World Performance of HER2 Testing—National Surgical Adjuvant Breast and Bowel Project Experience. JNCI J Natl Cancer Inst [Internet]. 2002 Jun 5;94(11):852–4. Available from: https://doi.org/10.1093/jnci/94.11.852

20. Wani MC, Taylor HL, Wall ME, Coggon P, McPhail AT. Plant antitumor agents. VI. The isolation and structure of taxol, a novel antileukemic and antitumor agent from Taxus brevifolia. J Am Chem Soc. 1971

May;93(9):2325–7.

21. Fitzpatrick FA, Wheeler R. The immunopharmacology of paclitaxel (Taxol), docetaxel (Taxoteree), and related agents. Int Immunopharmacol. 2003 Dec;3(13–14):1699–714.

22. Parness J, Horwitz SB. Taxol binds to polymerized tubulin in vitro. J Cell Biol. 1981 Nov;91(2 Pt 1):479–87.

23. Frederiks CN, Lam SW, Guchelaar HJ, Boven E. Genetic polymorphisms and paclitaxel- or docetaxel-induced toxicities: A systematic review. Cancer Treat Rev. 2015 Dec;41(10):935–50.

24. Heidenreich A, Bracarda S, Mason M, Ozen H, Sengelov L, Van Oort I, et al. Safety of cabazitaxel in senior adults with metastatic castration-resistant prostate cancer: Results of the European compassionate-use programme. Eur J Cancer. 2014 Apr 1;50(6):1090–9.

25. Gao F, Wang D, Huang X. Synthesis, isolation, stereostructure and cytotoxicity of paclitaxel analogs from cephalomannine. Fitoterapia. 2013 Oct 1;90:79–84.

26. Raajasekar A, Burdette-Radoux S. Pathologic complete response after neoadjuvant paclitaxel and carboplatin chemotherapy for stage II-III breast cancer: A community cancer center experience. J Clin Oncol. 2015 Oct 1;33:43.

27. Broderick SR. Adjuvant and Neoadjuvant Immunotherapy in Non-small Cell Lung Cancer. Thorac Surg Clin. 2020 May;30(2):215–20.

28. Krown SE, Moser CB, MacPhail P, Matining RM, Godfrey C, Caruso SR, et al. Treatment of advanced AIDS-associated Kaposi sarcoma in resource-limited settings: a three-arm, open-label, randomised, non-inferiority trial. Lancet (London, England). 2020 Apr;395(10231):1195–207.

29. Slamon D, Eiermann W, Robert N, Pienkowski T, Martin M, Rolski J, et al. Phase III Randomized Trial Comparing Doxorubicin and Cyclophosphamide Followed by Docetaxel (AC->T) with Doxorubicin and Cyclophosphamide Followed by Docetaxel and Trastuzumab (AC->TH) with Docetaxel, Carboplatin and Trastuzumab (TCH) in Her2neu Positive . Cancer Res. 2010 Feb 10;69:62.

30. Capelletto E, Migliorino MR, Morabito A, Chiari R, Grossi F, Tiseo M, et al. Final results of the SENECA (SEcond line NintEdanib in non-small cell lung

CAncer) trial. Lung Cancer. 2019 Aug;134:210–7.

31. Gravis G. Systemic treatment for metastatic prostate cancer. Asian J Urol [Internet]. 2019;6(2):162–8. Available from: https://www.sciencedirect.com/science/article/pii/S2214388219300104

32. Moiseyenko VM, Ajani J, Tjulandin SA, Majlis A, Constenla M, Boni C, et al. Final results of a randomized controlled phase III trial (TAX 325) comparing docetaxel (T) combined with cisplatin (C) and 5-fluorouracil (F) to CF in patients (pts) with metastatic gastric adenocarcinoma (MGC). J Clin Oncol [Internet]. 2005 Jun 1;23(16_suppl):4002. Available from: https://doi.org/10.1200/jco.2005.23.16_suppl.4002

33. Cohen EEW, Karrison TG, Kocherginsky M, Mueller J, Egan R, Huang CH, et al. Phase III Randomized Trial of Induction Chemotherapy in Patients With N2 or N3 Locally Advanced Head and Neck Cancer. J Clin Oncol [Internet]. 2014 Jul 21;32(25):2735–43. Available from: https://doi.org/10.1200/JCO.2013.54.6309

34. Simondsen K, Kolesar J. New treatment options for castration-resistant prostate cancer. Am J Heal Pharm [Internet]. 2013 May 15;70(10):856–65. Available from: https://doi.org/10.2146/ajhp110586

35. Soliman SSM, Raizada MN. Interactions between Co-Habitating fungi Elicit Synthesis of Taxol from an Endophytic Fungus in Host Taxus Plants [Internet]. Vol. 4, Frontiers in microbiology. Department of Plant Agriculture, University of Guelph Guelph, ON, Canada ; Faculty of Pharmacy, Zagazig University Zagazig, Egypt.; 2013. p. 3. Available from: http://europepmc.org/abstract/MED/23346084

36. Evans W. Trease and Evans' Pharmacognosy. 16th ed. Saunders; 2009. 416–27 p.

37. Noguchi S. Predictive factors for response to docetaxel in human breast cancers. Cancer Sci [Internet]. 2006 Sep 1;97(9):813–20. Available from: https://doi.org/10.1111/j.1349-7006.2006.00265.x

38. Imran M, Saleem S, Chaudhuri A, Ali J, Baboota S. Docetaxel: An update on its molecular mechanisms, therapeutic trajectory and nanotechnology in the treatment of breast, lung and prostate cancer. J Drug Deliv Sci Technol [Internet]. 2020;60:101959. Available from: https://www.sciencedirect.com/science/article/pii/S177322472031248X

39. Carbognin L, Sperduti I, Nortilli R, Brunelli M, Vicentini C, Pellini F, et al. Balancing activity and tolerability of neoadjuvant paclitaxel- and docetaxel-based chemotherapy for HER2-positive early stage breast cancer: sensitivity analysis of randomized trials. Cancer Treat Rev. 2015 Mar;41(3):262–70.

40. Baker J, Ajani J, Scotté F, Winther D, Martin M, Aapro MS, et al. Docetaxel-related side effects and their management. Eur J Oncol Nurs [Internet]. 2009;13(1):49–59. Available from: https://www.sciencedirect.com/science/article/pii/S1462388908001324

41. Karahalil B, Yardım-Akaydin S, Baytas S. An overview of microtubule targeting agents for cancer therapy. Arch Ind Hyg Toxicol. 2019 Sep 1;70:160–72.

42. Fojo T. The Role of Microtubules in Cell Biology, Neurobiology, and Oncology. 2008.

43. Ganju A, Yallapu MM, Khan S, Behrman SW, Chauhan SC, Jaggi M. Nanoways to overcome docetaxel resistance in prostate cancer. Drug Resist Updat [Internet]. 2014;17(1):13–23. Available from: https://www.sciencedirect.com/science/article/pii/S1368764614000065

44. Ho MY, Mackey JR. Presentation and management of docetaxel-related adverse effects in patients with breast cancer. Cancer Manag Res. 2014;6(1):253.

45. Zhao P, Astruc D. Docetaxel Nanotechnology in Anticancer Therapy. ChemMedChem [Internet]. 2012 Jun 1;7(6):952–72. Available from: https://doi.org/10.1002/cmdc.201200052

46. ten Tije AJ, Verweij J, Loos WJ, Sparreboom A. Pharmacological effects of formulation vehicles : implications for cancer chemotherapy. Clin Pharmacokinet. 2003;42(7):665–85.

47. van Zuylen L, Verweij J, Sparreboom A. Role of formulation vehicles in taxane pharmacology. Invest New Drugs. 2001 May;19(2):125–41.

48. Clarke SJ, Rivory LP. Clinical Pharmacokinetics of Docetaxel. Clin Pharmacokinet [Internet]. 1999;36(2):99–114. Available from: https://doi.org/10.2165/00003088-199936020-00002

49. Baker SD, Sparreboom A, Verweij J. Clinical Pharmacokinetics of Docetaxel. Clin Pharmacokinet [Internet]. 2006;45(3):235–52. Available from: https://doi.org/10.2165/00003088-200645030-00002

50. Sadat Tabatabaei Mirakabad F, Nejati-Koshki K, Akbarzadeh A, Yamchi MR, Milani M, Zarghami N, et al. PLGA-based nanoparticles as cancer drug delivery systems. Asian Pac J Cancer Prev. 2014;15(2):517–35.

51. Astete C, Sabliov C. Synthesis and characterization of PLGA nanoparticles. J Biomater Sci Polym Ed. 2006 Feb 1;17:247–89.

52. Lü J-M, Wang X, Marin-Muller C, Wang H, Lin PH, Yao Q, et al. Current advances in research and clinical applications of PLGA-based nanotechnology. Expert Rev Mol Diagn [Internet]. 2009;9(4):325–41. Available from: http://europepmc.org/abstract/MED/19435455

53. Anderson JM, Shive MS. Biodegradation and biocompatibility of PLA and PLGA microspheres. Adv Drug Deliv Rev [Internet]. 2012;64:72–82. Available from: https://www.sciencedirect.com/science/article/pii/S0169409X12002645

54. Mir M, Ahmed N, Rehman AU. Recent applications of PLGA based nanostructures in drug delivery. Colloids Surf B Biointerfaces. 2017 Nov;159:217–31.

55. Jain RA. The manufacturing techniques of various drug loaded biodegradable poly(lactide-co-glycolide) (PLGA) devices. Biomaterials. 2000 Dec;21(23):2475–90.

56. Dang Y, Guan J. Nanoparticle-based drug delivery systems for cancer therapy. Smart Mater Med [Internet]. 2020;1:10–9. Available from: https://www.sciencedirect.com/science/article/pii/S2590183420300028

57. Obeidat WM, Price JC. Viscosity of polymer solution phase and other factors controlling the dissolution of theophylline microspheres prepared by the emulsion solvent evaporation method. J Microencapsul. 2003;20(1):57–65.

58. Jahan S, Haddadi A. Investigation and optimization of formulation parameters on preparation of targeted anti-CD205 tailored PLGA nanoparticles. Int J Nanomedicine. 2015 Dec 10;10:7371.

59. Kou G, Gao J, Wang H, Chen H, Li B, Dapeng Z, et al. Preparation and Characterization of Paclitaxel-loaded PLGA Nanoparticles Coated with Cationic SM5-1 Single-chain Antibody. J Biochem Mol Biol. 2007 Oct 1;40:731–9.

60. Gao J, Kou G, Wang H, Chen H, Li B, Lu Y, et al. PE38KDEL-loaded anti-HER2 nanoparticles inhibit breast tumor progression with reduced toxicity and

immunogenicity. Breast Cancer Res Treat. 2008 Jun 1;115:29–41.

61. Sun B, Ranganathan B, Feng S-S. Multifunctional poly(d,l-lactide-co-glycolide)/montmorillonite (PLGA/MMT) nanoparticles decorated by Trastuzumab for targeted chemotherapy of breast cancer. Biomaterials [Internet]. 2008;29(4):475–86. Available from: https://www.sciencedirect.com/science/article/pii/S0142961207007909

62. Gao L, Zhang D, Chen M. Drug nanocrystals for the formulation of poorly soluble drugs and its application as a potential drug delivery system. J Nanoparticle Res. 2008 May 1;10:845–62.

63. Junyaprasert VB, Morakul B. Nanocrystals for enhancement of oral bioavailability of poorly water-soluble drugs. Asian J Pharm Sci [Internet]. 2015;10(1):13–23. Available from: https://www.sciencedirect.com/science/article/pii/S1818087614000555

64. Khadka P, Ro J, Kim H, Kim I, Kim JT, Kim H, et al. Pharmaceutical particle technologies: An approach to improve drug solubility, dissolution and bioavailability. Asian J Pharm Sci [Internet]. 2014;9(6):304–16. Available from: https://www.sciencedirect.com/science/article/pii/S1818087614000348

65. Davis ME, Chen ZG, Shin DM. Nanoparticle therapeutics: an emerging treatment modality for cancer. Nat Rev Drug Discov. 2008 Sep;7(9):771–82.

66. Peer D, Karp JM, Hong S, Farokhzad OC, Margalit R, Langer R. Nanocarriers as an emerging platform for cancer therapy. Nat Nanotechnol. 2007 Dec;2(12):751–60.

67. Pérez-Herrero E, Fernández-Medarde A. Advanced targeted therapies in cancer: Drug nanocarriers, the future of chemotherapy. Eur J Pharm Biopharm [Internet]. 2015;93:52–79. Available from: https://www.sciencedirect.com/science/article/pii/S0939641115001514

68. Podesta JE, Kostarelos K. Chapter Seventeen - Engineering Cationic Liposome: siRNA Complexes for In Vitro and In Vivo Delivery. In: Düzgünes NBT-M in E, editor. Liposomes, Part F [Internet]. Academic Press; 2009. p. 343–54. Available from: https://www.sciencedirect.com/science/article/pii/S0076687909640179

69. Shao J, Fang Y, Zhao R, Chen F, Yang M, Jiang J, et al. Evolution from small molecule to nano-drug delivery systems: An emerging approach for cancer therapy of ursolic acid. Asian J Pharm Sci [Internet]. 2020;15(6):685–

700. Available from: https://www.sciencedirect.com/science/article/pii/S1818087619306816

70. Casamonti M, Risaliti L, Vanti G, Piazzini V, Bergonzi MC, Bilia AR. Andrographolide Loaded in Micro- and Nano-Formulations: Improved Bioavailability, Target-Tissue Distribution, and Efficacy of the "King of Bitters." Engineering [Internet]. 2019;5(1):69–75. Available from: https://www.sciencedirect.com/science/article/pii/S2095809918309962

71. Kratz F, Warnecke A. Finding the optimal balance: Challenges of improving conventional cancer chemotherapy using suitable combinations with nano-sized drug delivery systems. J Control Release [Internet]. 2012;164(2):221–35. Available from: https://www.sciencedirect.com/science/article/pii/S0168365912004580

72. Lamch Ł, Pucek A, Kulbacka J, Chudy M, Jastrzębska E, Tokarska K, et al. Recent progress in the engineering of multifunctional colloidal nanoparticles for enhanced photodynamic therapy and bioimaging. Adv Colloid Interface Sci [Internet]. 2018;261:62–81. Available from: https://www.sciencedirect.com/science/article/pii/S0001868618302082

73. Li S-D, Huang L. Pharmacokinetics and biodistribution of nanoparticles. Mol Pharm. 2008;5(4):496–504.

74. Chu KS, Schorzman AN, Finniss MC, Bowerman CJ, Peng L, Luft JC, et al. Nanoparticle drug loading as a design parameter to improve docetaxel pharmacokinetics and efficacy. Biomaterials [Internet]. 2013;34(33):8424–9. Available from: https://www.sciencedirect.com/science/article/pii/S014296121300820X

75. Rafiei P, Haddadi A. Docetaxel-loaded PLGA and PLGA-PEG nanoparticles for intravenous application: pharmacokinetics and biodistribution profile. Int J Nanomedicine. 2017;12:935–47.

76. Zhao Y-Z, van Breemen RB, Nikolic D, Huang C-R, Woodbury CP, Schilling A, et al. Screening Solution-Phase Combinatorial Libraries Using Pulsed Ultrafiltration/Electrospray Mass Spectrometry. J Med Chem [Internet]. 1997 Dec 1;40(25):4006–12. Available from: https://doi.org/10.1021/jm960729b

77. Chu Y-H, Dunayevskiy YM, Kirby DP, Vouros P, Karger BL. Affinity Capillary Electrophoresis−Mass Spectrometry for Screening Combinatorial Libraries. J Am Chem Soc [Internet]. 1996 Jan 1;118(33):7827–35. Available from: https://doi.org/10.1021/ja960213h

78. Zhang N, Fountain ST, Bi H, Rossi DT. Quantification and Rapid Metabolite Identification in Drug Discovery Using API Time-of-Flight LC/MS. Anal Chem [Internet]. 2000 Feb 1;72(4):800–6. Available from: https://doi.org/10.1021/ac9911701

79. Yu X, Cui D, Davis MR. Identification of in vitro metabolites of indinavir by "intelligent automated LC-MS/MS" (INTAMS) utilizing triple quadrupole tandem mass spectrometry. J Am Soc Mass Spectrom [Internet]. 1999;10(2):175–83. Available from: https://www.sciencedirect.com/science/article/pii/S1044030598001329

80. Ma Y, Li P, Chen D, Fang T, Li H, Su W. LC/MS/MS quantitation assay for pharmacokinetics of naringenin and double peaks phenomenon in rats plasma. Int J Pharm [Internet]. 2006;307(2):292–9. Available from: https://www.sciencedirect.com/science/article/pii/S0378517305006782

81. Lee H, Shen S, Grinberg N. Identification and Control of Impurities for Drug Substance Development using LC/MS and GC/MS. J Liq Chromatogr Relat Technol. 2008 Sep 1;31:2235–52.

82. Wu Y. The use of liquid chromatography-mass spectrometry for the identification of drug degradation products in pharmaceutical formulations. Biomed Chromatogr. 2000 Oct;14(6):384–96.

83. Domon B, Aebersold R. Mass Spectrometry and Protein Analysis. Science (80-) [Internet]. 2006 Apr 14;312(5771):212 LP – 217. Available from: http://science.sciencemag.org/content/312/5771/212.abstract

84. Núñez O, Gallart-Ayala H, Martins CPB, Lucci P, Busquets R. State-of-the-art in fast liquid chromatography–mass spectrometry for bio-analytical applications. J Chromatogr B [Internet]. 2013;927:3–21. Available from: https://www.sciencedirect.com/science/article/pii/S1570023213000147

85. Lee MS, Kerns EH. LC/MS applications in drug development. Mass Spectrom Rev [Internet]. 1999 Jan 1;18(3-4):187–279. Available from: https://doi.org/10.1002/(SICI)1098-2787(1999)18:3/4%3C187::AID-MAS2%3E3.0.CO

86. Pavelić SK, Markova-Car E, Klobučar M, Spaventi LS and R. Technological Advances in Preclinical Drug Evaluation: The Role of -Omics Methods [Internet]. Vol. 27, Current Medicinal Chemistry. 2020. p. 1337–49. Available from: http://www.eurekaselect.com/node/173419/article

87. Zhang X, Li Q, Xu Z, Dou J. Mass spectrometry-based metabolomics in health and medical science: a systematic review. RSC Adv [Internet]. 2020;10(6):3092–104. Available from: http://dx.doi.org/10.1039/C9RA08985C

88. Miller R.A., Spellman D.S. (2014) Mass Spectrometry-Based Biomarkers in Drug Development. In: Woods A., Darie C. (eds) Advancements of Mass Spectrometry in Biomedical Research. Advances in Experimental Medicine and Biology, vol 806. Springer, Cham. https: In.

89. Rappold BA. Special Considerations for Liquid Chromatography–Tandem Mass Spectrometry Method Development. Clin Lab Med [Internet]. 2018;38(3):539–51. Available from: https://www.sciencedirect.com/science/article/pii/S0272271218311478

90. El-Aneed A, Cohen A, Banoub J. Mass Spectrometry, Review of the Basics: Electrospray, MALDI, and Commonly Used Mass Analyzers. Appl Spectrosc Rev [Internet]. 2009 Apr 1;44(3):210–30. Available from: https://doi.org/10.1080/05704920902717872

91. Buse J, Badea I, Verrall RE, El-Aneed A. Tandem mass spectrometric analysis of novel diquaternary ammonium gemini surfactants and their bromide adducts in electrospray-positive ion mode ionization. J Mass Spectrom [Internet]. 2011 Oct 1;46(10):1060–70. Available from: https://doi.org/10.1002/jms.1988

92. Donkuru M, Chitanda JM, Verrall RE, El-Aneed A. Multi-stage tandem mass spectrometric analysis of novel β-cyclodextrin-substituted and novel bis-pyridinium gemini surfactants designed as nanomedical drug delivery agents. Rapid Commun Mass Spectrom. 2014 Apr;28(7):757–72.

93. Al-Dulaymi M, El-Aneed A. Tandem mass spectrometric analysis of novel peptide-modified gemini surfactants used as gene delivery vectors. J Mass Spectrom. 2017 Jun;52(6):353–66.

94. Mohammed-Saeid W, Buse J, Badea I, Verrall R, El-Aneed A. Mass spectrometric analysis of amino acid/di-peptide modified gemini surfactants used as gene delivery agents: Establishment of a universal mass spectrometric fingerprint. Int J Mass Spectrom [Internet]. 2012;309:182–91. Available from: https://www.sciencedirect.com/science/article/pii/S1387380611004179

95. Jin W, Badea I, Leary SC, El-need A. The determination of gemini surfactants used as gene delivery agents in cellular matrix using validated tandem mass spectrometric method. J Pharm Biomed Anal. 2019 Feb 5;164:164–72.

96. Al-Dulaymi M, Michel D, Chitanda JM, Badea I, El-Aneed A. The development of simple flow injection analysis tandem mass spectrometric methods for the cutaneous determination of peptide-modified cationic gemini surfactants used as gene delivery vectors. J Pharm Biomed Anal. 2018 Sep 10;159:536–47.

97. Buse J, Purves RW, Verrall RE, Badea I, Zhang H, Mulligan CC, et al. The development and assessment of high-throughput mass spectrometry-based methods for the quantification of a nanoparticle drug delivery agent in cellular lysate. J Mass Spectrom [Internet]. 2014 Nov 1;49(11):1171–80. Available from: https://doi.org/10.1002/jms.3444

98. Buse J, Badea I, Verrall RE, El-Aneed A. A general liquid chromatography tandem mass spectrometry method for the quantitative determination of diquaternary ammonium gemini surfactant drug delivery agents in mouse keratinocytes' cellular lysate. J Chromatogr A [Internet]. 2013;1294:98–105. Available from: https://www.sciencedirect.com/science/article/pii/S0021967313006286

99. Jin W, Purves R, Krol E, Badea I, El-Aneed A. Mass Spectrometric Detection and Characterization of Metabolites of Gemini Surfactants Used as Gene Delivery Vectors. J Am Soc Mass Spectrom. 2020 Feb;31(2):366–78.

100. Cui M, Song F, Zhou Y, Liu Z, Liu S. Rapid identification of saponins in plant extracts by electrospray ionization multi-stage tandem mass spectrometry and liquid chromatography/tandem mass spectrometry. Rapid Commun Mass Spectrom [Internet]. 2000 Jul 30;14(14):1280–6. Available from: https://doi.org/10.1002/1097-0231(20000730)14:14%3C1280::AID-RCM26%3E3.0.CO

101. Jiang K, Gachumi G, Poudel A, Shurmer B, Bashi Z, El-Aneed A. The Establishment of Tandem Mass Spectrometric Fingerprints of Phytosterols and Tocopherols and the Development of Targeted Profiling Strategies in Vegetable Oils. J Am Soc Mass Spectrom [Internet]. 2019 Sep 1;30(9):1700–12. Available from: https://pubs.acs.org/doi/abs/10.1021/jasms.8b06084

102. Poudel A, Gachumi G, Badea I, Bashi ZD, El-Aneed A. The simultaneous quantification of phytosterols and tocopherols in liposomal formulations using validated atmospheric pressure chemical ionization- liquid chromatography – tandem mass spectrometry. J Pharm Biomed Anal [Internet]. 2020;183:113104. Available from: https://www.sciencedirect.com/science/article/pii/S0731708519323611

103. Busardò FP, Carlier J, Giorgetti R, Tagliabracci A, Pacifici R, Gottardi M, et al. Ultra-High-Performance Liquid Chromatography-Tandem Mass Spectrometry Assay for Quantifying Fentanyl and 22 Analogs and Metabolites in Whole Blood, Urine, and Hair [Internet]. Vol. 7, Frontiers in Chemistry . 2019. p. 184. Available from: https://www.frontiersin.org/article/10.3389/fchem.2019.00184

104. Castro-Perez J, Plumb R, Liang L, Yang E. A high-throughput liquid chromatography/tandem mass spectrometry method for screening glutathione conjugates using exact mass neutral loss acquisition. Rapid Commun Mass Spectrom. 2005;19(6):798–804.

105. Foltz DJ, Castro-Perez J, Riley P, Entwisle JR, Baker TR. Narrow-bore sample trapping and chromatography combined with quadrupole/time-of-flight mass spectrometry for ultra-sensitive identification of in vivo and in vitro metabolites. J Chromatogr B, Anal Technol Biomed life Sci. 2005 Oct;825(2):144–51.

106. Kostiainen R, Kotiaho T, Kuuranne T, Auriola S. Liquid chromatography/atmospheric pressure ionization-mass spectrometry in drug metabolism studies. J Mass Spectrom. 2003 Apr;38(4):357–72.

107. Castro-Perez JM. Current and future trends in the application of HPLC-MS to metabolite-identification studies. Drug Discov Today [Internet]. 2007;12(5):249–56. Available from: https://www.sciencedirect.com/science/article/pii/S1359644607000499

108. Cui L, Lu H, Lee YH. Challenges and emergent solutions for LC-MS/MS based untargeted metabolomics in diseases. Mass Spectrom Rev [Internet]. 2018 Nov 1;37(6):772–92. Available from: https://doi.org/10.1002/mas.21562

109. Ortmayr K, Causon TJ, Hann S, Koellensperger G. Increasing selectivity and coverage in LC-MS based metabolome analysis. TrAC Trends Anal Chem [Internet]. 2016;82:358–66. Available from: https://www.sciencedirect.com/science/article/pii/S016599361630108X

110. Suárez M, Caimari A, del Bas JM, Arola L. Metabolomics: An emerging tool to evaluate the impact of nutritional and physiological challenges. TrAC Trends Anal Chem [Internet]. 2017;96:79–88. Available from: https://www.sciencedirect.com/science/article/pii/S0165993617300997

111. Khamis MM, Adamko DJ, El-Aneed A. Strategies and chalenges in method development and validation for the absolute quantification of endogenous

biomarker metabolites using liquid chromatography- tandem mass spectrometry. Mass Spectrom Rev [Internet]. 2021 Jan 1;40(1):31–52. Available from: https://doi.org/10.1002/mas.21607

112. Lopes BT, Caldeira MJ, Gaspar H, Antunes AMM. Metabolic Profile of Four Selected Cathinones in Microsome Incubations: Identification of Phase I and II Metabolites by Liquid Chromatography High Resolution Mass Spectrometry [Internet]. Vol. 8, Frontiers in Chemistry . 2021. p. 1241. Available from: https://www.frontiersin.org/article/10.3389/fchem.2020.609251

113. Demeiry M El, Ali A, Abouleila Y, Zarad W, El-Gendy H, Salam RA, et al. Direct infusion nano-electrospray ionization mass spectrometry for therapeutic drug monitoring of ciprofloxacin and its metabolites in human saliva. J Pharm Biomed Anal [Internet]. 2021;195:113866. Available from: https://www.sciencedirect.com/science/article/pii/S0731708520317532

114. Hopfgartner G, Husser C, Zell M. Rapid Screening and Characterization of Drug Metabolites using a New Quadrupole–Linear Ion Trap Mass Spectrometer. J Mass Spectrom. 2003 Mar 1;38:138–50.

115. Kozar N, Kruusmaa K, Bitenc M, Argamasilla R, Adsuar A, Takač I, et al. Identification of Novel Diagnostic Biomarkers in Breast Cancer Using Targeted Metabolomic Profiling. Clin Breast Cancer [Internet]. 2020; Available from: https://www.sciencedirect.com/science/article/pii/S1526820920302329

116. van der Berg C, Venter G, van der Westhuizen FH, Erasmus E. Development and validation of LC-ESI-MS/MS methods for quantification of 27 free and conjugated estrogen-related metabolites. Anal Biochem [Internet]. 2020;590:113531. Available from: https://www.sciencedirect.com/science/article/pii/S0003269719308504

117. Chen D-R, Hsieh W-C, Liao Y-L, Lin K-J, Wang Y-F, Lin P-H. Imbalances in the disposition of estrogen and naphthalene in breast cancer patients: a potential biomarker of breast cancer risk. Sci Rep [Internet]. 2020;10(1):11773. Available from: https://doi.org/10.1038/s41598-020-68814-5

118. Bolton JL, Thatcher GRJ. Potential Mechanisms of Estrogen Quinone Carcinogenesis. Chem Res Toxicol [Internet]. 2008 Jan 1;21(1):93–101. Available from: https://doi.org/10.1021/tx700191p

119. Chovan LE, Black-Schaefer C, Dandliker PJ, Lau YY. Automatic mass spectrometry method development for drug discovery: application in metabolic stability assays. Rapid Commun Mass Spectrom [Internet]. 2004 Dec 30;18(24):3105–12. Available from: https://doi.org/10.1002/rcm.1735

120. Di L, Kerns E, Hong Y, Kleintop T, McConnell O, Huryn D. Optimization of a Higher Throughput Microsomal Stability Screening Assay for Profiling Drug Discovery Candidates. J Biomol Screen. 2003 Aug 1;8:453–62.

121. Chen X, Li Y. Identification of the stable and reactive metabolites of tetrahydropiperine using ultrahigh-performance liquid chromatography combined with diode-array detection and high-resolution mass spectrometry. Rapid Commun Mass Spectrom [Internet]. 2021 Jan 30;35(2):e8975. Available from: https://doi.org/10.1002/rcm.8975

122. Awad H, Khamis M, El-Aneed A. Mass Spectrometry, Review of the Basics: Ionization. Appl Spectrosc Rev. 2015 Feb 1;50.

123. van der Gugten JG. Tandem mass spectrometry in the clinical laboratory: A tutorial overview. Clin Mass Spectrom [Internet]. 2020;15:36–43. Available from: https://www.sciencedirect.com/science/article/pii/S2376999819300418

124. Glish GL, Vachet RW. The basics of mass spectrometry in the twenty-first century. Nat Rev Drug Discov [Internet]. 2003;2(2):140–50. Available from: https://doi.org/10.1038/nrd1011

125. Kumbhar PS, Diwate SK, Mali UG, Shinde TU, Disouza JI, Manjappa AS. Development and validation of RP-HPLC method for simultaneous estimation of docetaxel and ritonavir in PLGA nanoparticles. Ann Pharm Françaises [Internet]. 2020;78(5):398–407. Available from: https://www.sciencedirect.com/science/article/pii/S0003450920300845

126. Du P, Li N, Wang H, Yang S, Song Y, Han X, et al. Development and validation of a rapid and sensitive UPLC–MS/MS method for determination of total docetaxel from a lipid microsphere formulation in human plasma. J Chromatogr B [Internet]. 2013;926:101–7. Available from: https://www.sciencedirect.com/science/article/pii/S1570023213000913

127. Fernández-del-Campo-García MT, Casas-Ferreira AM, Rodríguez-Gonzalo E, Moreno-Cordero B, Pérez-Pavón JL. Development of a fast and reliable methodology for the determination of polyamines in urine by using a guard column as a low-resolution fractioning step prior to mass spectrometry. Comparison with flow injection-mass spectrometry analysis. Microchem J

[Internet]. 2020;158:105223. Available from: https://www.sciencedirect.com/science/article/pii/S0026265X20314016

128. Rafiei P, Michel D, Haddadi A. Application of a Rapid ESI-MS/MS Method for Quantitative Analysis of Docetaxel in Polymeric Matrices of PLGA and PLGA-PEG Nanoparticles through Direct Injection to Mass Spectrometer. Am J Anal Chem. 2015 Jan 1;6:164–75.

129. Guitton J, Cohen S, Tranchand B, Vignal B, Droz J-P, Guillaumont M, et al. Quantification of docetaxel and its main metabolites in human plasma by liquid chromatography/tandem mass spectrometry. Rapid Commun Mass Spectrom. 2005;19(17):2419–26.

130. Yamaguchi H, Fujikawa A, Ito H, Tanaka N, Furugen A, Miyamori K, et al. A rapid and sensitive LC/ESI–MS/MS method for quantitative analysis of docetaxel in human plasma and its application to a pharmacokinetic study. J Chromatogr B [Internet]. 2012;893–894:157–61. Available from: https://www.sciencedirect.com/science/article/pii/S1570023212000785

131. Gao S, Zhou J, Zhang F, Miao H, Yun Y, Feng J, et al. Rapid and Sensitive Liquid Chromatography Coupled With Electrospray Ionization Tandem Mass Spectrometry Method for the Analysis of Paclitaxel, Docetaxel, Vinblastine, and Vinorelbine in Human Plasma. Ther Drug Monit. 2013 Dec 20;36.

132. Kort A, Hillebrand MJX, Cirkel GA, Voest EE, Schinkel AH, Rosing H, et al. Quantification of cabazitaxel, its metabolite docetaxel and the determination of the demethylated metabolites RPR112698 and RPR123142 as docetaxel equivalents in human plasma by liquid chromatography-tandem mass spectrometry. J Chromatogr B Anal Technol Biomed Life Sci. 2013 Apr 5;925:117–23.

133. Corona G, Elia C, Casetta B, Frustaci S, Toffoli G. High-throughput plasma docetaxel quantification by liquid chromatography-tandem mass spectrometry. Clin Chim Acta. 2011 Jan;412(3–4):358–64.

134. Du P, Han X, Li N, Wang H, Yang S, Song Y, et al. Development and validation of an ultrafiltration-UPLC-MS/MS method for rapid quantification of unbound docetaxel in human plasma. J Chromatogr B Anal Technol Biomed Life Sci. 2014 Sep 15;967:28–35.

135. Rosing H, Lustig V, Koopman FP, ten Bokkel Huinink WW, Beijnen JH. Bio-analysis of docetaxel and hydroxylated metabolites in human plasma by high-performance liquid chromatography and automated solid-phase extraction. J

Chromatogr B Biomed Sci Appl [Internet]. 1997;696(1):89–98. Available from: https://www.sciencedirect.com/science/article/pii/S0378434797002090

136. Ciccolini J, Catalin J, Blachon MF, Durand A. Rapid high-performance liquid chromatographic determination of docetaxel (Taxoteree) in plasma using liquid-liquid extraction. J Chromatogr B Biomed Sci Appl. 2001 Aug;759(2):299–306.

137. Navarrete A, Martínez-Alcázar MP, Durán I, Calvo E, Valenzuela B, Barbas C, et al. Simultaneous online SPE–HPLC–MS/MS analysis of docetaxel, temsirolimus and sirolimus in whole blood and human plasma. J Chromatogr B [Internet]. 2013;921–922:35–42. Available from: https://www.sciencedirect.com/science/article/pii/S1570023213000597

138. Parise RA, Ramanathan RK, Zamboni WC, Egorin MJ. Sensitive liquid chromatography–mass spectrometry assay for quantitation of docetaxel and paclitaxel in human plasma. J Chromatogr B [Internet]. 2003;783(1):231–6. Available from: https://www.sciencedirect.com/science/article/pii/S1570023202006591

139. Hendrikx JJMA, Hillebrand MJX, Thijssen B, Rosing H, Schinkel AH, Schellens JHM, et al. A sensitive combined assay for the quantification of paclitaxel, docetaxel and ritonavir in human plasma using liquid chromatography coupled with tandem mass spectrometry. J Chromatogr B Anal Technol Biomed Life Sci. 2011 Oct 15;879(28):2984–90.

140. US Department of Health and Human Services FDA, Center for Drug Evaluation and Research. FDA Guidance for Industry: Bioanalytical Method Validation. Rockville, MD, 2018 [Internet]. [cited 2021 Mar 17]. Available from: https://www.fda.gov/files/drugs/published/Bioanalytical-Method-Validation-Guidance-for-Industry.pdf

141. European Medicines Agengy CfMPfHUC. Guidelines on Bioanalytical Method Validation. London, UK, 2011 [Internet]. [cited 2021 Mar 17]. Available from: https://www.ema.europa.eu/en/documents/scientific-guideline/guideline-bioanalytical-method-validation_en.pdf

142. Khamis MM, Adamko DJ, El-Aneed A. Development of a validated LC-MS/MS method for the quantification of 19 endogenous asthma/COPD potential urinary biomarkers. Anal Chim Acta [Internet]. 2017;989:45–58. Available from: https://www.sciencedirect.com/science/article/pii/S0003267017308966

143. Xu QA MT. LC-MS in drug bioanalysis. New York: Springer; 2012.

144. Mülhopt S, Diabaté S, Dilger M, Adelhelm C, Anderlohr C, Bergfeldt T, et al. Characterization of Nanoparticle Batch-To-Batch Variability. Nanomaterials. 2018 May 8;8.

145. Yeap SP, Lim J, Ngang HP, Ooi BS, Ahmad AL. Role of Particle-Particle Interaction Towards Effective Interpretation of -Average and Particle Size Distributions from Dynamic Light Scattering (DLS) Analysis. J Nanosci Nanotechnol. 2018;18(10):6957.

146. Mudalige T, Qu H, Van Haute D, Ansar SM, Paredes A, Ingle T. Chapter 11 - Characterization of Nanomaterials: Tools and Challenges. In: López Rubio A, Fabra Rovira MJ, martínez Sanz M, Gómez-Mascaraque LGBT-N for FA, editors. Micro and Nano Technologies [Internet]. Elsevier; 2019. p. 313–53. Available from: https://www.sciencedirect.com/science/article/pii/B9780128141304000117

147. Blanco E, Shen H, Ferrari M. Principles of nanoparticle design for overcoming biological barriers to drug delivery. Nat Biotechnol [Internet]. 2015;33(9):941–51. Available from: https://doi.org/10.1038/nbt.3330

148. Furinss BS, Hannaford AJ, Smith PWG, Tatchell AR. Vogel's textbook of practical organic chemistry. 1989;

149. Kulsirirat T, Sathirakul K, Kamei N, Takeda-Morishita M. The in vitro and in vivo study of novel formulation of Andrographolide PLGA nanoparticle embedded into gelatin-based hydrogel to prolong delivery and extend residence time in joint. Int J Pharm [Internet]. 2021;120618. Available from: https://www.sciencedirect.com/science/article/pii/S0378517321004233

150. Hamzaoui A, Laraba-Djebari F. Development and evaluation of polymeric nanoparticles as a delivery system for snake envenoming prevention. Biologicals [Internet]. 2021;70:44–52. Available from: https://www.sciencedirect.com/science/article/pii/S104510562100018X

151. Haddadi A, Chaffey A, Ng SH, Yalamati D, Wilson HL. Combination of Innate Immune Modulators as Vaccine Adjuvants in Mice. Vaccines. 2020 Oct;8(4).

152. Jahan ST, Sadat SMA, Yarahmadi M, Haddadi A. Potentiating Antigen Specific Immune Response by Targeted Delivery of the PLGA-Based Model Cancer Vaccine. Mol Pharm [Internet]. 2019 Feb 4;16(2):498–509. Available

from: https://doi.org/10.1021/acs.molpharmaceut.8b00700

153. Mousavi L, Mohd Salleh R, Murugaiyah V. Toxicology Assessment of Ocimum tenuiflorum L. Leaves Extracts on Streptozotocin-Induced Diabetic Rats. Malaysian J Microsc. 2018 Jan 1;14:124–56.

154. Kulkarni SA, Feng S-S. Effects of particle size and surface modification on cellular uptake and biodistribution of polymeric nanoparticles for drug delivery. Pharm Res. 2013 Oct;30(10):2512–22.

155. He C, Hu Y, Yin L, Tang C, Yin C. Effects of particle size and surface charge on cellular uptake and biodistribution of polymeric nanoparticles. Biomaterials [Internet]. 2010;31(13):3657–66. Available from: https://www.sciencedirect.com/science/article/pii/S0142961210000979

156. Florence AT, Hillery AM, Hussain N, Jani PU. Nanoparticles as carriers for oral peptide absorption: Studies on particle uptake and fate. J Control Release [Internet]. 1995;36(1):39–46. Available from: https://www.sciencedirect.com/science/article/pii/016836599500059H

157. Fang C, Shi B, Pei Y-Y, Hong M-H, Wu J, Chen H-Z. In vivo tumor targeting of tumor necrosis factor-α-loaded stealth nanoparticles: Effect of MePEG molecular weight and particle size. Eur J Pharm Sci [Internet]. 2006;27(1):27–36. Available from: https://www.sciencedirect.com/science/article/pii/S0928098705002472

158. Gaumet M, Vargas A, Gurny R, Delie F. Nanoparticles for drug delivery: The need for precision in reporting particle size parameters. Eur J Pharm Biopharm [Internet]. 2008;69(1):1–9. Available from: https://www.sciencedirect.com/science/article/pii/S0939641107002895

159. Gamvrellis A, Leong D, Hanley J, Xiang S, Mottram P, Plebanski M. Vaccines that facilitate antigen entry into dendritic cells. Immunol Cell Biol. 2004 Nov 1;82:506–16.

160. Hamdy S, Haddadi A, Shayeganpour A, Samuel J, Lavasanifar A. Activation of Antigen-Specific T Cell-Responses by Mannan-Decorated PLGA Nanoparticles. Pharm Res. 2011 May 11;28:2288–301.

161. Hobbs SK, Monsky WL, Yuan F, Roberts WG, Griffith L, Torchilin VP, et al. Regulation of transport pathways in tumor vessels: role of tumor type and microenvironment. Proc Natl Acad Sci. 1998;95(8):4607–12.

162. Vácha R, Martinez-Veracoechea FJ, Frenkel D. Receptor-mediated

endocytosis of nanoparticles of various shapes. Nano Lett. 2011 Dec;11(12):5391–5.

163. Ding H, Ma Y. Role of physicochemical properties of coating ligands in receptor-mediated endocytosis of nanoparticles. Biomaterials [Internet]. 2012;33(23):5798–802. Available from: https://www.sciencedirect.com/science/article/pii/S0142961212004942

164. Cheaburu-Yilmaz CN, Karasulu HY, Yilmaz O. Chapter 13 - Nanoscaled Dispersed Systems Used in Drug-Delivery Applications. In: Vasile CBT-PN in N, editor. Micro and Nano Technologies [Internet]. Elsevier; 2019. p. 437–68. Available from: https://www.sciencedirect.com/science/article/pii/B9780128139325000133

165. Malek MNFA, Hussin NM, Embong NH, Bhuyar P, Rahim MHA, Govindan N, et al. Ultrasonication: a process intensification tool for methyl ester synthesis: a mini review. Biomass Convers Biorefinery [Internet]. 2020; Available from: https://doi.org/10.1007/s13399-020-01100-6

166. Sandhya M, Ramasamy D, Sudhakar K, Kadirgama K, Harun WSW. Ultrasonication an intensifying tool for preparation of stable nanofluids and study the time influence on distinct properties of graphene nanofluids – A systematic overview. Ultrason Sonochem [Internet]. 2021;73:105479. Available from: https://www.sciencedirect.com/science/article/pii/S1350417721000201

167. Morsali A, Panjehpour A. Ultrasonic-assisted synthesis of nano-structured lead(II) coordination polymers as precursors for preparation of lead(II) oxide nanoparticles. Inorganica Chim Acta [Internet]. 2012;391:210–7. Available from: https://www.sciencedirect.com/science/article/pii/S0020169312002836

168. Liu Z, Yang L. Antisolvent precipitation for the preparation of high polymeric procyanidin nanoparticles under ultrasonication and evaluation of their antioxidant activity in vitro. Ultrason Sonochem [Internet]. 2018;43:208–18. Available from: https://www.sciencedirect.com/science/article/pii/S1350417718300877

169. Morsali A, Monfared HH, Morsali A, Janiak C. Ultrasonic irradiation assisted syntheses of one-dimensional di(azido)-dipyridylamine Cu(II) coordination polymer nanoparticles. Ultrason Sonochem [Internet]. 2015;23:208–11. Available from: https://www.sciencedirect.com/science/article/pii/S1350417714001916

170. Tang ESK, Huang M, Lim LY. Ultrasonication of chitosan and chitosan nanoparticles. Int J Pharm [Internet]. 2003;265(1):103–14. Available from: https://www.sciencedirect.com/science/article/pii/S0378517303004083

171. Lii C, Chen C-H, Yeh A-I, Lai VM-F. Preliminary study on the degradation kinetics of agarose and carrageenans by ultrasound. Food Hydrocoll [Internet]. 1999;13(6):477–81. Available from: https://www.sciencedirect.com/science/article/pii/S0268005X99000314

172. Abdelwahed W, DEGOBERT G, Stainmesse S, Fessi H. Freeze-Drying of Nanoparticles: Formulation, Process and Storage Considerations. Adv Drug Deliv Rev. 2007 Jan 1;58:1688–713.

173. Chen G, Wang W. Role of Freeze Drying in Nanotechnology. Dry Technol [Internet]. 2007 Feb 12;25(1):29–35. Available from: https://doi.org/10.1080/07373930601161179

174. Konan YN, Gurny R, Allémann E. Preparation and characterization of sterile and freeze-dried sub-200 nm nanoparticles. Int J Pharm [Internet]. 2002;233(1):239–52. Available from: https://www.sciencedirect.com/science/article/pii/S0378517301009449

175. Chang L (Lucy), Shepherd D, Sun J, Ouellette D, Grant KL, Tang X (Charlie), et al. Mechanism of protein stabilization by sugars during freeze-drying and storage: Native structure preservation, specific interaction, and/or immobilization in a glassy matrix? J Pharm Sci [Internet]. 2005;94(7):1427–44. Available from: https://www.sciencedirect.com/science/article/pii/S0022354916373154

176. Kumar S, Gokhale R, Burgess DJ. Sugars as bulking agents to prevent nano-crystal aggregation during spray or freeze-drying. Int J Pharm [Internet]. 2014;471(1):303–11. Available from: https://www.sciencedirect.com/science/article/pii/S037851731400413X

177. Holzer M, Vogel V, Mäntele W, Schwartz D, Haase W, Langer K. Physico-chemical characterisation of PLGA nanoparticles after freeze-drying and storage. Eur J Pharm Biopharm [Internet]. 2009;72(2):428–37. Available from: https://www.sciencedirect.com/science/article/pii/S0939641109000563

178. Hirsjärvi S, Peltonen L, Hirvonen J. Effect of Sugars, Surfactant, and Tangential Flow Filtration on the Freeze-Drying of Poly(lactic acid) Nanoparticles. AAPS PharmSciTech [Internet]. 2009;10(2):488–94. Available from: https://doi.org/10.1208/s12249-009-9236-z

179. Shahgaldian P, Gualbert J, Aïssa K, Coleman AW. A study of the freeze-drying conditions of calixarene based solid lipid nanoparticles. Eur J Pharm Biopharm [Internet]. 2003;55(2):181–4. Available from: https://www.sciencedirect.com/science/article/pii/S0939641102001960

180. Anhorn MG, Mahler H-C, Langer K. Freeze drying of human serum albumin (HSA) nanoparticles with different excipients. Int J Pharm [Internet]. 2008;363(1):162–9. Available from: https://www.sciencedirect.com/science/article/pii/S0378517308004936

181. Lee MK, Kim MY, Kim S, Lee J. Cryoprotectants for freeze drying of drug nano-suspensions: Effect of freezing rate. J Pharm Sci [Internet]. 2009;98(12):4808–17. Available from: https://www.sciencedirect.com/science/article/pii/S0022354916331926

182. Daughton CG. Emerging pollutants, and communicating the science of environmental chemistry and mass spectrometry: pharmaceuticals in the environment. J Am Soc Mass Spectrom [Internet]. 2001;12(10):1067–76. Available from: https://www.sciencedirect.com/science/article/pii/S1044030501002872

183. Yu D, Zhang S, Feng A, Xu D, Zhu Q, Mao Y, et al. Methotrexate, doxorubicin, and cisplatinum regimen is still the preferred option for osteosarcoma chemotherapy: A meta-analysis and clinical observation. Medicine (Baltimore). 2019 May;98(19):e15582.

184. Calza P, Medana C, Sarro M, Rosato V, Aigotti R, Baiocchi C, et al. Photocatalytic degradation of selected anticancer drugs and identification of their transformation products in water by liquid chromatography–high resolution mass spectrometry. J Chromatogr A [Internet]. 2014;1362:135–44. Available from: https://www.sciencedirect.com/science/article/pii/S0021967314012837

185. Khalin I, Severi C, Heimburger D, Wehn A, Hellal F, Reisch A, et al. Dynamic tracing using ultra-bright labelling and multi-photon microscopy identifies endothelial uptake of poloxamer 188 coated poly(lactic-co-glycolic acid) nano-carriers in vivo bioRxiv [Internet]. 2021 Jan 1;2020.11.19.385062. Available from: http://biorxiv.org/content/early/2021/06/04/2020.11.19.385062.abstract

186. Zhang E, Zhukova V, Semyonkin A, Osipova N, Malinovskaya Y, Maksimenko O, et al. Release kinetics of fluorescent dyes from PLGA

nanoparticles in retinal blood vessels: In vivo monitoring and ex vivo localization. Eur J Pharm Biopharm Off J Arbeitsgemeinschaft fur Pharm Verfahrenstechnik eV. 2020 May;150:131–42.

187. Vij N, Min T, Marasigan R, Belcher CN, Mazur S, Ding H, et al. Development of PEGylated PLGA nanoparticle for controlled and sustained drug delivery in cystic fibrosis. J Nanobiotechnology [Internet]. 2010;8(1):22. Available from: https://doi.org/10.1186/1477-3155-8-22

188. Rong L, Zhou S, Liu X, Li A, Jing T, Liu X, et al. Trastuzumab-modified DM1-loaded nanoparticles for HER2(+) breast cancer treatment: an in vitro and in vivo study. Artif cells, nanomedicine, Biotechnol. 2018 Dec;46(8):1708–18.

189. Steinhauser I, Spänkuch B, Strebhardt K, Langer K. Trastuzumab-modified nanoparticles: optimisation of preparation and uptake in cancer cells. Biomaterials. 2006 Oct;27(28):4975–83.

190. Zhang X, Liu J, Li X, Li F, Lee RJ, Sun F, et al. Trastuzumab-Coated Nanoparticles Loaded With Docetaxel for Breast Cancer Therapy. Dose Response. 2019;17(3):1559325819872583.

APPENDIX

Supplementary figures

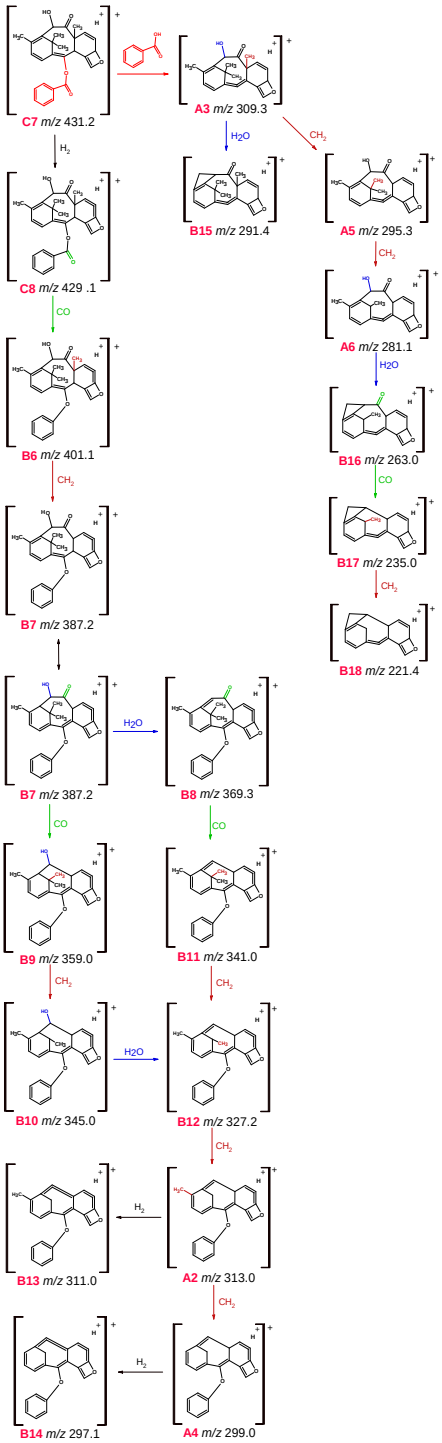

Figure S1. The remaining proposed MS/MS fragmentation of paclitaxel.

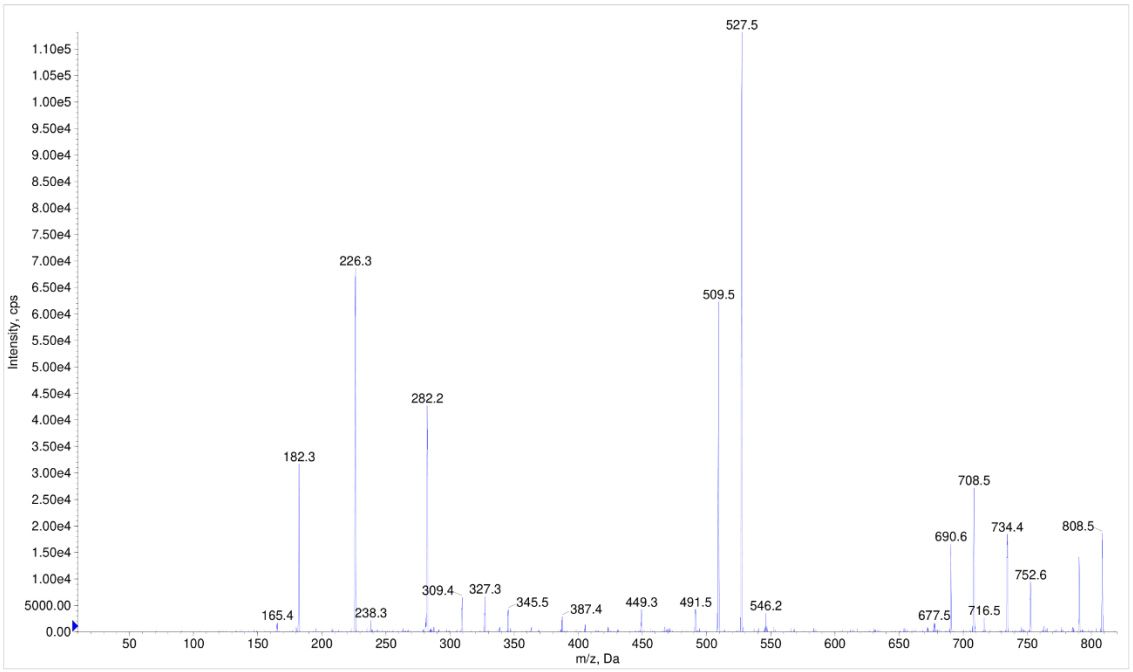

Figure S2. MS/MS spectrum of docetaxel.

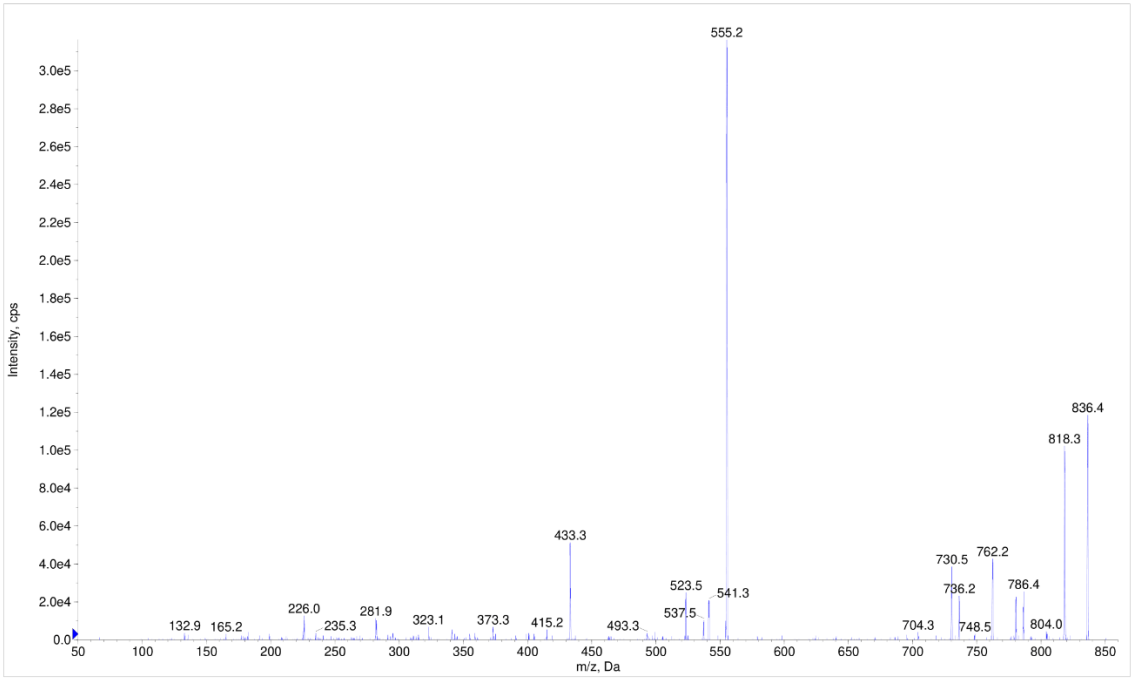

Figure S3. MS/MS spectrum of cabazitaxel.

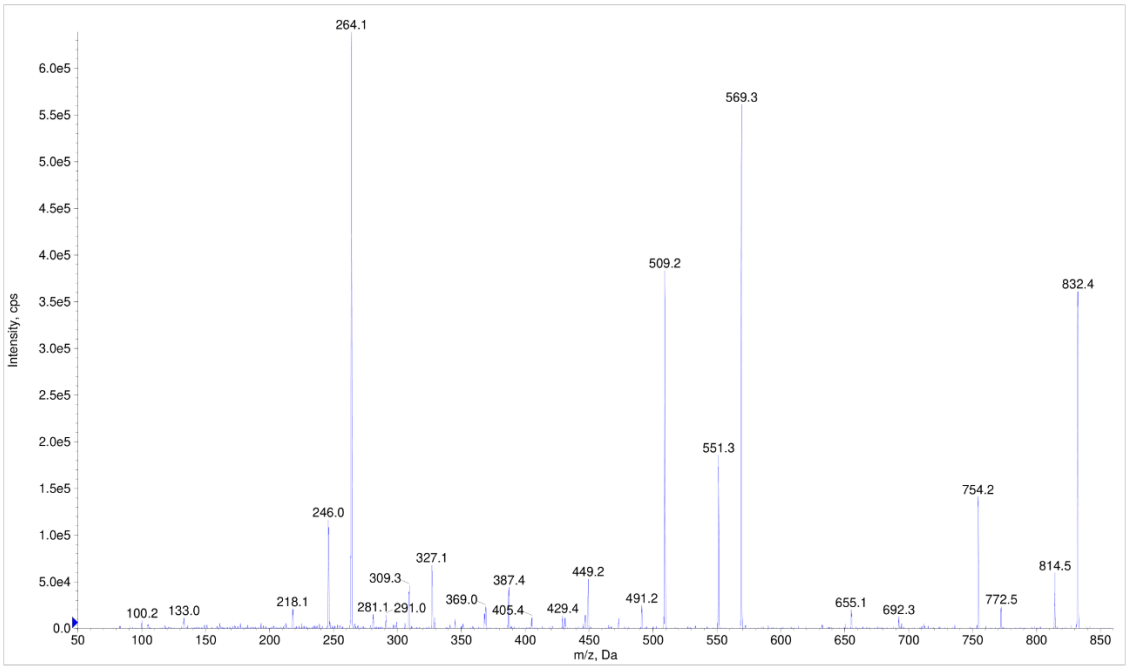

Figure S4. MS/MS spectrum of cephalomannine.

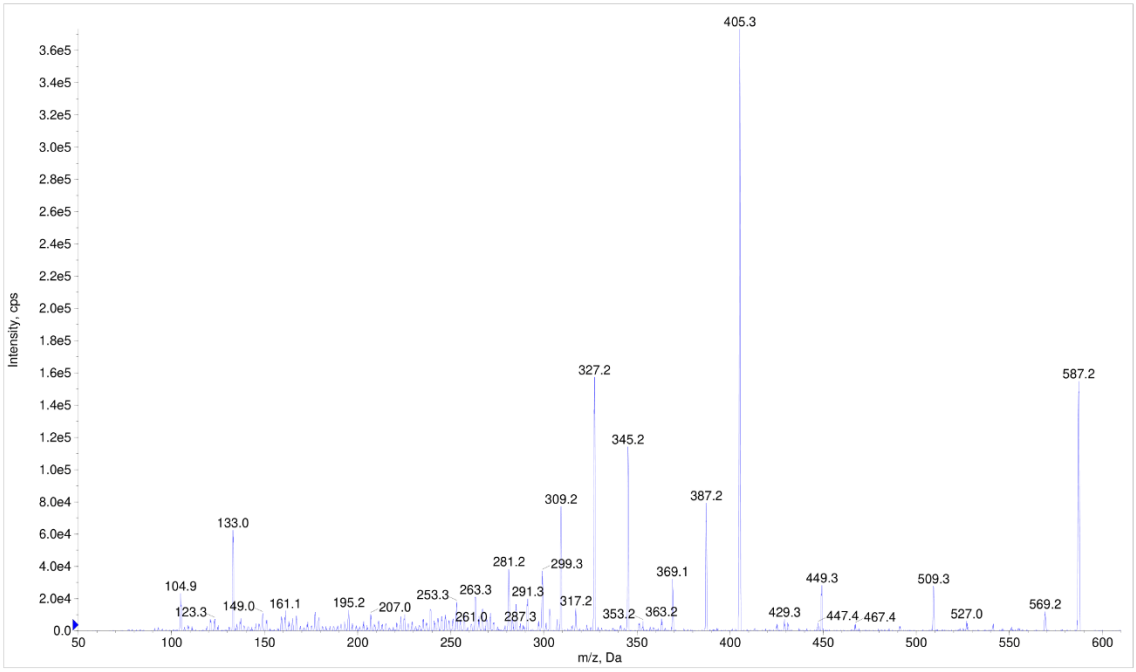

Figure S5. MS/MS spectrum of baccatin III.

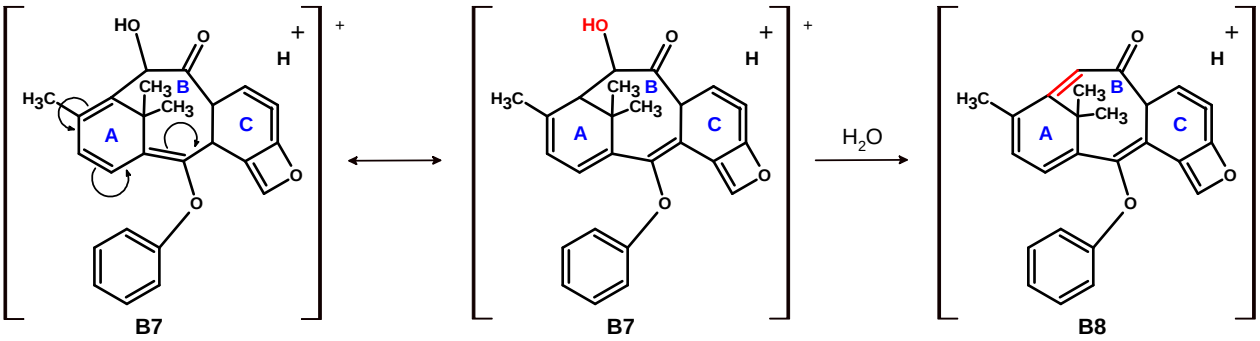

Figure S6. Resonance mechanism for the ion B7 at *m/z* 387.2 that makes it possible for the subsequent loss of H_2O from the B-ring.

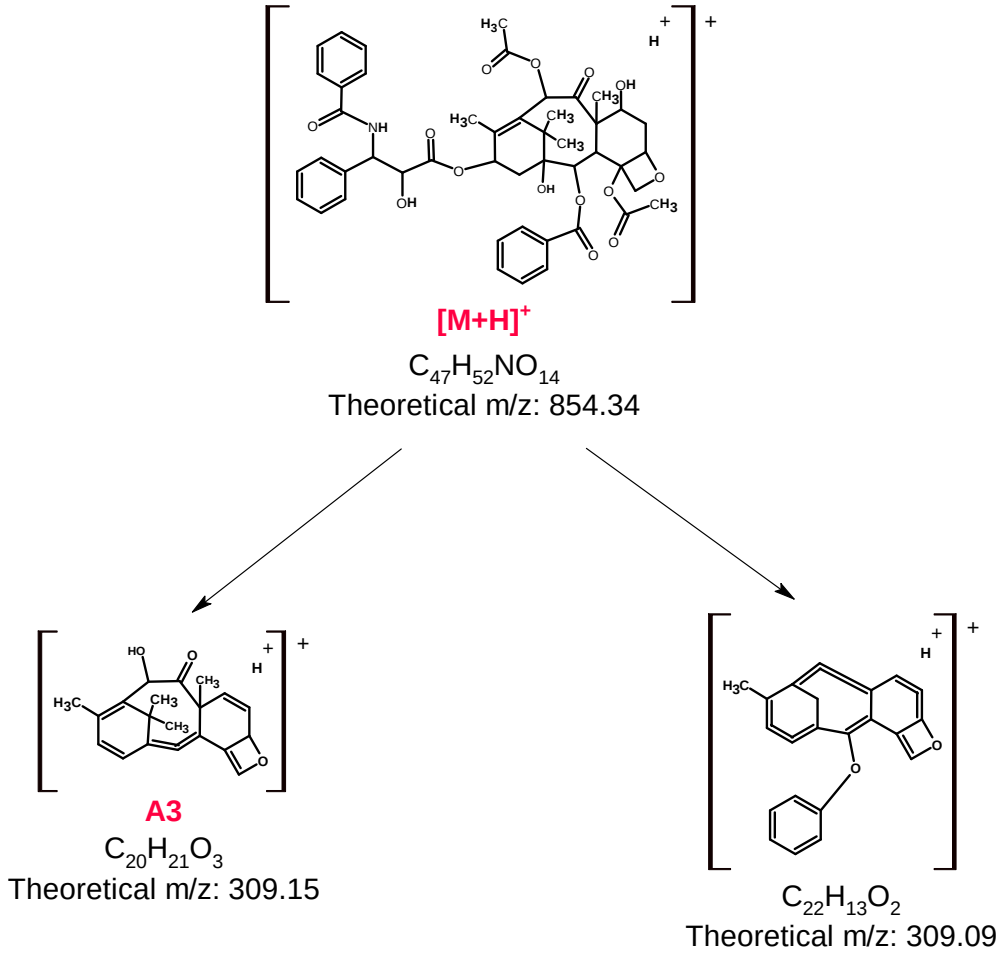

Figure S7. The structures of the two theoretically possible ions representing *m/z* 309.3. MS^3 analysis showed that the only logical structure is A3 (the structure on the left with an m/z value of 309.15).

Supplementary tables

Table S1. MS^3 analysis for cabazitaxel.

Precursor ion	First generation product ions (MS/MS)	Second generation product ions (MS^3)
836.4 $[M+H]^+$	818.4 [B1]	786.3 [C1], 762.3, 730.5 [S1], 555.3 [S3], 505.1 [A1]
	804.4	786.3 [C1], 748.5, 730.5 [S1], 541.3
	786.3	730.5 [S1]
	780.4	736.2, 718.3
	762.2	730.5 [S1], 555.3 [S3], 537.2
	736.2	718.3, 704.3, 555.3 [S3], 523.2 [C4], 341.0 [B8]
	730.5 [S1]	523.2 [C4], 341.0 [B8], 463.1 [C6]
	718.3	704.3, 555.3 [S3]
	555.3 [S3]	523.2 [C4], 505.1 [A1], 433.4, 401.1 [B11], 373.0 [A2]
	523.2 [C4]	521.2, 505 [A1], 493 [B17], 463.1 [C6], 341.0 [B8]
	505.1 [A1]	463.1 [C6], 341.0 [B8]
	493.3 [B17]	475.1, 415.1 [B6]
	463.1 [C6]	445.1 [C7]
	445.1 [C7]	443.1 [C8], 341.0 [B8]
	443.1 [C8]	415.1 [B6]
	433.4	415.1 [B6], 401.1 [B11], 373.0 [A2], 341.0 [B8]
	415.1 [B6]	401.1 [B11]
	401.0 [B11]	387.1 [B12]
	387 [B12]	373.0 [A2], 341.0 [B8]
	373.0 [A2]	341.0 [B8]
	282.3 [S5]	226.1, 164.9
	226.1	164.9

Table S2. MS^3 analysis for docetaxel.

Precursor ion	First generation product ions (MS/MS)	Second generation product ions (MS^3)
808.3 $[M+H]^+$	790.4 [B1]	776.2, 734.2, 690.3 [C1], 509.2 [C4]
	752.6	708.5, 690.3 [C1]
	734.2	690.3 [C1], 672.2 [S1], 568.1 [B5], 509.2 [C4], 327.2 [B10]
	708.5	690.3 [C1], 527.2 [S3]
	690.3 [C1]	672.2 [S1], 568.1 [B5], 527.2 [S3], 509.2 [C4], 491.0 [A1]
	672.2 [S1]	612.2 [C3], 550.2 [B3], 472.1
	550.2 [B3]	472.1
	527.2 [S3]	509.2 [C4], 491.0 [A1], 449.2 [C6], 327.2 [B10], 309.3 [A3]
	509.2 [C4]	491.0 [A1], 449.2 [C6], 431.1 [C7], 387.2 [B8], 281.0 [A6]
	491.0 [A1]	449.2 [C6], 431.1 [C7], 369.2, 309.3 [A3]
	449.2 [C6]	431.1 [C7], 421.1 [B6], 327.2 [B10], 309.3 [A3]
	431.1 [C7]	309.3 [A3], 295.0 [A6], 281.0 [A6]
	421.1 [B6]	419.1 [C8], 405.4 [B7], 387.2 [B8]
	419.1 [C8]	405.4 [B7], 387.2 [B8]
	405.4 [B7]	387.2 [B8], 387.2 [B8], 299.0 [A4]
	387.2 [B8]	369.2, 359.1 [B11], 345.4 [B12], 327.2 [B10], 299.0 [A4]
	369.2	341.1 [B9], 327.2 [B10]
	359.1 [B11]	345.4 [B12], 327.2 [B10]
	345.4 [B12]	327.2 [B10], 299.0 [A4]
	341.1 [B9]	327.2 [B10]
	327.2 [B10]	313.0 [A2], 299.0 [A4]
	313.0 [A2]	299.0 [A4]
	309.3 [A3]	295.0 [A5], 263.4 [B16], 239.2 [B17]
	295.0 [A5]	281.0 [A6], 263.4 [B16]
	282.2 [S5]	254.2 [S7], 226.1
	281.0 [A6]	263.4 [B16], 239.2 [B17]
	254.2 [S7]	238.3, 165.2
	238.3	165.2
	226.1	182.1

Table S3. MS^3 analysis for cephalomannine.

Precursor ion	First generation product ions (MS/MS)	Second generation product ions (MS^3)
832.3 $[M+H]^+$	814.5 [B1]	772.5 [B2], 754.2 [C1], 655.1 [S2], 569.3 [S3], 551.3 [C4], 491.2 [A1], 309.3 [A3], 264.1 [S5], 246.0 [S6]
	772.5 [B2]	754.2 [C1], 509.2 [S4], 327.1 [B12], 264.1 [S5], 246.0 [S6]
	754.2 [C1]	694.3 [C2], 655.1 [S2], 264.1 [S5], 509.2 [S4], 491.2 [A1], 309.3 [A3], 264.1 [S5]
	694.3 [C2]	692.3, 674.3 [S1], 429.2 [C7]
	692.3	674.3 [S1], 429.2 [C7], 264.1 [S5], 246.0 [S6], 218.1 [S7]
	674.3 [S1]	660.3, 646.3, 632.2
	660.3	646.3, 632.2
	655.1 [S2]	509.2 [S4], 491.2 [A1], 449.2 [C6], 431.1 [C5], 387.4 [B7], 327.1 [B12], 309.3 [A3], 267.3 [B18]
	646.3	632.2
	569.3 [S3]	551.3 [C4], 509.2 [S4], 387.4 [B7], 327.1 [B12], 309.3 [A3]
	551.3 [C4]	509.2 [S4], 491.2 [A1], 369.0 [B8], 309.3 [A3]
	509.2 [S4]	491.2 [A1], 449.2 [C6], 327.1 [B12], 267.3 [B18]
	491.2 [A1]	449.2 [C6], 431.1 [C5], 309.3 [A3], 341.0 [B11]
	449.2 [C6]	447.3 [C8], 431.1 [C5], 327.1 [B12], 309.3 [A3]
	447.3 [C8]	429.2 [C7], 419.3, 387.4 [B7]
	431.1 [C5]	429.2 [C7], 309.3 [A3], 281.1 [A6]
	429.2 [C7]	401.0 [B6], 387.4 [B7], 369.0 [B8], 327.1 [B12]
	419.3	405.4
	401.0 [B6]	387.4 [B7], 327.1 [B12]
	387.4 [B7]	369.0 [B8], 311.0 [A2]
	369.0 [B8]	341.0 [B11], 327.1 [B12], 325.0 [B13]
	341.0 [B11]	327.1 [B12], 311.0 [A2]
	327.1 [B12]	325.0 [B13]
	325.0 [B13]	311.0 [A2]
	309.3 [A3]	295.0 [A5], 291.0 [B15], 281.1 [A6], 267.3 [B18]
	295.0 [A5]	281.1 [A6], 267.3 [B18]
	281.1 [A6]	267.3 [B18]
	264.1 [S5]	246.0 [S6], 218.1 [S7]
	246.0 [S6]	218.1 [S7]

Table S4. MS^3 analysis for baccatin III.

Precursor ion	First generation product ions (MS/MS)	Second generation product ions (MS^3)
587.2 $[M+H]^+$	569.2 [C4]	527.0 [S4], 467.4 [C3], 387.2 [B8], 327.2, 239.0 [B17]
	527.0 [S4]	509.3 [A1], 491.2 [C5], 467.4 [C3], 309.2 [A3]
	509.3 [A1]	491.2 [C5], 449.3 [C6], 431.2 [C7], 309.2 [A3], 291.3 [B15]
	491.2 [C5]	449.3 [C6], 431.2 [C7], 421.1 [B6]
	449.3 [C6]	447.4 [C8], 431.2 [C7], 431.2 [C7], 327.2, 309.2 [A3], 291.3 [B15], 281.2 [A6], 263.3
	431.2 [C7]	309.2 [A3], 295.0 [A5], 291.3 [B15]
	421.1 [B6]	419.1, 405.3 [B7]
	419.1	405.3 [B7], 387.2 [B8], 377.2 [B9], 325.0 [B13]
	405.3 [B7]	387.2 [B8], 377.2 [B9], 363.2 [B10], 369.1, 345.2 [B12]
	387.2 [B8]	369.1, 327.2
	377.2 [B9]	363.2 [B10], 345.2 [B12]
	369.1	341.0 [B11], 341.0 [B11], 327.2, 325.0 [B13], 311.0
	363.2 [B10]	345.2 [B12], 317.2 [A2], 299.3
	345.2 [B12]	327.2, 317.2 [A2], 299.3, 327.2, 325.0 [B13]
	341.0 [B11]	327.2
	327.2	325.0 [B13], 311.0
	325.0 [B13]	311.0
	317.2 [A2]	299.3
	309.2 [A3]	295.0 [A5], 291.3 [B15], 281.2 [A6], 267.0 [B18], 263.3, 261.0, 195.2
	295.0 [A5]	281.2 [A6], 267.0 [B18]
	291.3 [B15]	287.3, 277.0, 263.3, 261.0, 235.3
	281.2 [A6]	267.0 [B18], 265.3, 253.3, 239.0 [B17], 195.2
	277.0	263.3, 261.0, 235.3
	267.0 [B18]	265.3, 253.3, 239.0 [B17], 195.2
	263.3	261.0, 235.3
	253.3	195.2